# Computational Studies of Premixed Flame Characteristics with Surface Effects

by

Jingjing Li

A dissertation submitted in partial fulfillment
of the requirements for the degree of
Doctor of Philosophy
(Mechanical Engineering)
in The University of Michigan
2008

Doctoral Committee:

Associate Professor Hong G. Im, Chair
Professor Arvind Atreya
Professor Margaret S. Wooldridge
Assistant Professor Matthias Ihme

# Acknowledgements

This thesis is the result of six years of work whereby I have been accompanied and supported by many people. It is a pleasant aspect that I have now the opportunity to express my gratitude for all of them.

The first person I would like to thank is my advisor Professor Hong G. Im. During these years, he was always available when I needed his advises or help. His overly enthusiasm and integral view on research and his mission for providing 'only high-quality work and not less', has made a deep impression on me. I owe him lots of gratitude for having me shown this way of research. He could not even realize how much I have learned from him. I am really glad that I have come to be his student.

I would like to thank my colleague James Wiswall for his effort in providing me with valuable experimental data. I also want to thank James' advisor, Professor Wooldridge, for her precious opinion on simulation/experiments data comparison issues.

My lab members of CRFL all gave me the feeling of being at home at work. I especially want to show my appreciation to Dr. Ramanan Sankaran and Dr. Chunsang Yoo for their selfless help to me on the realm of research and life. I would also like to thank the other members of my PhD committee who monitored my work and took effort in reading and providing me with valuable comments on this thesis.

I am very grateful for my husband Dong Yang, for his patience during this period. I was impossible to finished the study without his support from all aspects.

This work was financially supported by the National Science Foundation, CAREER program.

# Table of Contents

**Acknowledgements** ii

**List of Figures** v

**Abstract** viii

**1 Introduction** 1

**2 Extinction Characteristics of Catalyst-Assisted Combustion with Variable Strain Rate** 10

2.1 Model Configuration . . . . . 10

2.1.1 Formulation . . . . . 11

2.1.2 Arc-length Continuation . . . . . 14

2.1.3 Computational Conditions . . . . . 16

2.2 Results and Discussion . . . . . 17

2.2.1 Flame temperature and extinction behavior . . . . . 17

2.2.2 Effects of equivalence ratio . . . . . 27

2.2.3 Effects of heat loss . . . . . 29

2.2.4 Parametric mapping of combustion regimes . . . . . 32

2.3 Conclusions . . . . . 34

**3 Effects of Dilution on the Extinction Characteristics of Strained Lean Premixed Flames Assisted by Catalytic Reaction** 37

3.1 Model Description . . . . . 38

3.2 Results and Discussion . . . . . 39

3.2.1 Steady response: effects of dilution . . . . . 39

3.2.2 Unsteady response to oscillatory strain rate . . . . . 45

3.2.3 Dynamic flammability limit . . . . . 46

3.3 Conclusions . . . . . 47

**4 Experimental Validation** **51**
4.1 Experimental Configuration . . . 52
4.2 Model Adjustment . . . 52
4.3 Results and Discussion . . . 57
4.3.1 Comparison with Experiment . . . 57
4.3.2 Assessment of Flammability Extension . . . 60
4.4 Conclusions . . . 65

**5 Flame Propagation and Extinction in a Narrow Channel** **70**
5.1 Numerical Model and Computational Condition . . . 70
5.2 Results and Discussion . . . 72
5.2.1 Effects of heat loss and mixture composition on the flame shape . . . 72
5.2.2 Flame propagation speed change . . . 74
5.3 Conclusions . . . 78

**6 Conclusions** **81**
6.1 Directions for Future Work . . . 84

**Bibliography** **86**

# List of Figures

Figure


1.1 Examples of micro-combustor designed in model of macro-combustor, combustion chamber assemblied with turbine together [1, 2]. . . . . 2

1.2 Examples of micro-combustor without moving part, left one collect combustion energy though thermionic emission [3], right one use thermophotovoltaic component: (a) without cooling fins, (b) with cooling fins [4]. . . . 3

1.3 Experimental setup . . . . . 7

2.1 Schematic of the stagnation-point flow configuration . . . . . 11

2.2 Finite-volume, spacial-difference stencil for the stagnation flow equations . 14

2.3 Maximum temperature and its location versus the nominal strain rate for $\phi = 0.8$, $h = 8$W/m$^2$-K. The cases with and without surface reactions are compared. . . . . 18

2.4 Maximum temperature and profiles of $CH_4$, $CO_2$, CO, and $H_2$ concentrations at point A. . . . . 20

2.5 Profiles of O, H, and OH concentrations at point A. . . . . 21

2.6 Maximum temperature and profiles of $CH_4$, $CO_2$, CO, and $H_2$ concentrations at point B. . . . . 22

2.7 Profiles of O, H, and OH concentrations at point B. . . . . 23

2.8 Maximum temperature and profiles of $CH_4$, $CO_2$, CO, and $H_2$ concentrations at point C. . . . . 24

2.9 Profiles of O, H, and OH concentrations at point C. . . . . 25

2.10 Maximum temperature versus strain rate for various equivalence ratio conditions with adiabatic surface. . . . . 28

2.11 Solid line: the ratio of the extinction strain rate in the lower branch to that in the upper branch in the presence of catalytic reaction. Dotted line: the ratio of the extinction strain rate in the lower branch to the pure homogeneous combustion without catalytic reaction. Curves are plotted as function of $\phi$ under the same conditions in Fig. 2.10. . . . . 30

2.12 Maximum temperature versus strain rate for $\phi = 0.8$ and various heat loss conditions. The conductivity $h$ has the unit of $\mathrm{W/m^2 - K}$. . . . . 31

2.13 Maximum temperature versus strain rate for various heat source conditions and $\phi = 0.8$. The unit for $\dot{q}$ is $\mathrm{W/m^2}$. . . . . 33

2.14 Mapping of catalytic combustion response for various $\phi$ and $k$. A typical temperature versus strain rate response behavior in each regime is represented by the insets: Regime I has two isolated branches; Regime II has connected two distinct branches; Regime III is a surface-dominant reaction with no significant gas-phase reaction. . . . . 35

3.1 Maximum temperature as a function of the equivalence ratio for various levels of nitrogen dilution for adiabatic surface. Lines without symbols: without surface reactions. Lines with symbols: with surface reactions. . . . 40

3.2 Lean extinction limits as a function of the nitrogen dilution for various surface thermal conditions, for S=277$\mathrm{s^{-1}}$. Lines without symbols: without surface reactions. Lines with symbols: with surface reactions. . . . . 42

3.3 Normalized maximum amplitude of temperature variation as a function of frequency for the flames subjected to oscillatory strain rates. Lines without symbols: without surface reactions. Lines with symbols: with surface reactions. . . . . 44

3.4 Unsteady flame temperature response to the equivalence ratio various frequencies. . . . . 49

3.5 Difference between the dynamic flammability extension of a flame with and without surface reaction ($\Delta\phi_s - \Delta\phi_g$), as a function of frequency, for various dilution and surface thermal conditions. . . . . 50

4.1 PIV image of flow velocity vector [5]. . . . . 53

4.2 Numerical and experimental flow axial velocity profile along nozzle center line with chemical reaction. . . . . 54

4.3 Numerical and experimental flow axial velocity profile along nozzle center line without chemical reaction. . . . . 55

4.4 $k_{eff}$ versus the stagnation plane temperature for various strain rate and equivalence ratio conditions, with a noncatalytic surface. . . . . 58
4.5 $k_{eff}$ versus the stagnation plane temperature for various strain rate and equivalence ratio conditions, with a catalytic surface. . . . . 59
4.6 Extinction stagnation surface temperature from numerical and experimental results for catalytic/noncatalytic surface condition. Two equations for $k_{cata}/k_{noncata}$ is applied in calculation. . . . . 61
4.7 Extinction equivalence ratio from numerical and experimental results for catalytic/noncatalytic surface condition. Two equations for $k_{cata}/k_{noncata}$ is applied in calculation. . . . . 62
4.8 Extinction stagnation surface temperature from numerical and experimental results for catalytic/noncatalytic surface condition. Same equation for $k_{cata}/k_{noncata}$ is applied in calculation. . . . . 63
4.9 Extinction equivalence ratio from numerical results for catalytic/noncatalytic surface condition. Average nozzle velocity 74.4 cm/s, adiabatic wall. . . . . 66
4.10 Extinction equivalence ratio from numerical results for catalytic/noncatalytic surface condition. Average nozzle velocity 74.4 cm/s, heat loss condition $h = k/\delta = 7.874W/m^2 - K$. . . . . 67
4.11 Extinction equivalence ratio from numerical results for catalytic/noncatalytic surface condition. Average nozzle velocity 138.6 cm/s, adiabatic wall. . . . 68
4.12 Extinction equivalence ratio from numerical results for catalytic/noncatalytic surface condition. Average nozzle velocity 138.6 cm/s, heat loss condition $h = k/\delta = 7.874W/m^2 - K$. . . . . 69

5.1 Schematic diagram of how Galilean transformation for velocity works. . . . 72
5.2 Flame shape change with heat loss in 2 mm channel, H2/air at $\phi = 0.5$. . . 73
5.3 Flame shape change with equivalence ratio in 2 mm channel, $h = 32e - 9W/m^2 - K$. . . . . 75
5.4 Flame shape with equivalence ratio in 0.7 mm channel, $h = 40e - 9W/m^2 - K$. . . . . 76
5.5 2 mm channel. . . . . 77
5.6 0.7 mm channel. . . . . 79
5.7 Extinction equivalence ratio with different wall heat loss and channel width. 80

# Abstract

As a fundamental study to understand characteristics in catalyst-assisted combustion, numerical simulations of two canonical models are performed.

For a stagnation-point flow combustor with a catalytic surface, parametric studies are conducted to investigate the effects of strain rate, equivalence ratio and heat loss on the combustion and extinction modes. The steady results showed that catalysis can largely extend the strain-induced extinction limit, while suppressing the gas phase reaction at lower strain rates. The temperature versus strain rate response curves exhibit multiple branches of stable solutions, implying a possibility of hysteresis behavior in a coupled homogeneous-heterogeneous reactor. In the lean extinction limit investigation, results show that the level of flammability extension by surface reaction depends strongly on the mixture dilution, such that the benefit of catalyst-assisted lean combustion can be fully realized only with a diluted system. These observations are explained by consideration of characteristic time scales calculated from the fuel consumption rate. The extinction response to an oscillatory strain rate also shows consistent behavior. Experimental validation was carried out to demonstrate simulation conclusions. It was found the substrate surface heat loss condition is a key factor to match simulation result with experimental results. Radiation and conductive heat loss through the surface in the experiment could be modeled as one effective heat loss coefficient, and that coefficient is relevant to both the flow rate (related with strain rate) and the surface temperature at that time. Thus an iteration process could be used to find the extinction condition for a fixed flow rate.

Parametric studies on heat loss, equivalence ratio and device dimension for micro-

channel flow configuration are conducted to research the combustion stability at near quenching conditions. A parallel DNS code supplemented by flame position capturing ability is applied. The results show the flame quenching condition is mainly affected by channel width and equivalence ratio at current parameter range. Channel wall heat loss shows influence on flame propagation speed but not on quenching conditions. Flame shape is affected by both equivalence ratio and heat loss.

This whole research is expected to provide insight into improving the overall combustion stability and efficiency of catalyst-assisted combustors.

# Chapter 1

# Introduction

With the recent advances in the fabrication technologies for micro electro-mechanical systems (MEMS), there is strong research interest in developing miniature power generation systems with a dimension ranging from a few centimeters to a fraction of a millimeter [6]. If such a devices can be developed and the target design specifications are met, the application areas of the micro-engines are countless; most notably the batteries for portable electronics, small-scale aerospace propulsion systems, and military applications, to name a few.

Among many alternative energy sources for the future, combustion still appears to be the most effective means for compact power generation devices in favor of its high energy density. Typical hydrocarbon fuel has a specific energy of 45 MJ/kg, while in comparison a high-performance battery has the energy density of about 1.2 MJ/kg [7]. Thus, the micro-combustor system only needs to be as efficient as 3% to compete against commercial batteries. Furthermore, if carefully operated, the product gases consisting mainly of $CO_2$ and water will have less adverse environmental impact compared to exhausted batteries. All these aspects show many great promises in the pursuit of micro-combustor research.

Thus far, a major effort in the micro-combustor design has been based on the concept of a miniature version of the macro-scale counterpart [1, 8, 9, 10, 11, 12, 13, 14]. Figure 1.1 shows some of such examples. In this case, the high temperature and high pressure product gases are used to rotate turbines, push pistons or other movable components to generate

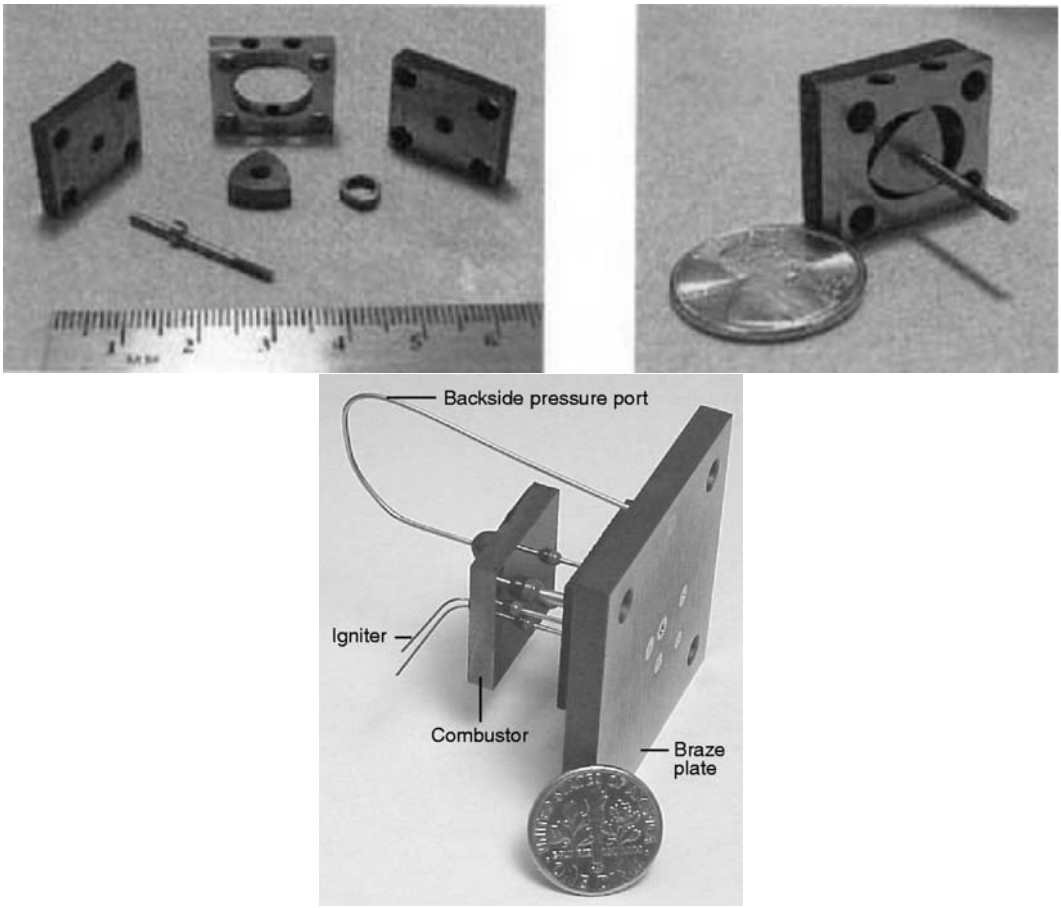


Figure 1.1: Examples of micro-combustor designed in model of macro-combustor, combustion chamber assemblied with turbine together [1, 2].

electric energy. Typical sizes of such devices are usually several centimeters and the fabrication involves complicated mechanical and electrical process. The anticipated efficiency is claimed to be as high as 40%-70%. However, the mechanical friction and wear of the high-speed moving parts remain a serious concern. An alternative approach is to use a simple geometric configuration such as cylindrical or rectangular combustion chamber and generate electric power through the use of thermoelectric, thermionic or thermophotovoltaic components [3, 4, 15, 16, 17]. As illustrated in Fig. 1.2, their simple configuration and the lack of moving components working at high temperature offer a design that is durable and easy to fabricate, although achieving high efficiency through the thermoelectric means can be a challenge.

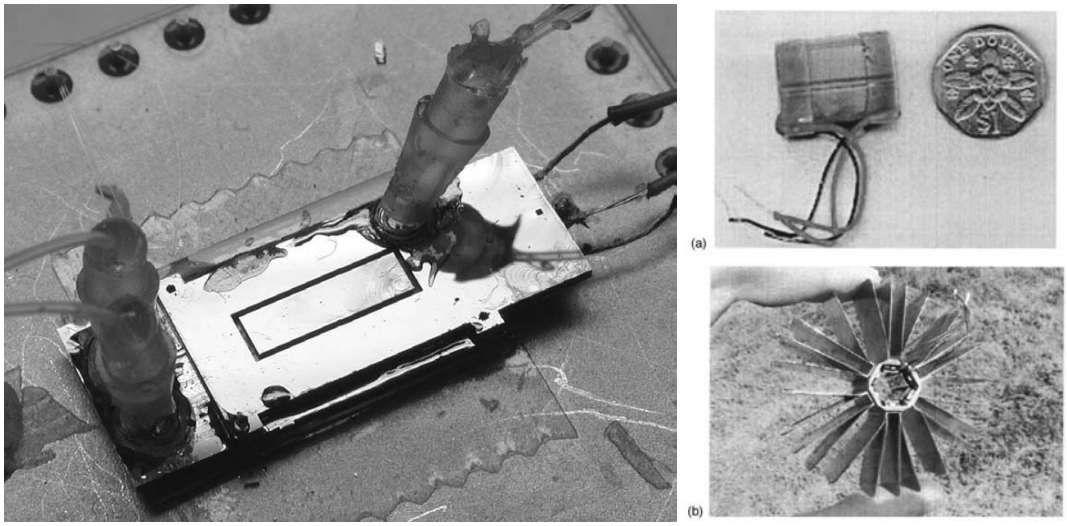


Figure 1.2: Examples of micro-combustor without moving part, left one collect combustion energy though thermionic emission [3], right one use thermophotovoltaic component: (a) without cooling fins, (b) with cooling fins [4].

In either approach, one of the major challenges in combustion aspects is to achieve stable chemical reaction in a device that suffers from a large amount of heat loss due to its high surface-to-volume ratio. It is well known that combustion cannot be sustained in a dimension smaller than the quenching distance due to the overwhelming heat loss compared to the heat generated by the flames. To overcome this difficulty, catalytic materials are used as a means to sustain and stabilize combustion in the presence of large surface area [13, 16]. In fact, catalytic technology have long been used in the automotive application to process post-combustion gases to reduce emissions. Catalytic combustion has also been used in gas turbines to achieve low-temperature stable combustion to reduce NOx [18, 19]. In the micro-combustor application, catalytic materials embedded on the reactor surface can extend the quenching limits so that stable combustion can be achieved under conditions that are otherwise nonflammable. Therefore, unlike the large-scale catalytic combustor, development of micro-combustors faces drastically different challenges in identifying optimal operating conditions and meeting design targets. For example, achieving self-sustained combustion to overcome the quenching distance may be more important than establishing

low-temperature and low-NOx combustion as would be the case in the gas turbine application. In a premixed combustion mode, increased viscous friction due to reduced dimension has also been found to be an additional source of combustion instability [20]. Therefore, it is of great interest to understand fundamental characteristics of the coupled effects of surface and gas-phase chemical reactions that are more relevant in the micro-combustor application.

The present research mainly focuses on micro-combustor without moving parts, in an anticipation that the simple configuration and continuous combustion behavior allow easy development of robust and portable combustor devices. In particular, a stagnation-point flow is used as a model problem in the present study. This configuration has not only been considered as an on-chip micro-combustor design [21], but it also serves as an excellent canonical configuration in which the coupling of surface and gas-phase combustion can be extensively investigated over a wide range of physical parameters, such as the equivalence ratio, flow strain rates, and heat loss to the surface. Extensive numerical calculations of steady and unsteady flame behavior will be performed using detailed reaction mechanisms [22] that have been validated against experimental measurements.

A number of asymptotic analysis have been performed for a stagnation-point flow configuration employing simple chemistry. An earlier study by Law *et al.* [23] showed that the catalytic extension of the extinction limit of a stretched premixed flame is possible when the Lewis number of the deficient reactant is less than unity. Margolis *et al.* [24] analyzed a similar system in the near-unity Lewis number limit considering both surface reaction and volumetric heat loss, and showed that catalytic reaction can significantly extend the extinction limits caused by flame stretch and heat loss. In addition, he found that multiple solution branches appear corresponding to different surface temperatures, suggesting that different solution branches may be expected depending on the boundary and initial conditions of the problem.

Many recent experimental and computational studies of catalytic reactions have primar-

ily focused on their ignition characteristics. Fernandes *et al.* [25] experimentally examined the auto-ignition behavior of $H_2/O_2$ mixtures over a platinum foil and demonstrated that the catalytic surface can extend the flammability limit on stagnation-point flow. On the other hand, it has also been found that the catalytic surface may inhibit gas phase reaction [26]. Veser *et al.* [27] experimentally obtained bifurcation diagrams to characterize the ignition behavior of hydrocarbons over platinum plate. While these studies have provided valuable information regarding the basic ignition characteristics, further work is needed to understand the ignition as well as extinction characteristics of catalytic combustion over a wide range of heat loss, mixture composition, and flow strain conditions that are relevant to the micro-combustor application. The present work will provide extensive simulation data to address many fundamental issues related to this subject.

Besides whole process of combustion with variable strain rate, micro-combustor's performance under near extinction condition due to low temperature is also a interesting issue. For micro-combustors, high combustion temperature is undesirable since it adversely affect the mechanical and chemical structures of the interior parts. This problem can be alleviated by achieving low-temperature combustion using lean reactant mixtures. Another benefit of lean combustion is lower pollutant emission such as NOx or soot. However, low temperature combustion is more difficult to achieve in micro-combustors because their high surface-to-volume ratio causes a large heat loss compare to macro-scale combustors. A feasible approach to overcome this difficulty is to employ surface reaction using a catalytic material to assist stable combustion. It is therefore of fundamental importance to assess the extent of flammability enhancement due to the surface reaction, especially under lean mixture conditions.

Flammability extension by catalytic reaction has been studied in various configurations. Park *et al.*[28] performed a numerical study of hydrogen/air stagnation-point flow model with a platinum catalyst, and showed that catalytic reaction can extend both lean and rich flammability limits. Seo *et al.* [29] experimentally investigated a channel flow combustor

with a palladium catalyst to determine the minimum surface temperature for sustained combustion. They reported an interesting observation that, when the liquefied natural gas-air ratio was 4.25%, the minimum preheat temperature at which the flame extincts was lower than the preheat temperature of surface extinction. When the fuel-air ratio was 3.86% or less, the preheat temperature for flame extinction was higher than that of surface extinction. These results suggest that successful application of catalyst-assisted micro-combustion depends on parametric conditions of the combustion systems.

Another issue of fundamental interest is the effect of unsteadiness. Due to the small dimension, a micro-combustor is subject to larger variability in operating conditions because there are large uncertainties and technical difficulties in maintaining the constant inlet parameter conditions such as the flow rate, composition, and surface heat loss in small scale devices. It has also been understood that flames near extinction conditions are in general more sensitive to external perturbations [30], which can sometimes lead to combustion instability. Therefore, the flammability extension by catalytic reactions must be carefully examined under unsteady conditions. A number of studies exist on the response of strained flames to unsteady strain rate [30, 31, 32, 33, 34, 35] and composition fluctuations [36, 37]. In this study, these issues are investigated in a system with homogeneous/heterogeneous reactions. In particular, the concept of the dynamic flammability limit [37] and its extension due to catalytic reactions are explored.

Therefore, there is motivation to conduct numerical simulation to examine the effects of mixture dilution and surface thermal conditions on the lean extinction limit for a steady system. Subsequently, flame behavior in response to unsteady strain rate and equivalence ratio is investigated in the context of the flammability extension by catalytic reaction.

Though catalytic reaction shows a lot of benefits in simulation study such as extension of extinction strain rate, lower extinction equivalence ratio and temperature in diluted system, enhanced environmental disturbance resistance, corresponding experimental study is need to demonstrate those conclusion. To validate the findings from the modeling studies,

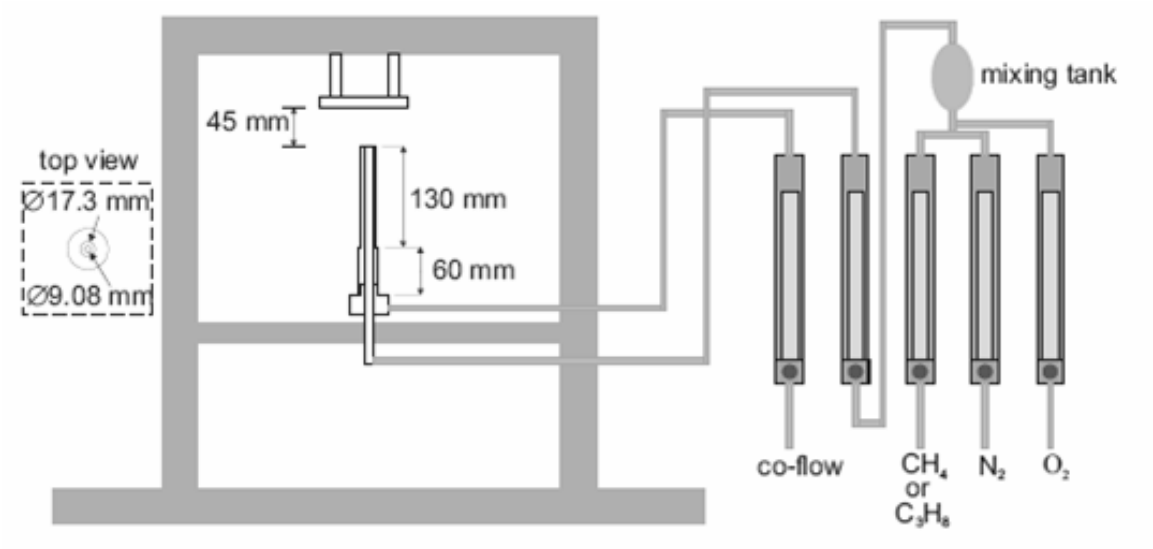


Figure 1.3: Experimental setup

experimental studies [5] have been conducted recently by setting up a compact stagnation-point flow combustor as shown in Fig. 1.3. The silicon wafer substrate (stagnation plate) was coated with platinum to assess the catalytic effects. Experimental measurements were performed under similar conditions of mixture composition and strain rate. In contrast to the computational predictions, however, the measured surface temperature at extinction was consistently lower by at least several hundreds K, even with a significant amount of external heating on the substrate. Furthermore, the difference in the lean flammability limit between the catalytic and non-catalytic surface conditions was found to be insignificant. After careful examinations, the main cause for the discrepancies was the larger amount of heat loss associated in the experimental apparatus.

To reconcile the discrepancies between modeling and experimental studies, we thus attempt to reproduce the experimental conditions with a better estimate of the heat loss effect. This is not a trivial task, because heat transfer between the hot catalytic surface and the surrounding combustion gases involve all heat transfer modes - radiation, conduction and convection. Conductive and convective heat transfer effects between the surface and surrounding gases can be combined in terms of the effective heat transfer coefficient

because both are linearly proportional to the temperature difference. On the other hand, radiative heat loss is harder to estimate due to the lack of knowledge on the emissivity of the catalytic surface that also depend on temperature. Moreover, there are additional differences between the 1-D modeling and the actual experimental system which may actually reveal the effect of heat transfer in the transverse direction. The radial variation in the axial velocity at the nozzle exit due to the presence of boundary layers further contributes to the discrepancies. Therefore, in this study we attempt to revise the computational model to account for these additional effects associated with the experimental device, thereby achieving improved agreement between the modeling and experiment. Once the cross-validation is completed, then the numerical model can explore combustion characteristics in the parametric ranges that are beyond the capability of the current experimental setup.

Besides stagnation-point flow model, another canonical geometry to investigate micro-combustor is channel flow. The choice of the configuration is based on the practical relevance of some recent developments on micro-combustor. For example, the famous ”Swiss Roll” micro-combustor design [38] could be distinguished as a combination of stagnation-point flow and channel flow. Besides, as well as stagnation-point flow model was configured to analyze effect of strain rate, channel flow could be utilized to investigate effect of diffusion if fuel and oxidizer are introduced separately.

Previous investigation for channel flow are mostly concentrated on one-dimensional geometry, one step chemical mechanism or simplified mechanism. Limited research among them are for detailed chemistry and multi-dimensional configuration due to huge computer resource demand. Michaelis and Rogg [39] used a finite-element method to investigate a steadily propagating 2-D flame in channel with detailed chemical mechanism and refined mesh near flame. Galilean transformation in velocity is applied. Three kinds of boundary condition: non-slip adiabatic wall, non-slip isothermal wall, slip adiabatic wall are tested. Flame shape change was investigated without quantitive thermal boundary condition. Kurdyumov *et al.* [40] investigated the critical flashback condition of premixed flame

experimentally (propane/air) and theoretically (asymptotic) mainly focused on adiabatic wall and isothermal wall condition. Both experimental and numerical results shows the limit of flashback varies strongly with heat transfer to the wall. Pizza *et al.* [41] investigated the stabilization and dynamics of lean premixed hydrogen/air atmospheric-pressure flames in planar micro-channels of prescribed wall temperature with respect to the inflow velocity and channel height (0.3 to 1.0 mm) using direct numerical simulation with detailed chemistry and transport. Rich dynamics starting from periodic ignition and extinction of the flame and further transitioning to symmetric V-shaped flames, asymmetric flames, oscillating and pulsating flames, and finally again to asymmetric flames are observed as the inlet velocity is increased.

None of above research involved parametric study of channel size, equivalence ratio or wall heat loss for flame propagation or quenching behavior as what is done in this chapter. This research is a extension of micro-combustor performance investigation as in previous chapters but for a different micro-channel configuration. The whole research including both models are expected to provide direction into improving the combustion stability and efficiency of micro-combustors.

In the following, the modeling formulation and the associated numerical method will be described at beginning of each chapter. Detailed study method, observation and conclusions will be discussed within each chapter. In chapter 2, the steady combustion characteristics of methane over a platinum plate with continuously variable strain rate will be studied. Chapter 3 is system response to diluted/lean reactant and vibrating input. Chapter 4 is about experimental validation and potential to improve experimental results. Chapter 5 is for parallel DNS code computation on micro-channel model for different channel size, equivalence ratio and channel wall heat loss.

# Chapter 2

# Extinction Characteristics of Catalyst-Assisted Combustion with Variable Strain Rate

As a classical configuration in combustion and fluid mechanics research, stagnation-point flow model is applied in this chapter to investigate combustion stability and extinction criteria. Combustion process and extinction due to large strain rate with combination of different equivalence ratio and stagnation plane heat loss/heat supply are studied here. In the last, a plot indicates stagnation-point flow micro-combustor performance criteria under different combination of wall heat condition and equivalence ratio is presented. Through out this chapter, input parameters such as inlet flow rate, equivalence ratio, environmental temperature, nozzle distance and heat loss coefficient are all constant that conduce to steady response of the whole system.

## 2.1 Model Configuration

Figure 2.1 shows a schematic of the model. A combustible gas mixture is blown from the top of the catalytic surface, forming a stagnation-point flow configuration. This geometry represents a canonical problem of heterogeneous/homogeneous combustion subjected to a strained flow field, which introduces an additional variable that governs the quenching and flammability limit.

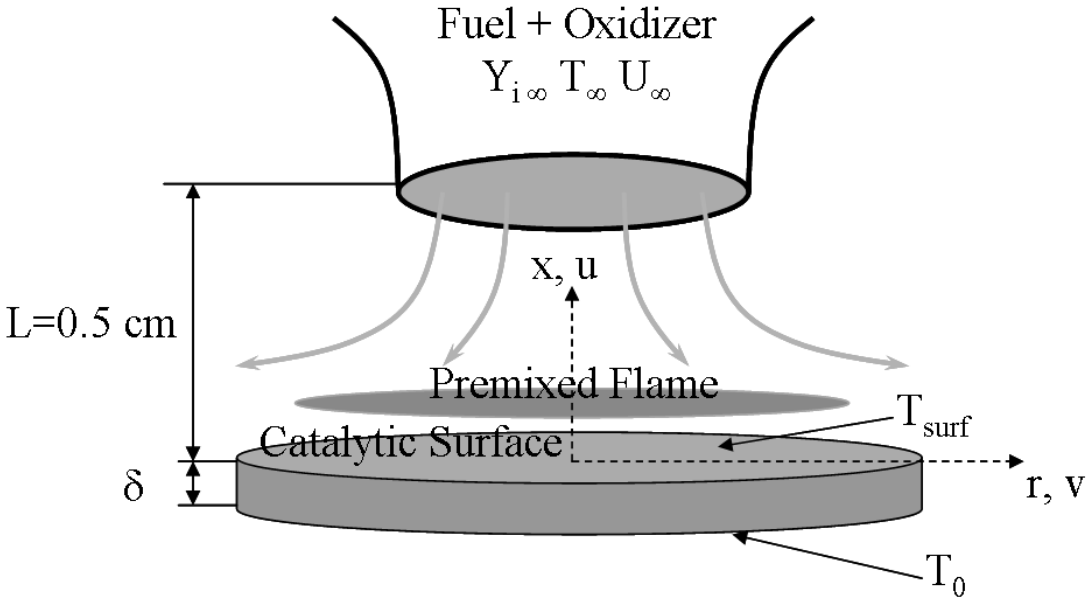


Figure 2.1: Schematic of the stagnation-point flow configuration

### 2.1.1 Formulation

The governing equations to describe the steady state combustion system are derived based on the solution similarity along the centerline, such that all the solution variables are assumed to be a function of $x$ only. The conservation equations for mass, axial momentum, radial momentum, energy, gas and surface species are written as:

$$\frac{\partial}{\partial x}(\rho u) + 2\rho V = 0, \tag{2.1}$$

$$\rho u\frac{\partial u}{\partial x} + \frac{\partial p}{\partial x} - 2\mu\frac{\partial V}{\partial x} - \frac{4}{3}\frac{\partial}{\partial x}\left(\mu\frac{\partial u}{\partial x}\right) + \frac{4}{3}\frac{\partial}{\partial x}(\mu V) = 0, \tag{2.2}$$

$$\rho u\frac{\partial V}{\partial x} + \rho V^2 - \frac{\partial}{\partial x}\left(\mu\frac{\partial V}{\partial x}\right) + \Lambda = 0, \quad \Lambda = \frac{1}{r}\frac{\partial p}{\partial r}, \tag{2.3}$$

$$\rho c_p u \frac{\partial T}{\partial x} - \frac{\partial}{\partial x}\left(\lambda \frac{\partial T}{\partial x}\right) - u\frac{\partial p}{\partial x} + \rho(\sum_k c_p Y_k V_k)\frac{\partial T}{\partial x} + \sum_k h_k W_k \omega_k = 0, \tag{2.4}$$

$$\rho u \frac{\partial Y_k}{\partial x} + \frac{\partial}{\partial x}\left(\rho Y_k V_k\right) - W_k \omega_k = 0, \quad k = 1, \cdots, K_g, \tag{2.5}$$

where $V = v/r$, $V_k$ is the diffusion velocity of species $k$ in the $x$-direction, $\mu$ is the molecular viscosity, $\lambda$ is the thermal conductivity, $c_p$ is the mixture specific heat, $W_k$ is the molecular weight of species $k$, $h_k$ is the enthalpy of formation, and $\omega_k$ is the molar reaction rate as defined in Chemkin [42]. $K_g$ and $K_s$ are the total number of gas-phase and surface species, respectively.

The above equations are subjected to the following boundary conditions. On the mixture inlet boundary, the variables are fixed as constants:

$$x = L, \quad u = U_\infty, \quad v = 0, \quad T = T_\infty, \quad p = p_0, \quad Y_k = Y_{k\infty}. \tag{2.6}$$

The surface boundary conditions are more complex. When the surface is inert, there is no surface reaction and the no-slip velocity boundary condition is applied. When the surface is reactive, the coupling between the gas phase and the surface is established through a mass-flux matching condition for each of the gas-phase species as

$$\rho Y_k (u_{st} + V_k) = \dot{\omega}_k W_k, \tag{2.7}$$

where the effect of surface chemistry appears in the Stefan velocity

$$u_{st} = (1/\rho)\sum \dot{s}_k W_k. \tag{2.8}$$

Surface species are computed by

$$\frac{\dot{s}_k}{\Gamma_n} = 0, \quad k = 1, \cdots, K_s. \tag{2.9}$$

Where $\Gamma_n$ is the surface site density for the site type $n$ and $\dot{s}_k$ is the generation rate of the $k$-th surface species. For both reacting and nonreacting surfaces, the no-slip condition for the radial velocity ($v = 0$) is applied [43]. Surface temperature is also computed from the energy conservation equation:

$$\lambda \frac{\partial T}{\partial x} - \sum_{k=1}^{K_g} \rho Y_k (V_k + u) h_k = \sum_{k=1}^{K_s} \dot{s}_k W_k h_k + \dot{q}, \tag{2.10}$$

where $\dot{q}$ is the energy source in the surface itself, so as to represent the effects such as electrical heating or conductive heat loss through the substrate.

Figure 2.2 shows the staggered grid system and the boundary conditions for individual equations used in the calculation. Similar to Raja *et al.* [43], the grid system is defined such that only the axial velocities are represented on the cell surfaces and all other variables are defined in the cell center. Therefore, the axial velocity at the surface (center of the first control volume) is $u_{st}$. To improve the stability of the system, an artificial dissipation term $\alpha \frac{\Delta x}{2u_r} \left( \frac{\partial^2 p}{\partial x^2} \right)$ is added to the continuity equation [44], where a proper scaling of the term ensures stability with little effect on the solution fidelity.

The computation is performed using a revised version of the OPUS package [45]. To simulate a reacting stagnation-point flow, the code is modified into the configuration in which a premixed fuel and oxidizer stream is supplied from $x = L$, and the other boundary ($x = 0$) is set as a solid surface. The surface reactions on the solid surface and their interface with gas phase reaction are fully incorporated [46]. Full steady and unsteady solution capabilities are implemented based on Twopnt[47] and DASPK[48], although only the steady solutions are presented in this chapter. The code is interfaced with Chemkin [42] and Transport [49] packages for computing detailed reaction rates and transport properties. To

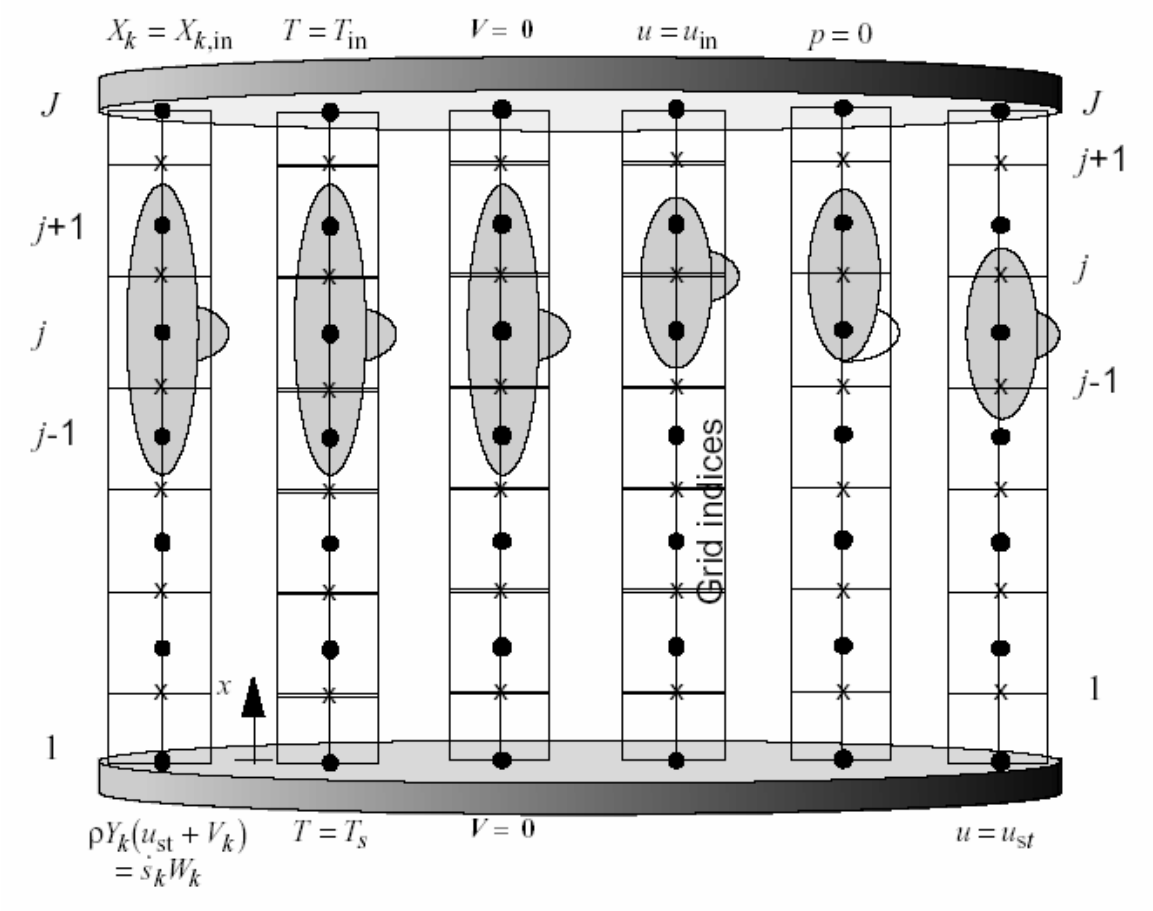


Figure 2.2: Finite-volume, spacial-difference stencil for the stagnation flow equations

generate the continuous steady combustion response curves around the ignition/extinction turning points, an arc-length continuation method [50] is employed in the code.

### 2.1.2 Arc-length Continuation

The system equations shown in the previous section can be represented as:

$$F(u; \lambda) = 0, \tag{2.11}$$

where $u$ is the solution vector with size $n$ and $\lambda$ is a parameter. The nonlinear system of equations is solved by the Newton iteration technique using the Twopnt subroutine [47]. However, the Newton method fails near the turning point because of the singular Jacobian

matrix $F_u = \dfrac{\partial F}{\partial u}$ if the method is applied directly to equation system (2.11).

In order to obtain the solution around the turning points, a new arc-length parameter $s$ is introduced such that

$$F(u(s); \lambda(s)) = 0. \tag{2.12}$$

Given a solution of $u_0$ and $\lambda_0$ at a previous continuation step, the continuation equation used to augment the equation (2.12) is

$$N = \frac{1}{n}\|u - u_0\|_2 + (\lambda - \lambda_0)^2 - (s - s_0)^2 = 0. \tag{2.13}$$

Taking the derivative of equation (2.12, 2.13) with respect to $s$ gives

$$F_u \dot{u} + F_\lambda \dot{\lambda} = 0, \tag{2.14}$$

$$\frac{1}{n}(u^T - {u_0}^T)\dot{u} + (\lambda - \lambda_0)\dot{\lambda} - (s - s_0) = 0 \tag{2.15}$$

where $\dot{u} = u_s$, $\dot{\lambda} = \lambda_s$. An Euler method is used for prediction of the solution for each new continuation step

$$u = u_0 + \dot{u}\Delta s,\ \lambda = \lambda_0 + \dot{\lambda}\Delta s, \tag{2.16}$$

and $\dot{u}$, $\dot{\lambda}$ are determined by solving the system of equations

$$\begin{bmatrix} F_u & F_\lambda \\ \dfrac{1}{n}(u^T - {u_0}^T) & \lambda - \lambda_0 \end{bmatrix} \begin{bmatrix} \dot{u} \\ \dot{\lambda} \end{bmatrix} = \begin{bmatrix} 0 \\ s - s_0 \end{bmatrix} \tag{2.17}$$

Newton's method is used as a corrector to obtain the solution $(u, \lambda)$ according to

$$\begin{bmatrix} F_u & F_\lambda \\ 2\dfrac{1}{n}(u^T - {u_0}^T) & 2(\lambda - \lambda_0) \end{bmatrix} \begin{bmatrix} \Delta u \\ \Delta\lambda \end{bmatrix} = - \begin{bmatrix} F \\ N \end{bmatrix} \tag{2.18}$$

It can be proved that even $F_u$ is singular, the left hand side matrix in the above two equations

will not be singular if $N$ and $\lambda$ are chosen properly [50].

### 2.1.3 Computational Conditions

To investigate the effects of the catalytic surface on the extinction limits, we first consider the strain-induced extinction characteristics for various conditions for the heat loss and mixture composition. The strain rate can be controlled by varying the inflow velocity at the nozzle. For the stagnation-flow configuration, the effective strain rate is usually defined as the radial velocity gradient, $\frac{1}{r}\frac{\partial}{\partial r}(vr)$, at the flame position [51]. In the present study, however, the primary reaction zone is often pushed to the wall with catalytic reaction, where the velocity gradient vanishes. Therefore, the strain rate is represented by the nominal velocity gradient based on the nozzle exit velocity and the system dimension, $S = \frac{U_\infty}{2L}$. Although this may not be the only way, it serves as a reasonable measure to characterize the flow time scale.

As for the boundary conditions, a mixture of methane and air at 300K is supplied through the nozzle located at $x$ = 0.5cm towards the catalytic surface located at $x$ = 0. A platinum plate is considered as a catalytic surface. The GRI-Mech 3.0 [42] is used for the detailed gas phase mechanism and thermal data, and the surface reaction mechanism for the methane-air system developed by Deutschmann [22] is adopted.

The surface temperature is determined by the heat generated from chemical reactions and heat loss to the environment through surface conduction. The thickness of substrate and the conductivity coefficient are denoted as $\delta$ and $k$, and the heat loss through the surface is described by the form $\dot{q} = h\,(T_{\text{surf}} - T_0)$, where $h = \frac{k}{\delta}$ is the effective heat transfer coefficient. For simplicity, different heat loss conditions are represented by varying $h$ only, while fixing the back substrate temperature, $T_0$, at 300K. Since the back substrate temperature in an actual combustor is expected to be higher than 300K, this implies that the $h$ used may be smaller than a realistic material property and the substrate thickness may result. For example, typical values of $h$ used in the parametric study are in the order of 10 W/m$^2$-

K. Considering a substrate thickness of 5 mm, the corresponding $k = 5 \times 10^{-2}$ W/m-K may appear too small for a practical solid material. However, this condition can also be interpreted as a convective heat loss with a heat transfer coefficient of 10 W/m$^2$-K for an ambient temperature at 300 K, since the heat resistance of the substrate is negligible compared to that between the plate and the surroundings. Therefore, the adopted heat loss parameter values indeed represent heat loss conditions for a real device.

## 2.2 Results and Discussion

### 2.2.1 Flame temperature and extinction behavior

The first part of the computational experiments is to characterize the steady combustion and extinction behavior as a function of the imposed strain rate. Using the arc-length continuation technique, a series of steady solutions can be obtained for various parametric conditions of the equivalence ratio and heat loss. Fig. 2.3 shows the maximum temperature and its corresponding location versus strain rate for $\phi = 0.8$. Since an adiabatic surface would always result in the maximum temperature attached to the surface, a finite amount of heat loss with $h = 8$ W/m$^2$-K is added to ensure non-trivial solutions. The results with and without considering the surface reactions are compared.

One of the main issues is to identify various combustion modes arising from the coupled effects of gas-phase and surface reactions. First, consider the pure gas-phase combustion behavior shown in Fig. 2.3 as a baseline case. As expected, we find a typical flame response, in that the flame temperature decreases as the strain rate increases until a turning point at which the flame extinction occurs. The corresponding flame location is also seen to approach the surface during the increase in the strain rate. Nevertheless, the maximum temperature location of the gas-phase reaction zone remains detached up to the extinction point due to the heat loss to the surface. This is consistent with previous theoretical prediction for a mixture with the effective Lewis number near unity [52].

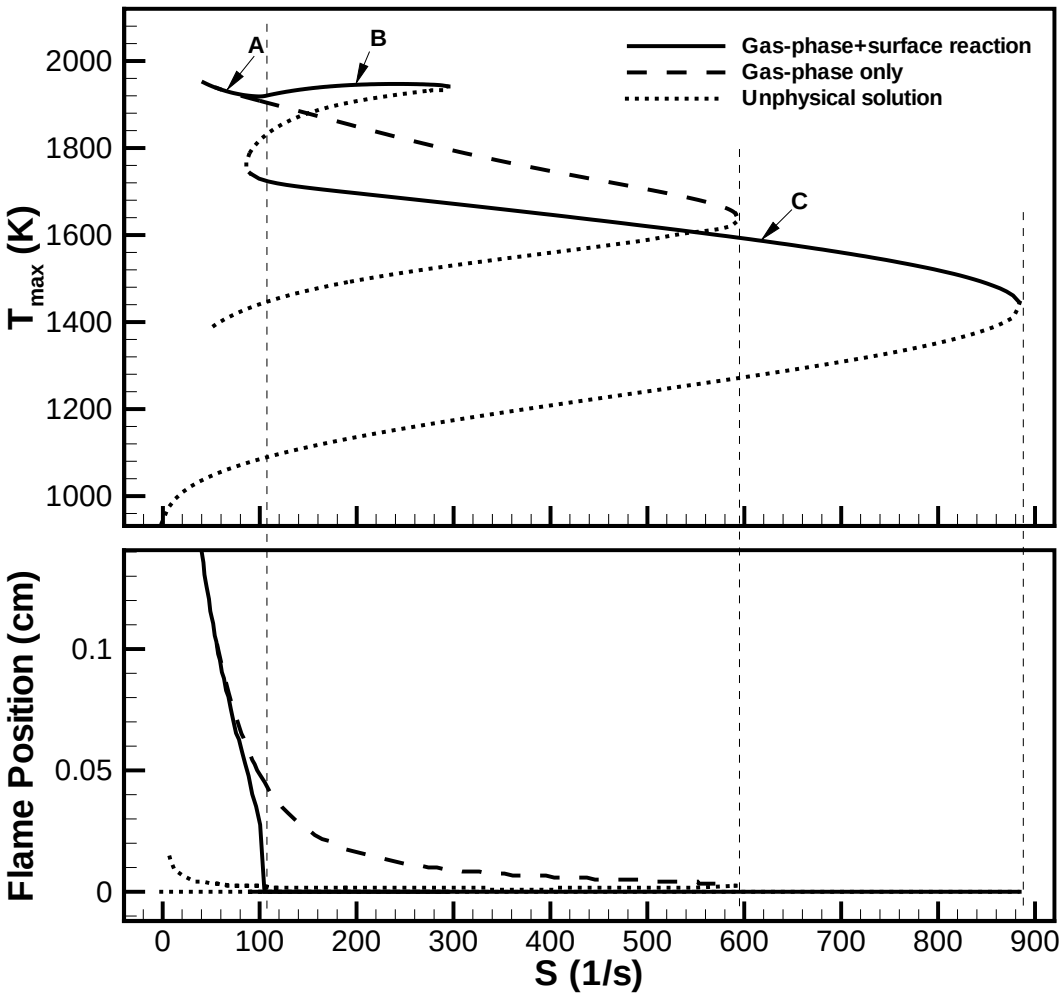


Figure 2.3: Maximum temperature and its location versus the nominal strain rate for $\phi = 0.8$, $h = 8$W/m$^2$-K. The cases with and without surface reactions are compared.

In the presence of surface reaction, however, this behavior is significantly modified. As the strain rate is increased, the gas-phase flame approaches the surface more rapidly and becomes attached (at $S \approx 100$ s$^{-1}$). One suggested explanation is that the catalytic surface reaction becomes more active by attracting the radicals generated in the gas-phase flame, thereby scavenging the radicals that are needed for the homogeneous reaction [53]. A more recent study interpreted this behavior as the catalytic production of $H_2O$ promoting the termination reaction, $H+O_2+M \rightarrow HO_2+M$, and the depletion of reactants near the surface [54]. As the strain rate is further increased, a turning point is reached and the system bifurcates to another stable combustion branch at lower temperatures. This second stable combustion branch, which is dominated by the surface reaction, is then eventually extinguished at a higher strain rate beyond which no stable combustion can exist. Comparing the extinction strain rates for the cases with and without surface reaction, it is readily seen that the catalytic surface reaction can substantially extend the range of stable combustion. This result also suggests that there can be a hysteresis effect that leads to a duality of the stable combustion modes (in the range of $S = 100 - 300$ s$^{-1}$).

The multiple solution branches shown in Fig. 2.3 suggest that catalyst-assisted combustion features three distinct combustion modes: detached gas-phase flames, attached combustion with intense gas-phase burning, and attached heterogeneous combustion. Representative points for these three modes are respectively denoted as symbols A-C in the figure, and the detailed major and minor species profiles are shown in Figs. 2.4 through 2.8. It is clearly seen that point A (Figs. 2.4 and 2.5) represents a detached gas-phase flame with radical species diffusing to the surface, point C (Figs. 2.8 and 2.9) indicates surface-dominant reactions with all the radical and product species emanating from the surface. Substantially reduced peak values of CO and $H_2$ concentrations for point C further suggest that the fundamental combustion mode is different from that of a gas-phase flame. In comparison, point B (Figs. 2.6 and 2.7) shows a structure in between A and C in that the maximum temperature is attached to the surface, yet the peak intermediate species con-

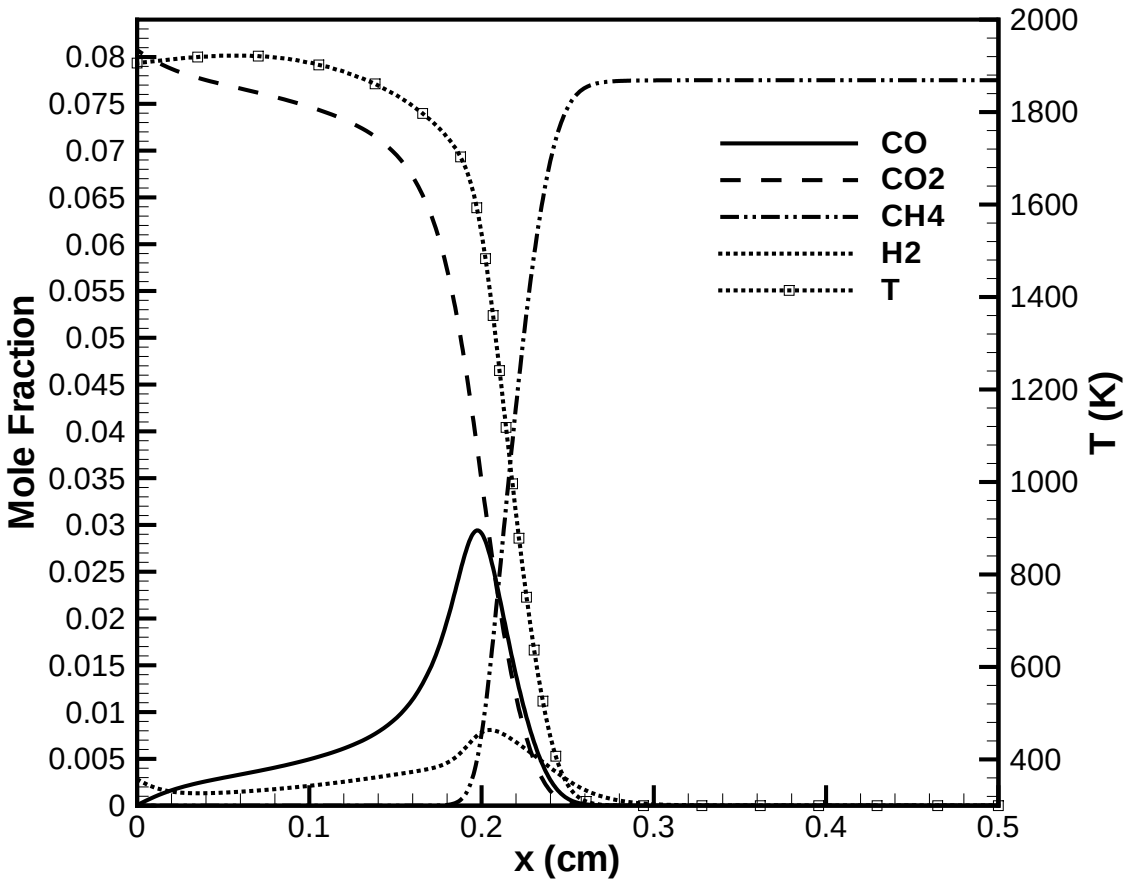


Figure 2.4: Maximum temperature and profiles of $CH_4$, $CO_2$, CO, and $H_2$ concentrations at point A.

centrations are detached into the gas-phase medium. Therefore, the upper-branch solutions represented by point B are characterized as an attached combustion mode with strong presence of gas-phase reactions. As a result, the maximum temperature (which occurs at the surface) in this branch increases with strain rate, because the reduced residence time in the gas-phase reaction zone allows increased leakage of intermediate combustible gases toward the catalytic surface, which has a sufficiently faster reaction time to complete combustion.

Strain-induced extinction is characterized as the condition at which the characteristic flow residence time becomes shorter than the characteristic chemical reaction time. There-

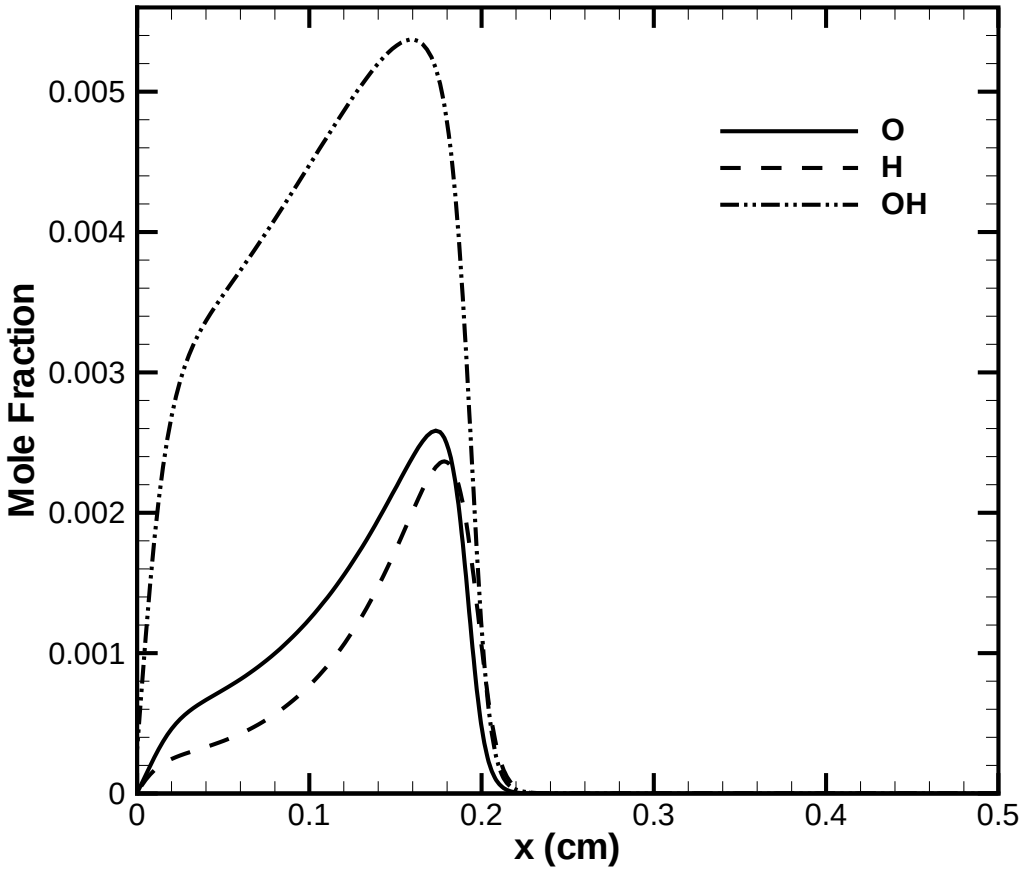


Figure 2.5: Profiles of O, H, and OH concentrations at point A.

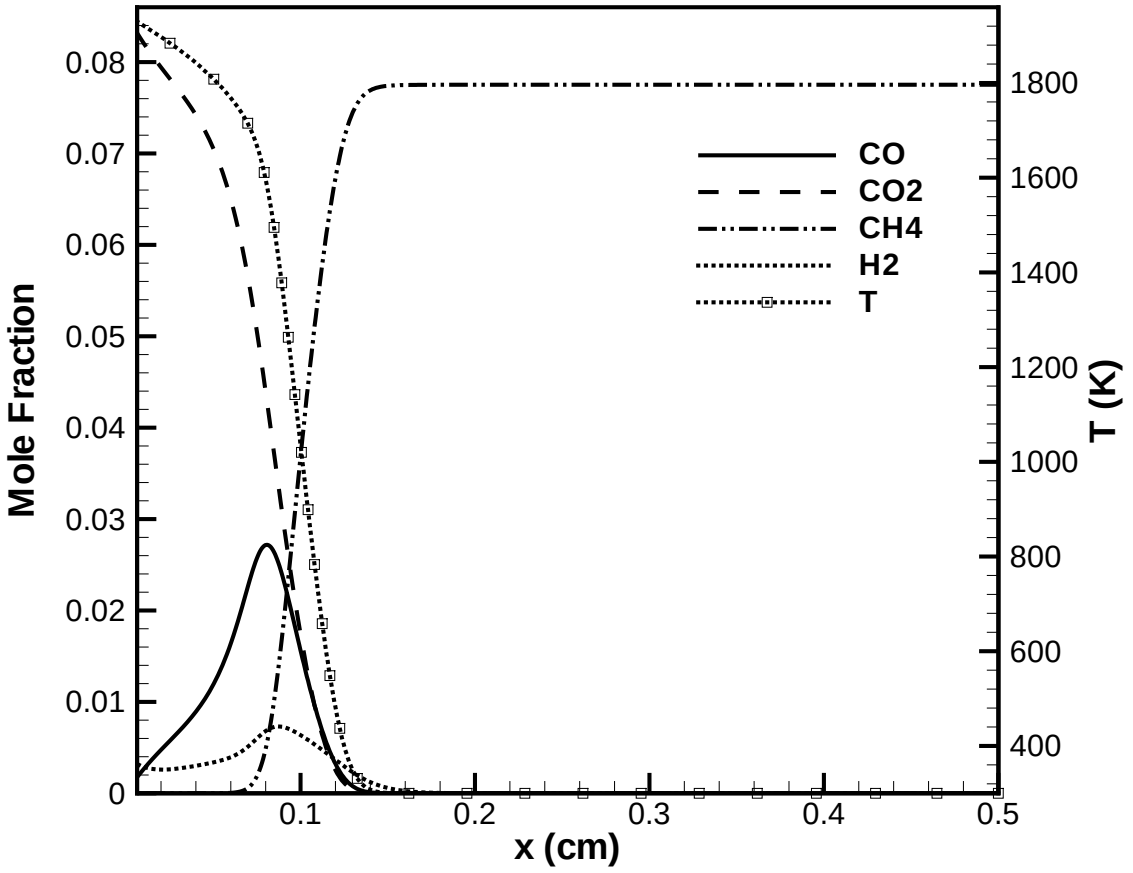


Figure 2.6: Maximum temperature and profiles of $CH_4$, $CO_2$, CO, and $H_2$ concentrations at point B.

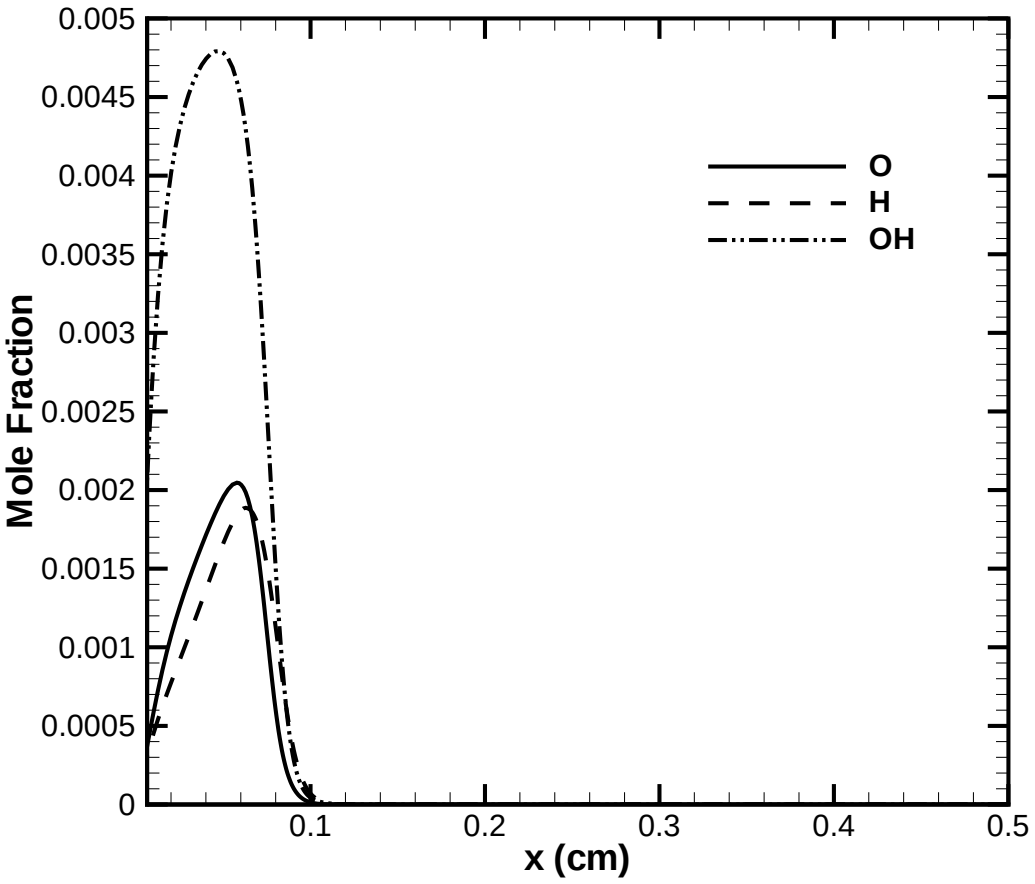


Figure 2.7: Profiles of O, H, and OH concentrations at point B.

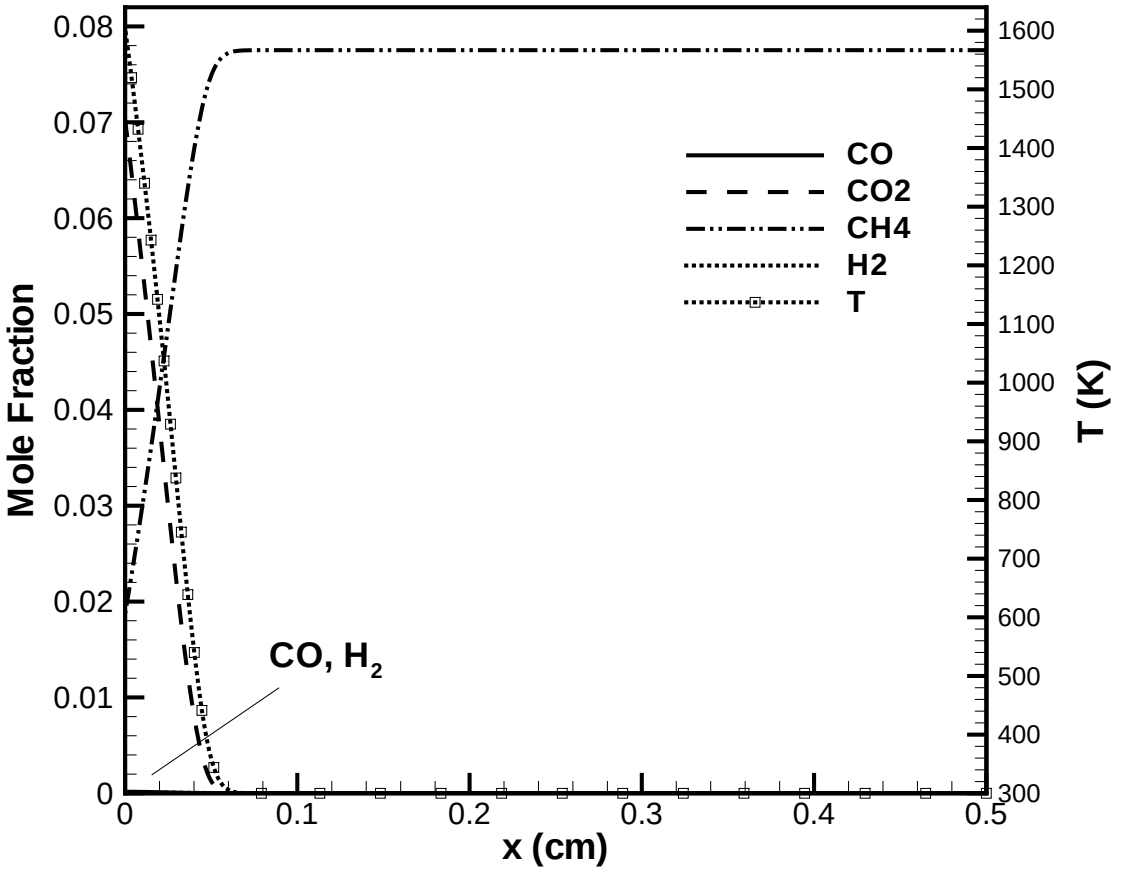


Figure 2.8: Maximum temperature and profiles of $CH_4$, $CO_2$, CO, and $H_2$ concentrations at point C.

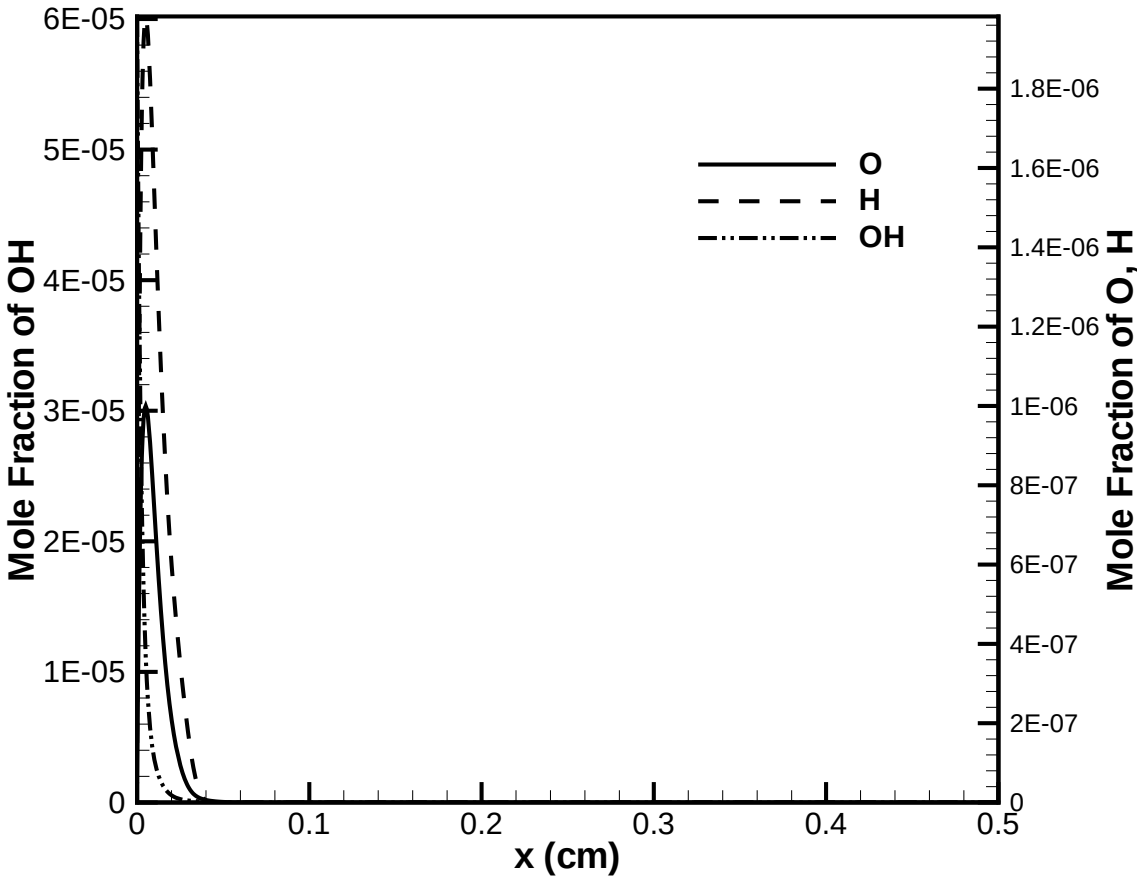


Figure 2.9: Profiles of O, H, and OH concentrations at point C.

fore, the fact that the catalytic reaction can sustain combustion at higher strain rates suggests that the characteristic time scale for the surface reactions is shorter than that for the gas-phase reactions. To confirm this argument, characteristic time scales for the gas-phase ($\tau_g$) and surface ($\tau_s$) reactions for the present system are defined based on the reaction rate of methane as

$$\tau_g = \frac{X_{\mathrm{CH_4}}}{\dot{\omega}_{\mathrm{CH_4}}} \frac{p}{R^0 T}, \tag{2.19}$$

$$\tau_s = \frac{X_{\mathrm{CH_4}} \Gamma}{\dot{\omega}_{\mathrm{CH_4}}}, \tag{2.20}$$

where the units are in seconds, $X_{CH_4}$ is mole fraction of methane at the nozzle inlet, $R^0$ is the universal gas constant, and $\Gamma$ is site density of surface species. For these quantities, $\dot{\omega}_{CH_4}$ for the surface reactions is determined at the catalytic surface, while for the gas-phase reactions the spatial maximum value of $\dot{\omega}_{CH_4}$ is used. Note that $\dot{\omega}_{CH_4}$ in Eqs. 2.19 and 2.20 have different units [46]. The characteristic times are evaluated at a fixed strain rate of $S = 179\mathrm{s}^{-1}$ for the conditions shown in Fig. 2.3. The results are found to be $\tau_g = 1.508 \times 10^{-4}$s and $\tau_s = 1.090 \times 10^{-5}$s, clearly demonstrating that the surface reaction is faster than gas-phase reaction as predicted. It is interesting to find that the upper branch solution (point B in Fig. 2.3) shows that $\tau = 1.602 \times 10^{-4}$s, further confirming that the reaction at this condition is dominated by the gas-phase chemistry even if the reaction appears to be attached to the surface. It is noted that consistent results in the characteristic times are found for different choices of the strain rate.

Another measure to characterize the reactivity and its sensitivity is the effective activation energy. Although detailed chemical mechanism is considered in this study, it is useful to identify such a quantity as a means to describe the phenomena based on a simple chemistry model. Considering the Arrhenius rate expression $\dot{\omega}_{\mathrm{CH_4}} \sim \exp(-E/RT)$, the effective activation temperature based on the methane consumption rate is determined as

$$T_a = \frac{E}{R} = -\frac{d \ln \dot{\omega}_{\mathrm{CH_4}}}{d(1/T)}. \tag{2.21}$$

All the values are measured at the location of maximum $\dot{\omega}$ at the fixed strain rate condition at $S = 179\text{s}^{-1}$. The temperature sensitivity is computed numerically by obtaining steady solutions with different levels of nitrogen dilution. The effective activation temperature is found to be 19,774K and 11,227K for the pure gas-phase and surface reactions, respectively, yielding the ratio of $\nu = 0.56$, which is similar to the suggested value in Ref. [24]. On the other hand, the effective activation temperature near point B in Fig. 2.3, in the presence of both gas-phase and surface reactions, is found to be much larger at 28,342K. While it is difficult to identify exactly which reactions are responsible for causing the high activation temperature, such an enhanced temperature sensitivity in a coupled gas-phase and surface reaction system should be noted.

### 2.2.2 Effects of equivalence ratio

The mixture equivalence ratio is an important parameter that determines the performance and the overall characteristics of the combustion system. It is of interest to examine how the behavior shown in Fig. 2.3 is modified with different mixture conditions. Fig. 2.10 shows the maximum temperature as a function of strain rate for different equivalence ratios. An adiabatic wall condition is used in these calculations. Due to the absence of the heat loss, the maximum temperature is always at the surface such that the detached combustion mode (as observed in the upper branch in Fig. 2.3) is hardly seen.

The most notable observation from Fig. 2.10 is that, as the equivalence ratio increases, the enhancement in the extinction strain rate is substantially larger compared to that obtained in the gas-phase flames. Approximately an order of magnitude increase in the extinction strain rate is observed for an increment in the equivalence ratio by 0.2. In a rich condition at $\phi = 1.4$, the extinction strain rate was beyond the range that the code could handle. Clearly, the catalytic reaction favors richer conditions for robust combustion, which contrasts typical gas-phase combustion behavior. On the other hand, the extinction limit extension on surface branch is not so obvious for equivalence ratios less than 0.6, suggesting

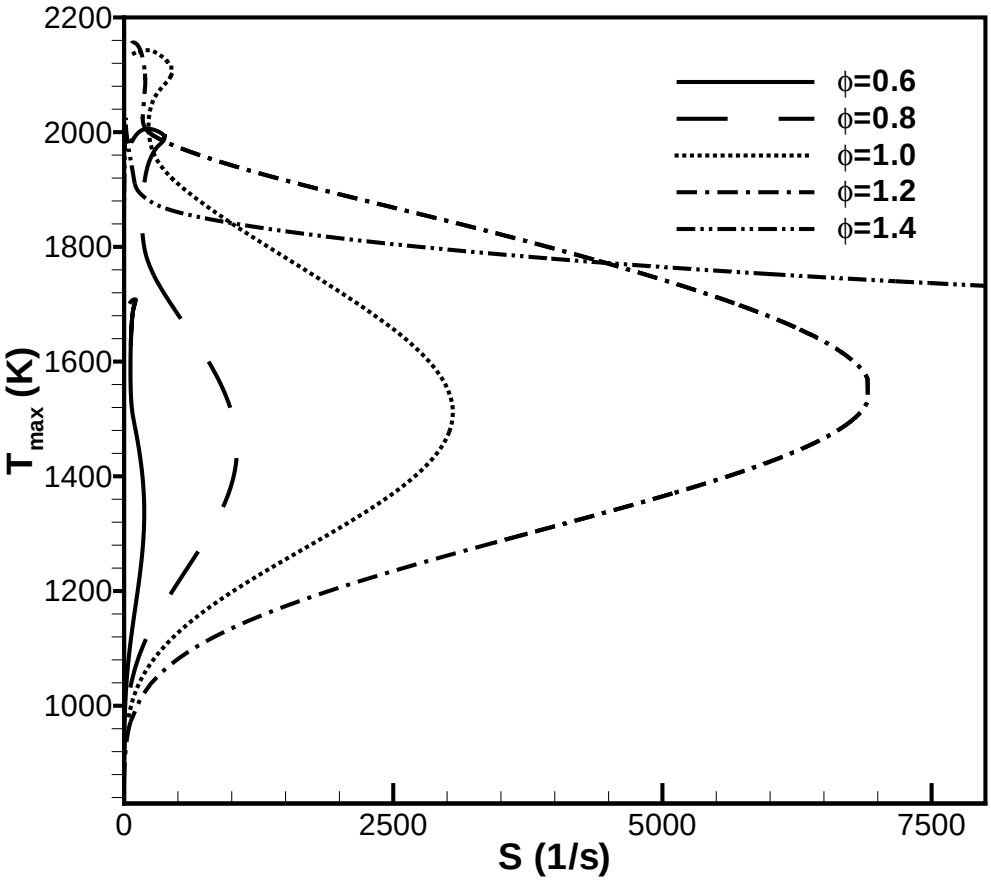


Figure 2.10: Maximum temperature versus strain rate for various equivalence ratio conditions with adiabatic surface.

that catalytic reaction does not significantly help extend the lean flammability limit.

To elaborate on this observation, the solid line in Fig. 2.11 shows the ratio between the extinction strain rate of the lower branch (surface dominant) and upper branch (gas phase dominant) in the presence of catalytic reaction. As a reference, the dotted line also denotes the ratio of the extinction strain rate for the lower branch to the extinction strain rate of the pure homogeneous combustion without catalytic surface. Both curves are plotted as a function of the equivalence ratio under the same conditions in Fig. 2.10. When $\phi$ is less than 0.6, the ratio is nearly 1, implying the surface reaction hardly affects the overall extinction strain rate. These results suggest that surface reaction depends largely on the intermediate hydrocarbon radicals generated by the gas-phase reaction. On the contrary, the concentration of oxidizer does not have a significant effect on the surface reaction.

### 2.2.3 Effects of heat loss

We next examine the effects of conductive heat loss to the catalytic surface. Figure 2.12 shows the maximum temperature versus strain rate for $\phi = 0.8$ and various heat conductivity $k$. As expected, a larger value of $k$ results in reduced extinction strain rates for both upper and lower branches due to the increased heat loss. It is of interest to note that, while the gas-phase extinction temperature is reduced with an increase heat loss, the minimum surface reaction temperature for the surface reaction branch remains almost constant for different heat losses. This contrasts the results in Fig. 2.10 where the extinction temperature varies significantly with the equivalence ratio, suggesting that the surface reactions are highly chemistry-controlled.

Another notable observation in Fig. 2.12 is that, as heat loss increases, the separation between the gas-phase branch and the surface reaction branch becomes larger, eventually leading to an island of the response in the surface chemistry-dominant regime that is separated from the upper branch gas-phase combustion regime. The low strain rate extinction of the surface reaction regime is believed to be due to the lack of intermediate reactants

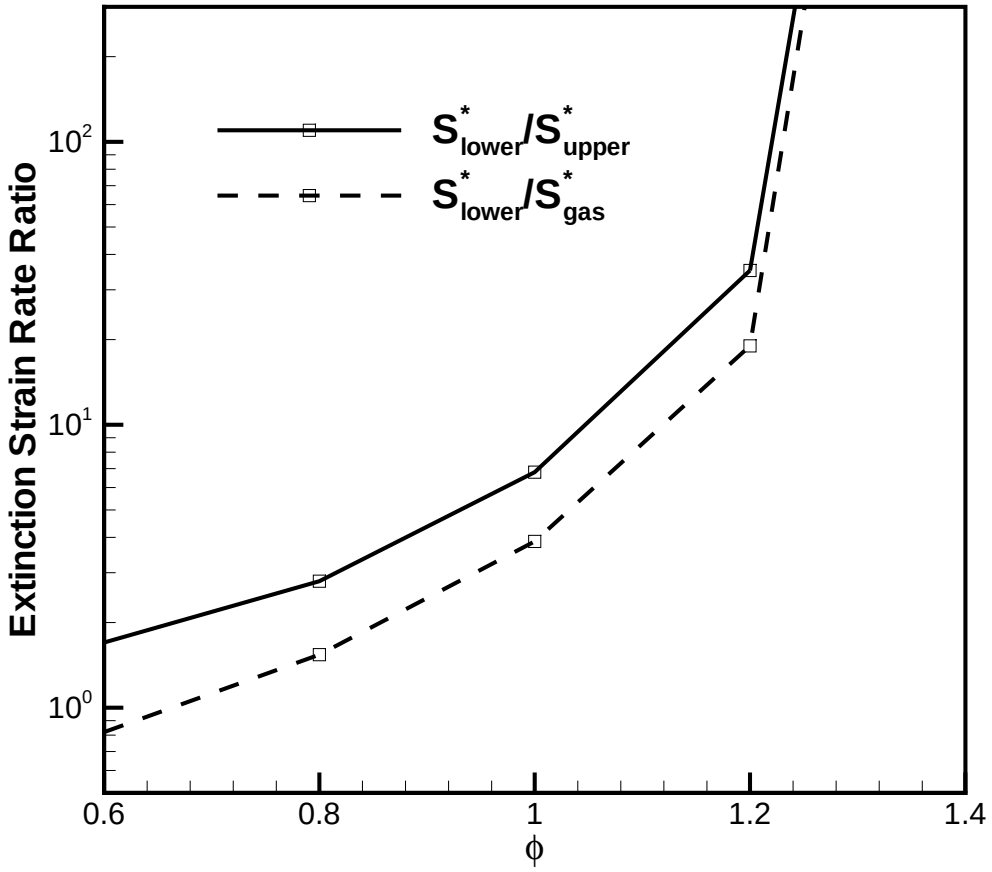


Figure 2.11: Solid line: the ratio of the extinction strain rate in the lower branch to that in the upper branch in the presence of catalytic reaction. Dotted line: the ratio of the extinction strain rate in the lower branch to the pure homogeneous combustion without catalytic reaction. Curves are plotted as function of $\phi$ under the same conditions in Fig. 2.10.

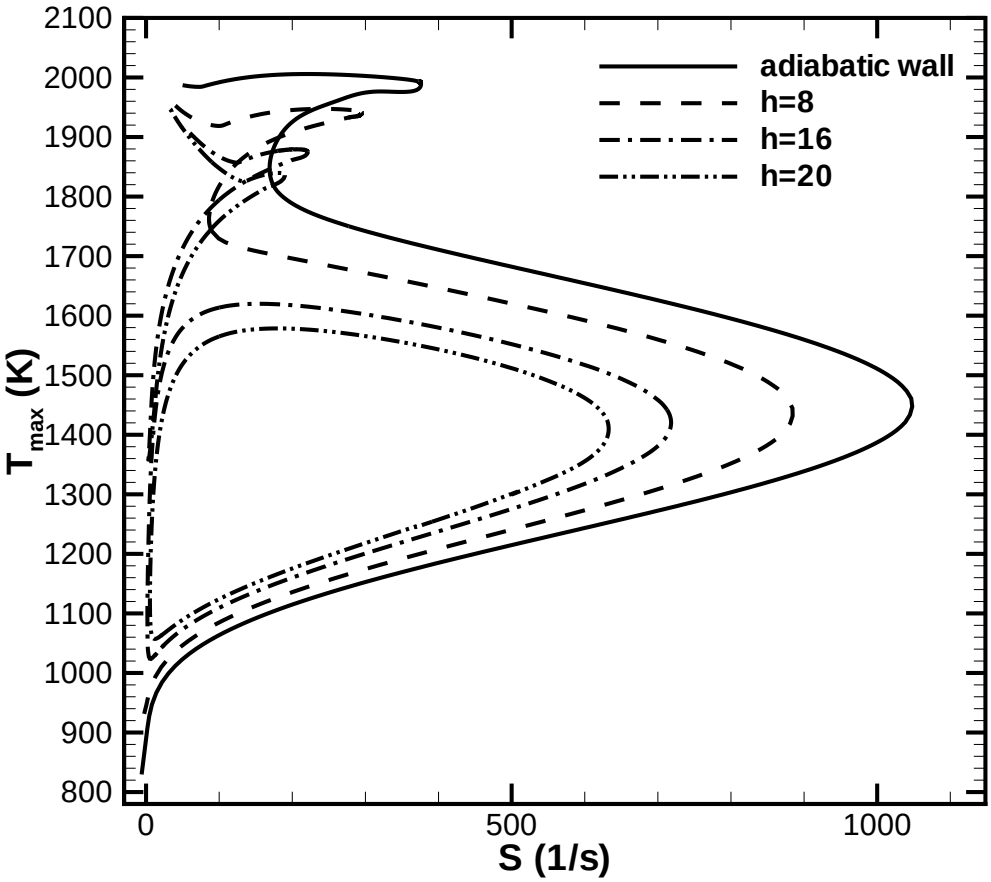


Figure 2.12: Maximum temperature versus strain rate for $\phi = 0.8$ and various heat loss conditions. The conductivity $h$ has the unit of $\mathrm{W/m^2 - K}$.

supplied from the gas phase reaction. This behavior resembles the low-stretch extinction of flames in the presence of radiative heat loss [55], and it is interesting to find a similar response in a surface-dominant reaction system.

Figure 2.13 shows a similar temperature response with an addition of heat to the catalytic surface. This case may represent a practical situation where the micro-combustor is sustained by an external heating mechanism. The results show that the basic two-branch behavior is maintained over a wide range of heat fluxes, while the curve is shifted to increase the extinction strain rate. Again, the gas-phase extinction temperature shows a moderate sensitivity to the amount of heat flux, while the surface reaction extinction temperature remains almost constant, further demonstrating the chemical dominance of the catalytic combustion.

### 2.2.4 Parametric mapping of combustion regimes

In the previous sections, we observed different characteristics of the steady combustion temperature versus the strain rate. In addition to the fact that the surface reaction can in general extend the extinction limit, the observations based on extensive parametric calculations are summarized as follows: (a) Two distinct stable combustion branches appear when there exists a finite amount of surface heat loss. The upper branch is primarily governed by the gas-phase flames, while the lower branch is dictated by the surface reaction; (b) There exists an optimal equivalence ratio to observe these two distinct branches, and the gas-phase branch vanishes for leaner or richer mixture; (c) For a rich mixture ($\phi > 1.2$) the surface reaction is so intense that no strain-induced extinction is observed; (d) For an appropriate equivalence ratio, the presence of two distinct branches become more pronounced as the heat loss is increased. At larger heat losses, the two branches separate out to form an isolated surface reaction response curve, exhibiting dual extinction behavior.

The equivalence ratio and heat loss have been the two major parameters in the present investigation. More extensive calculations have been performed to characterize the com-

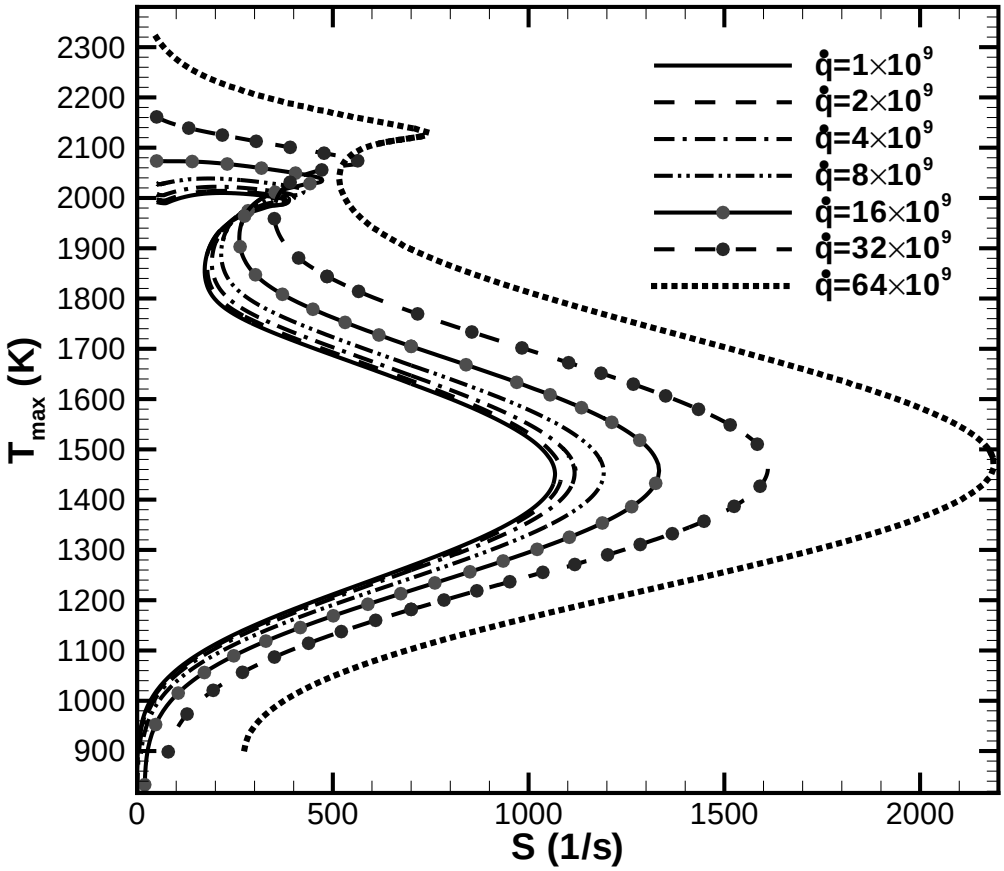


Figure 2.13: Maximum temperature versus strain rate for various heat source conditions and $\phi = 0.8$. The unit for $\dot{q}$ is $\mathrm{W/m^2}$.

bustion response with various combinations of the two parameters, and the results are plotted in Fig. 2.14. For all equivalence ratios, the system is found completely non-reactive if the surface heat loss is sufficiently large. The three regimes denote that the flame temperature versus strain rate response shows two isolated branches (I), a continuous curve with two distinct branches (II), and a monotonic response dominated by surface reaction (III). Such a parametric map can serve as a useful guidance in understanding the fundamental combustion characteristics inside a micro-combustor.

## 2.3 Conclusions

A computational study has been performed on a steady stagnation-point flow combustor with a catalytic surface. Premixed methane-air gas reacting on a platinum surface was investigated with detailed gas-phase and surface chemistry.

A main focus of the present work was to identify and characterize the strain-induced extinction limits over a range of physical parameters. An estimate of the characteristic chemical times based on the methane consumption rate confirms that the surface reaction has a significantly shorter characteristic time scales, thereby sustaining reaction at lower flow residence times.

The steady results showed that catalytic reaction can largely extend the extinction limit, while suppressing the gas phase reaction at lower strain rates. It was also found that the extension of the catalytic reaction quenching limit is highly sensitive to the mixture composition, suggesting the dominance of chemical aspects in catalytic combustion. The temperature versus strain rate response curves exhibit multiple branches of stable solutions, implying a possibility of hysteresis behavior in a coupled homogeneous-heterogeneous reactor. Characteristics of combustion behavior in each branch have been examined by the reaction zone structures.

Finally, three distinct steady combustion regimes have been identified in terms of the mixture equivalence ratio and heat loss: a surface-dominant monotonic response, contin-

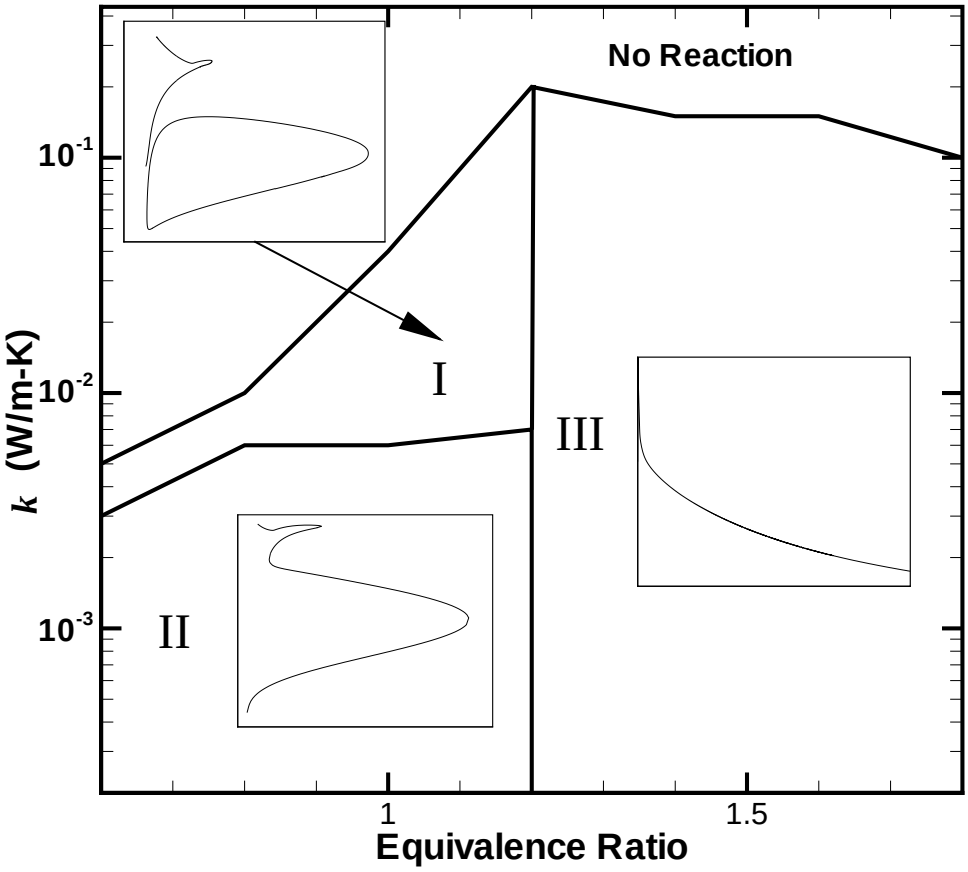


Figure 2.14: Mapping of catalytic combustion response for various $\phi$ and $k$. A typical temperature versus strain rate response behavior in each regime is represented by the insets: Regime I has two isolated branches; Regime II has connected two distinct branches; Regime III is a surface-dominant reaction with no significant gas-phase reaction.

uous two-branch response, and separated response showing an isolated surface-reaction island. This parametric mapping will be useful in identifying the operating conditions and combustion characteristics of micro-combustors. Further consideration of combustion response to unsteady strain rate, mixture composition, and substrate temperature will be undertaken in future studies.

# Chapter 3

# Effects of Dilution on the Extinction Characteristics of Strained Lean Premixed Flames Assisted by Catalytic Reaction

Combustion performance and extinction due to large strain rate with different wall heat condition and equivalence ratio were studied in previous chapter. It has been proved that catalytic surface reaction can extend extinction strain rate limit largely with proper input parameters. Temperature versus strain rate curves exhibit multi-branches which indicates more than one physical status could exist for same input conditions. Three combustor steady performance regimes with different range of equivalence ratio and wall heat condition are presented at last.

Despite strain rate, extinction due to lean equivalence ratio is studied in this chapter. Not like in previous chapter, both steady and unsteady environmental parameters are adopted here. Steady extinction lean limit is tested first. Periodic vibrating inlet equivalence ratio is then applied to test the catalytic reaction's ability to extend dynamic lean extinction limit. Vibrating strain rate input is also applied to validate the conclusion that benefits of catalytic reaction is caused by different characteristic reaction time scale between gas phase and surface catalytic reaction. Nitrogen dilution is proved to be able to enlarge reaction time scale discrepancy between gas phase and catalytic reaction further in this chapter.

## 3.1 Model Description

As shown in Fig. 2.1, the computational configuration is a stagnation-point flow where a mixture of methane and oxidizer is injected onto a platinum surface, forming a flame either in the flow field or on the catalytic surface. One-dimensional similarity formulation is derived with full consideration of detailed surface [22] and gas-phase [56] chemical kinetic models. The adopted surface mechanism has been validated for ignition behavior in both rich and lean conditions, and extinction under lean cases [22, 57]. Due to the lack of thermodynamic data for surface species, however, there may be some inconsistencies when the mechanism is used outside the conditions at which it was designed and tested. Since the present study explores mostly lean to near-stoichiometric conditions, the qualitative behavior and major findings of the study are expected to be valid.

As in our previous study [58], both steady and unsteady computations are performed by a modified version of OPUS [45] to incorporate solid wall and surface chemistry. A fixed zonal grid refinement is applied to provide sufficient resolution in the reaction zone near the solid surface. For all calculations, the inlet gas temperature and pressure is fixed at 300 K and 1 atm, respectively. The distance between the inlet and the catalytic surface is $L$ = 0.5 cm.

One of the main issues in this study is the effects of dilution on the separation of characteristic time scales for gas-phase and surface reactions. For this purpose, additional nitrogen is mixed into the air, measured by its mole fraction. For example, 10% nitrogen addition indicates that 0.1 mole nitrogen is added to 1 mole of air.

To study unsteady flame response, the reactant composition and flow strain rate are varied in time according to the following equations:

$$U_\infty(t) = U_\infty(0)[1 - B(1 - \cos(2\pi f t))], \tag{3.1}$$

$$X_{\mathrm{CH_4}}(t) = X_{\mathrm{CH_4}}(0)[1 - A(1 - \cos(2\pi f t))], \tag{3.2}$$

where $U_\infty$ is the axial velocity at the nozzle exit and $X$ is the mole fraction. The strain rate is then defined as the nominal velocity gradient, $S = U_\infty/(2L)$, due to the difficulty in defining the actual velocity gradient when the reaction occurs on the surface [58].

## 3.2 Results and Discussion

### 3.2.1 Steady response: effects of dilution

A baseline study of the flame structure and species profiles in response to the addition of the surface reaction has been investigated in our previous work [58]. In this chapter, the steady flame behavior subjected to reactant mixture dilution is first investigated, as an attempt to assess the effect of surface chemistry on extending the lean extinction limit at various level of gas mixture dilution. In general, it is anticipated that dilution lowers temperature and hence the reaction rate, such that the flame extinction occurs at a higher equivalence ratio. It is of interest to examine whether this effect applies to both homogeneous and heterogeneous reactions at a comparable level.

Figure 3.1 shows the maximum reaction zone temperature as a function of the mixture equivalence ratio for various nitrogen dilution levels, each case with and without surface reaction. For all the calculations, the strain rate was fixed at 277 $s^{-1}$ and the surface was considered adiabatic. The results for all cases show that the maximum temperature decreases as the equivalence ratio is reduced, eventually reaching the lean extinction limit. For the results with surface reactions, it is clearly seen that an increased amount of dilution lowers the reactivity such that extinction occurs at higher equivalence ratio. An important observation here is that the disparity between the lean extinction limit of homogeneous and heterogeneous combustion becomes larger as the level of dilution is increased. For example, in 0% dilution case the extinction limit for the homogeneous reaction is lower than that for the heterogeneous case. With 13% dilution, however, the heterogeneous combustion shows a much wider flammable range of the equivalence ratio. This implies that the sen-

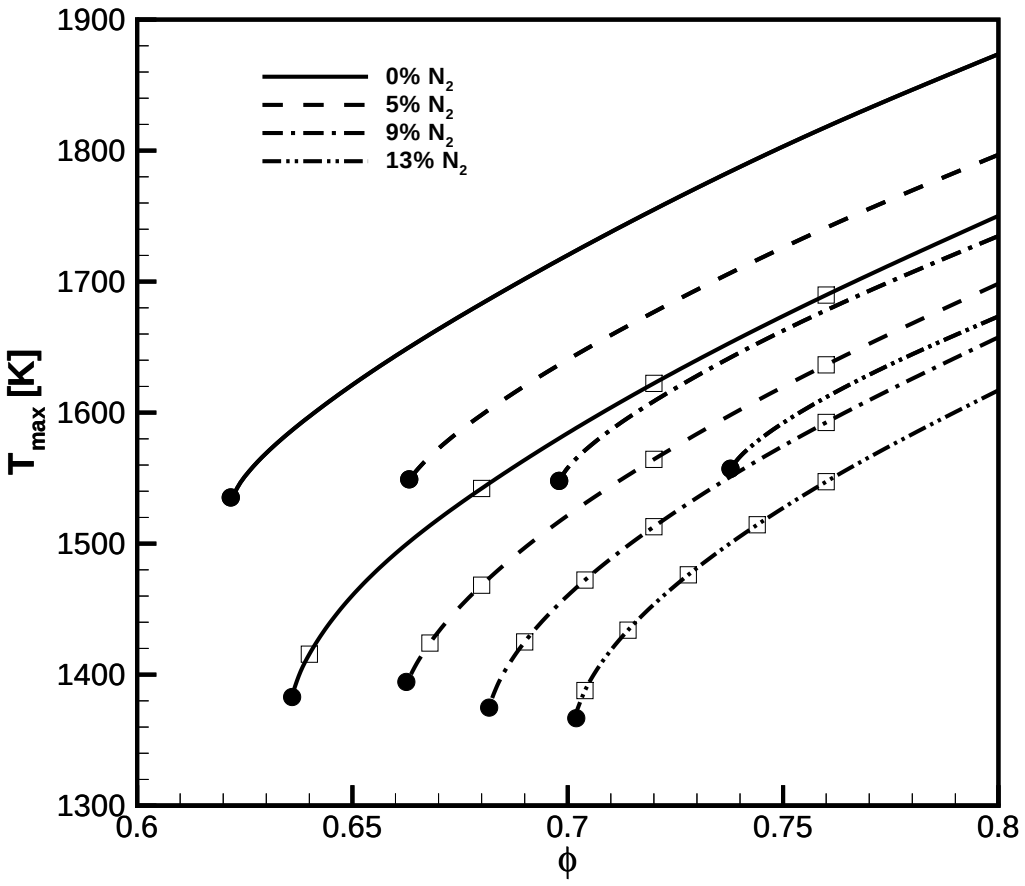


Figure 3.1: Maximum temperature as a function of the equivalence ratio for various levels of nitrogen dilution for adiabatic surface. Lines without symbols: without surface reactions. Lines with symbols: with surface reactions.

sitivity in the reduction of the characteristic reaction time scales to the mixture dilution is different between homogeneous and heterogeneous combustion processes. Therefore, it is expected that the benefit of flammability limit extension by catalytic reaction is greater as the reactant mixture is more diluted. This behavior was found to be qualitatively consistent for other values of the strain rate.

More extensive calculations were performed to determine the extinction limit extension over a range of nitrogen dilution. In addition to the adiabatic wall considered in the above,

we have also considered the cases where the catalytic surface is subjected to heat loss or heat addition. Heat loss from the surface is modeled by a general form: $\dot{q} = h(T_{\text{surf}} - T_0)$, where $T_0$ is the ambient temperature set at 300 K, and $h$ is the effective heat transfer coefficient accounting for the associated conductive and conductive modes. In this study, $h = 4$ W/m$^2$-K is used. For the heated surface case, a net power of $10^4$ W/m$^2$ is supplied to the substrate.

Figure 3.2 is plot of lean extinction limits as a function of the nitrogen dilution for various thermal conditions on the surface. For all surface conditions with zero dilution, it is interesting to note that catalytic reaction results in higher lean extinction limit. In other words, catalytic reaction actually leads to a narrower flammable range. The benefit of flammability extension by surface chemistry occurs only with nitrogen dilution of approximately 5% and above, and the level of extension continues to increase as the level of dilution increases. This behavior is attributed to the fact that, at such lean conditions, the addition of catalytic surface scavenges radicals generated from the gas-phase reactions, hence attenuating the overall reactivity of the system. This results provide an important practical implication that the use of surface reaction in a lean premixed micro-combustor may be applicable only with a significant level of dilution, which is rather a desirable feature for the purpose of achieving low temperature combustion.

Figure 3.2 also demonstrates that, while heat loss or heat supply on the surface can significantly affect the absolute level of the lean extinction limits, the difference between the homogeneous and heterogeneous extinction limits are largely unaffected by the surface thermal conditions. It is also noted that the crossover point between the homogeneous and heterogeneous limits, albeit marginally, tends to decrease toward a lower level of dilution for the heat addition case. This is because surface reaction can be more effectively enhanced by heat supply than homogeneous reaction.

The effect of nitrogen dilution is primarily to lower the flame temperature and thereby lengthening the characteristic chemical time scales relative to the characteristic flow res-

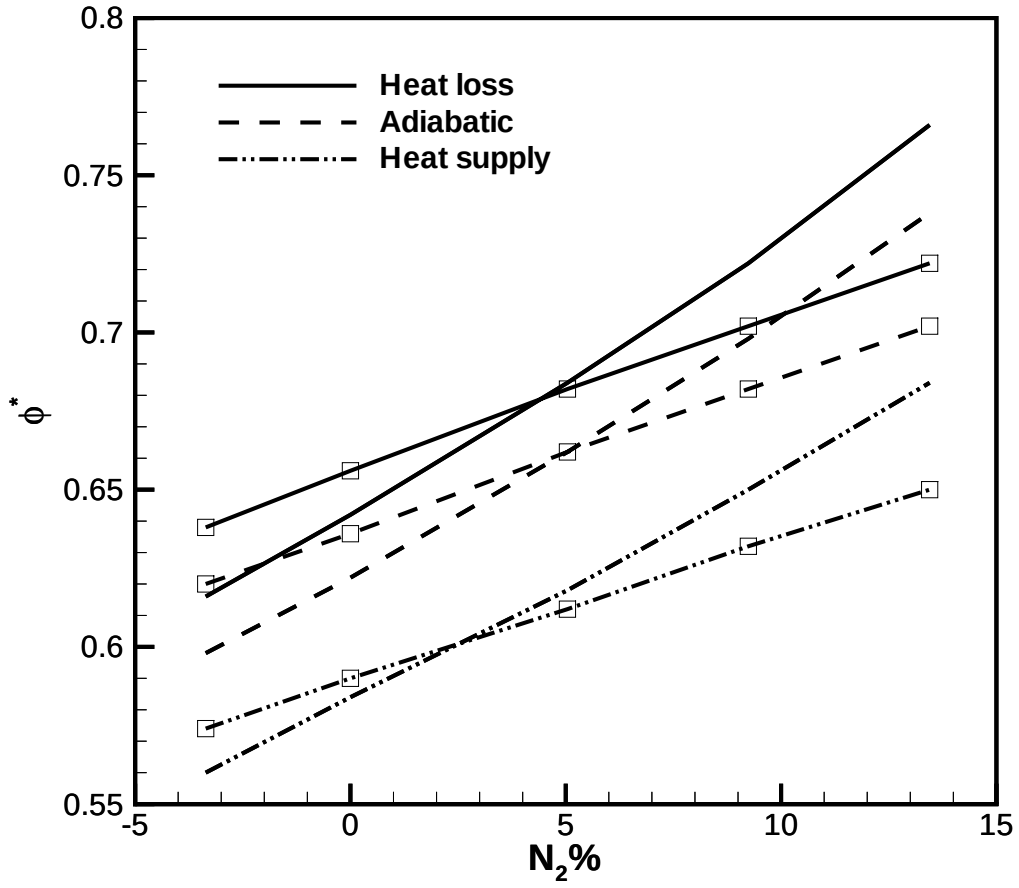


Figure 3.2: Lean extinction limits as a function of the nitrogen dilution for various surface thermal conditions, for S=277$s^{-1}$. Lines without symbols: without surface reactions. Lines with symbols: with surface reactions.

Table 3.1: Time scales of gas-phase and surface fuel consumption rates for various levels of dilution.

| | 0% $N_2$ | 9% $N_2$ | 13% $N_2$ |
|---|---|---|---|
| $\tau_g$ | $1.365\times10^{-4}$s | $2.076\times10^{-4}$s | $2.490\times10^{-4}$s |
| $\tau_s$ | $9.201\times10^{-6}$s | $8.696\times10^{-6}$s | $8.637\times10^{-6}$s |
| $\tau_g/\tau_s$ | 14.8 | 23.9 | 28.8 |

idence time. It is apparent that this effect is more pronounced in the gas-phase than on the surface. To verify this observation, the characteristic chemical time scales for the gas-phase and surface chemistry, $\tau_g$ and $\tau_s$ respectively, are defined based on the primary fuel consumption as equations 2.19 and 2.20 [58]

$$\tau_g = \frac{X_{\mathrm{CH_4}}}{\dot{\omega}_{\mathrm{CH_4}}} \frac{p}{R^0 T},$$

$$\tau_s = \frac{X_{\mathrm{CH_4}} \Gamma}{\dot{s}_{\mathrm{CH_4}}},$$

where the units are in seconds, $X_{\mathrm{CH_4}}$ is mole fraction of methane at the nozzle exit, $R^0$ is the universal gas constant, and $\Gamma$ is site density of the surface species. In determining the reaction rate, $\dot{s}_{\mathrm{CH_4}}$ for the surface reactions is evaluated at the catalytic surface, while for the gas-phase reactions the spatial maximum value of $\dot{\omega}_{\mathrm{CH_4}}$ is used. Note that $\dot{\omega}_{\mathrm{CH_4}}$ in Eq. (2.19) and $\dot{s}_{\mathrm{CH_4}}$ in Eq. (2.20) have different units [58]. The characteristic times are evaluated at a fixed strain rate of $S = 277\mathrm{s}^{-1}$ for the steady initial conditions shown in Fig. 3.3.

The results for the three dilution cases considered in Fig. 3.1 are summarized in Table 3.1. It is found that the gas-phase reaction time scales increases with dilution by several factors, while the surface reaction time scale remains almost the same. This confirms that the gas-phase reaction is more sensitive to dilution than surface reaction.

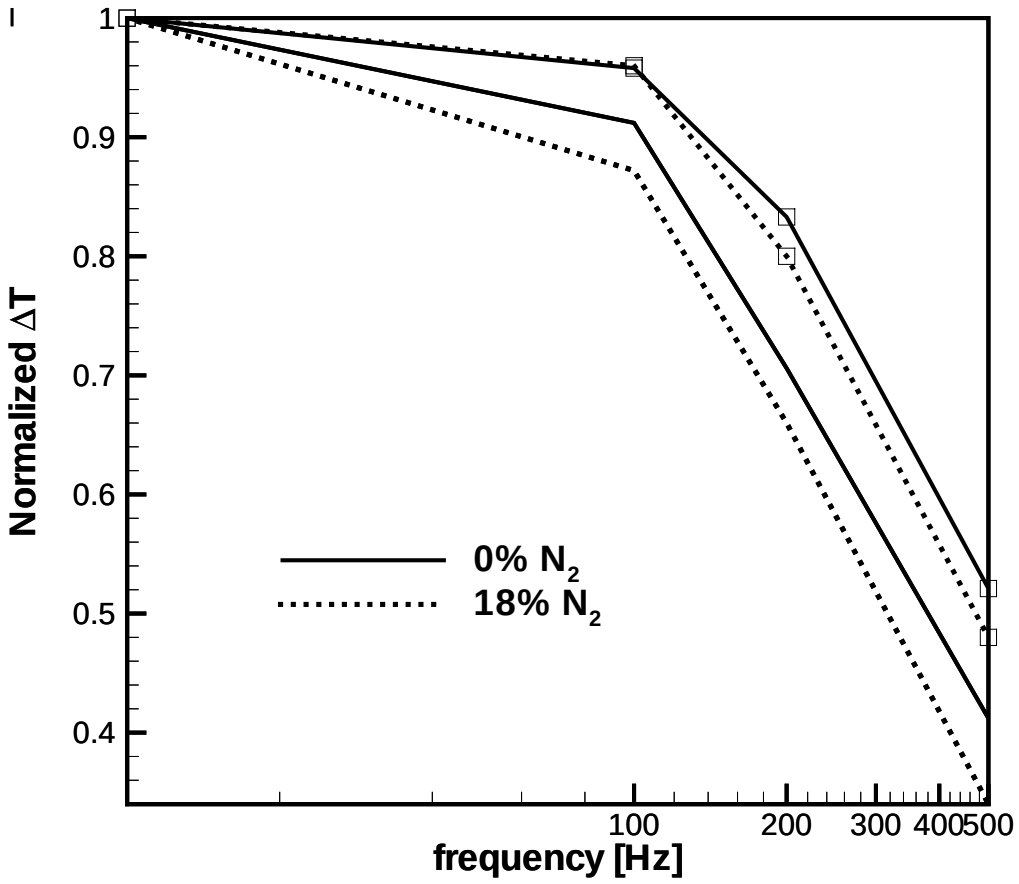


Figure 3.3: Normalized maximum amplitude of temperature variation as a function of frequency for the flames subjected to oscillatory strain rates. Lines without symbols: without surface reactions. Lines with symbols: with surface reactions.

### 3.2.2 Unsteady response to oscillatory strain rate

The effect of dilution on the chemical time scales has an additional implication in unsteady flame response. As reported in a number of previous studies [30, 33, 51], flames subjected to unsteady flow perturbation behave as a low-pass filter; the flame response becomes attenuated as the frequency of the external perturbation increases. In this case, the cut-off frequency beyond which the flame no longer responds to unsteady fluctuation depends on the characteristic time scale of the relevant chemical reactions.

The above consideration is extended to a system in the presence of heterogeneous combustion. A steady flame is now subjected to an oscillatory strain rate by imposing a sinusoidal velocity fluctuation as given by Eq. (3.1) for various frequencies. For these calculations, the equivalence ratio is fixed at $\phi = 0.8 (A = 0)$, and the initial strain rate is fixed at $S(0) = 277$ s$^{-1}$ with $B = 0.1$. The surface is considered adiabatic so that the maximum temperature always occurs at the surface for both catalytic or non-catalytic cases. To show the effect of dilution clearly, the 0% dilution case is compared to the 18% dilution case, which was the maximum value before extinction.

Figure 3.3 shows the amplitude of the maximum temperature oscillation, $\Delta T$, in response to the unsteady strain rate as a function of frequency. For each case, $\Delta T$ is normalized by the quasi-steady value ($f \rightarrow 0$). As the frequency of oscillation is increased, the flame temperature response for various conditions become attenuated at different cut-off frequencies. For either case of dilution, surface reactions have shorter characteristic time scales, such that the response is less attenuated at higher frequencies. The fact that the gas-phase reaction time scales are more sensitive to dilution is reflected in Fig. 3.3 in that the deviation of the two curves between 0% and 18% dilution cases is greater for the gas-phase than for the surface reaction. All these results are consistent with the discussion in the previous section.

### 3.2.3 Dynamic flammability limit

To further examine the effects of dilution on unsteady flame characteristics, we now study the unsteady flame response to oscillatory equivalence ratio as given by Eq. (3.2). The main interest is to identify the extension of lean flammable limit for a given strain rate as a function of frequency, following the concept of the dynamic flammability limit, which is defined as the minimum instantaneous equivalence ratio during the oscillation without extinction, introduced by Sankaran and Im [37]. For each frequency, $f$, we can determine the maximum allowable amplitude of oscillation, $A$, beyond which the flame extinguishes. This implies that the dynamic flammability limit is a function of frequency for the given strain rate, surface thermal condition, and the initial equivalence ratio. We attempt to conduct an analysis to a system in the presence of heterogeneous combustion, with an emphasis on the effects of nitrogen dilution, heat loss, and the frequency of the equivalence ratio oscillation.

The flame responses with and without catalytic reaction are compared under three cases: (a) 0% dilution without heat loss, (b) 13% dilution without heat loss, and (c) 13% dilution with heat loss. Following Eq. (3.2), the initial condition, $X_{\mathrm{CH_4}}(0)$, as been set such that the equivalence ratio, $\phi = 2X_{\mathrm{CH_4}}(0)/X_{\mathrm{O_2}}(0)$, is 0.68, 0.76, and 0.80 for cases (a) to (c), respectively. For all cases, the strain rate is set to 277 $\mathrm{s}^{-1}$.

Figures 3.4(a) to (c) shows the limit-cycle behavior of the maximum flame response for various frequencies of oscillation in $\phi_{\mathrm{flame}}$, which is determined at the upstream flame base at $T$ = 302 K. Since the amplitude of $\phi_{\mathrm{flame}}$ was taken to be the maximum without quenching the flame, the minimum equivalence ratio reached during the limit cycle is considered the dynamic flammability limit for a given frequency condition. Comparing Figs. 3.4(a) and (b), it is clear that the diluted case shows a greater extension of the lean flammability limit by adding the surface reaction; not only is the steady flammability limit further extended to a leaner condition, but the additional unsteady extension for the same frequency is also greater with surface reaction. This is attributed to the fact that the surface reaction is faster and thus can respond to the imposed oscillation more rapidly. Moreover, the surface

reaction case undergoes a larger excursion in the flame strength, hence there is a larger amount of excess enthalpy during a cycle to sustain combustion at leaner conditions. Similar behavior is also observed in Fig. 3.4(c) in the presence of heat loss, although the overall flammability limits are relatively higher than those in (b). As discussed in Fig. 3.2, the amount of flammability extension due to surface reaction is found to be rather insensitive to the surface thermal condition even considering unsteady situations.

To summarize the unsteady characteristics, it is of interest to compare the dynamic flammability extension between the cases with and without surface reaction, denoted by $\Delta\phi_s$ and $\Delta\phi_g$, respectively. Here $\Delta\phi$ is defined as the maximum flammability extension compared to the steady limit for a given frequency. Figure 3.5 shows the difference, $\Delta\phi_s - \Delta\phi_g$, as a function of frequency for the three cases shown in Fig. 3.4. Note that the increase in the curve with frequency indicates that the *additional* dynamic flammability extension due to surface reaction becomes greater as frequency increases. In other words, the benefit of surface reaction in extending flammability is greater for a larger level of unsteadiness. For 0% dilution, the curves fall into an negative region for frequencies above 200 Hz due to the fact that surface reaction acts negatively on the system flammability. However, there is a reversal in the curve at low frequencies below 200 Hz resulting in flammability enhancement by surface reaction even with 0% dilution. Therefore, the benefit of catalytic flammability extension is found to be greater with dilution, while the difference between the cases with and without heat loss appears to be insignificant.

## 3.3 Conclusions

In this chapter, steady and unsteady extinction characteristics of a stagnation-point flow combustor were analyzed with both homogeneous (methane-air) and heterogeneous (platinum) reactions considered. One of the key aspects of the study was the effect of mixture dilution on the aspects of flammability extension. For the system under study, it was found that surface reactions actually attenuates the range of lean flammability limit due to their

effect of radical scavenging. The benefit of catalytic reactions can indeed occur and it increases with additional dilution in the gas mixture, which is a desirable aspect in achieving low temperature combustion for micro-combustor application. While the surface heat loss expectedly lowers the overall flammability of the system, it was found that the level of flammability extension by surface reactions is rather insensitive to the surface thermal conditions.

Unsteady extinction behavior in response to oscillatory strain rate and equivalence ratio fluctuations showed overall consistent trend expected from the steady results. The overall flame response becomes attenuated as the frequency of oscillation increases, and the cut-off frequency depends on the characteristic time scales of the dominant chemical reactions. It was also found that the benefit of flammability extension by catalytic reactions can be greater as the level of unsteadiness increases. These results can provide insights into the development of robust micro-combustion devices.

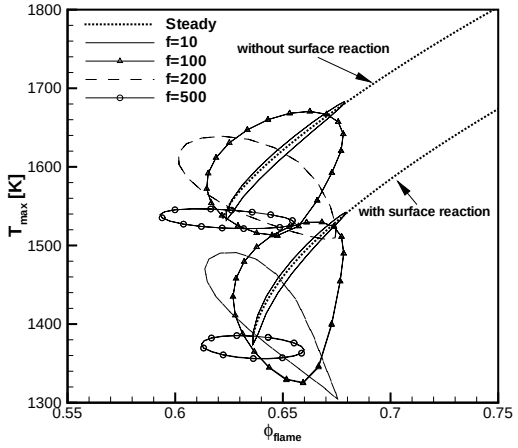


(a) 0% dilution without heat loss

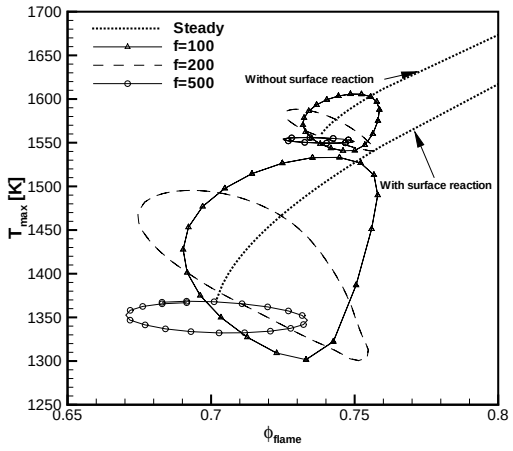


(b) 13% dilution without heat loss

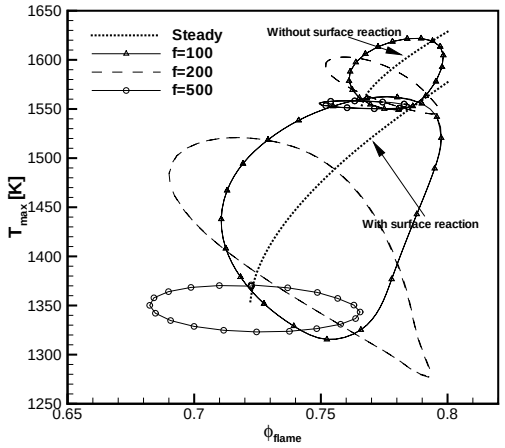


(c) 13% dilution with heat loss

Figure 3.4: Unsteady flame temperature response to the equivalence ratio various frequencies.

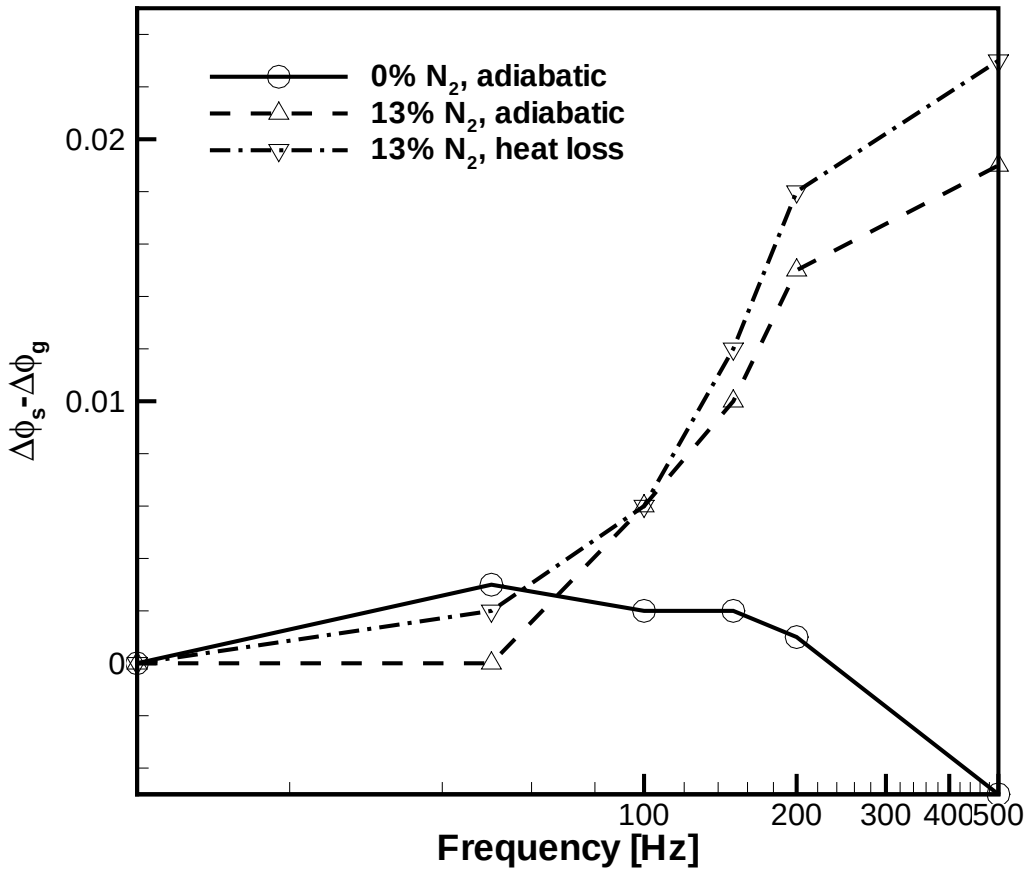


Figure 3.5: Difference between the dynamic flammability extension of a flame with and without surface reaction ($\Delta\phi_s - \Delta\phi_g$), as a function of frequency, for various dilution and surface thermal conditions.

# Chapter 4

# Experimental Validation

The computational studies in Chapters 2 and 3 demonstrated that the flammability and extinction limits can be extended in the presence of catalytic reaction. It was found that the flammability extension is more pronounced when nitrogen is added into the system as a diluent gas. These observations were explained based on the relative characteristic time scales of the gas-phase and surface reactions; the scale disparity becomes larger with dilution of mixture.

While the computational model allows systematic analysis of the extinction characteristics over a wide range of parameters, whether the observed behavior can be consistently reproduced in real devices must be validated. In particular, the computational studies in the previous chapters employed a prescribed heat transfer coefficient which may be different from practical conditions. Therefore, in this chapter we conduct calculations and validate against experimental measurements, with an attempt to match the heat loss effects as closely as possible.

The experimental work was undertaken as a collaborative effort by James Wiswall and Professor Margaret Wooldridge at the University of Michigan. Experiments were carried out with similar parameters range as in previous numerical results. Details of the experimental set-up and experimental procedure can be found in Ref. [5], which is briefly summarized in the following section.

## 4.1 Experimental Configuration

The schematic of the experimental configuration is shown in Fig. 1.3. Fuel, oxygen and nitrogen were conducted to a mixing tank to produce the premixed reactant. Rotameters of individual gas tanks are used to control the flow rate as well as the mixture equivalence ratio. Extra nitrogen was introduced through a co-flow tube outside the nozzle exit to create a boundary layer preventing reactant mixing with environmental air. Flow rate of co-flow nitrogen was also controlled by rotameter to suppress mixture parabolic velocity profile which could induce flame edge curve. A silicon wafer coated with Platinum was used as stagnation plane for catalytic cases and another exactly same bare silicon wafer served as stagnation plane of noncatalytic cases. Thermocouples were embedded into center of both sides of substrate to measure temperature [5]. Velocity can be measured from postprocessing of PIV data as in Figure 4.1.

The experimental measurement uncertainties are found to be $\pm 4$ cm/s for the average nozzle velocity, $-0.04$ to $0.02$ for the extinction equivalence ratio, and $\pm 5$ K for the temperature.

## 4.2 Model Adjustment

Figures 4.2 and 4.3 show the comparison between numerical and experimental results of the axial velocity profile along the centerline between the stagnation plane and the nozzle exit, with and without the flame, respectively. The discrete symbols in the figures which represent experimental results are postprocessing data from PIV measurement. The experimental velocity profile behaves consistently with the numerical data, but there exists a wide range of plateau region near the nozzle. This is attributed to the multi-dimensional effect present in the experimental system when the flow is far from the stagnation plane. Since the key parameter to compare the results are the strain rate (which is determined by the velocity gradient at the flame or at the stagnation plane), for consistent validation the

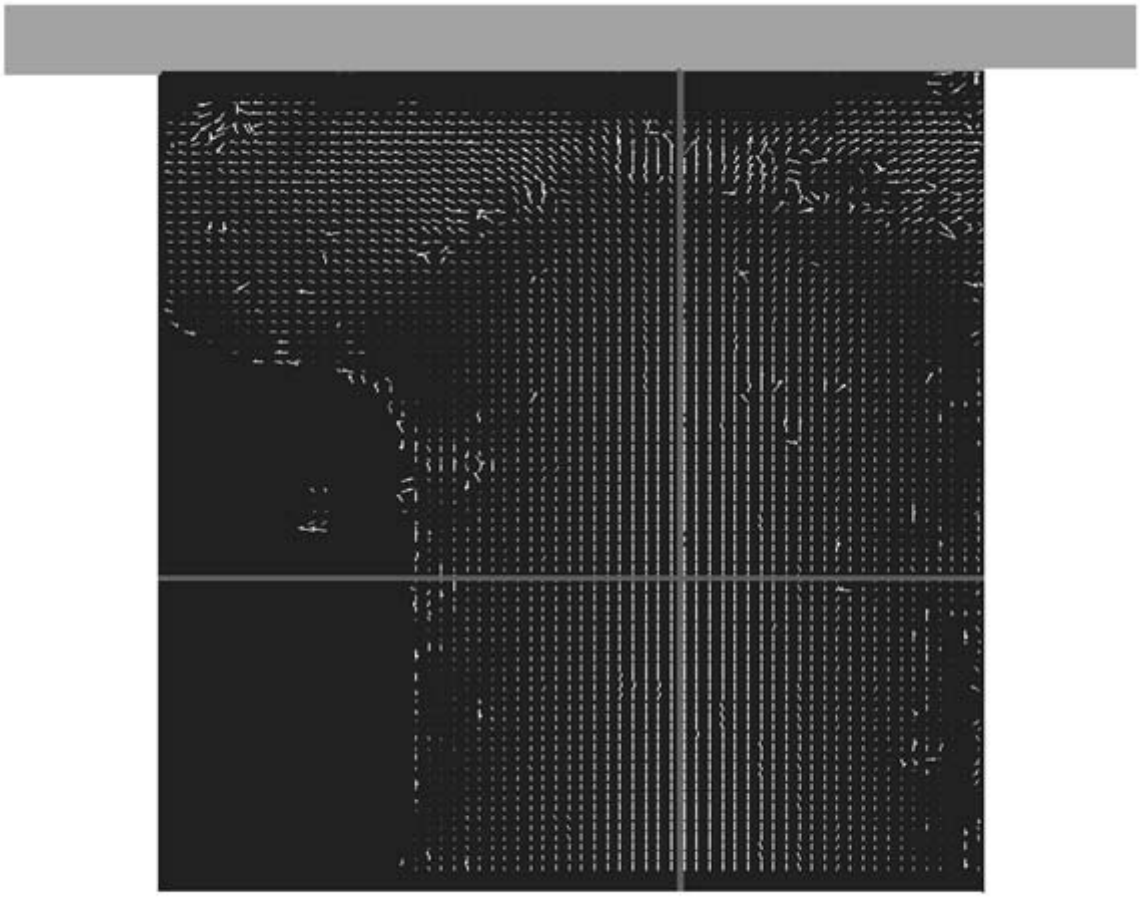

Figure 4.1: PIV image of flow velocity vector [5].

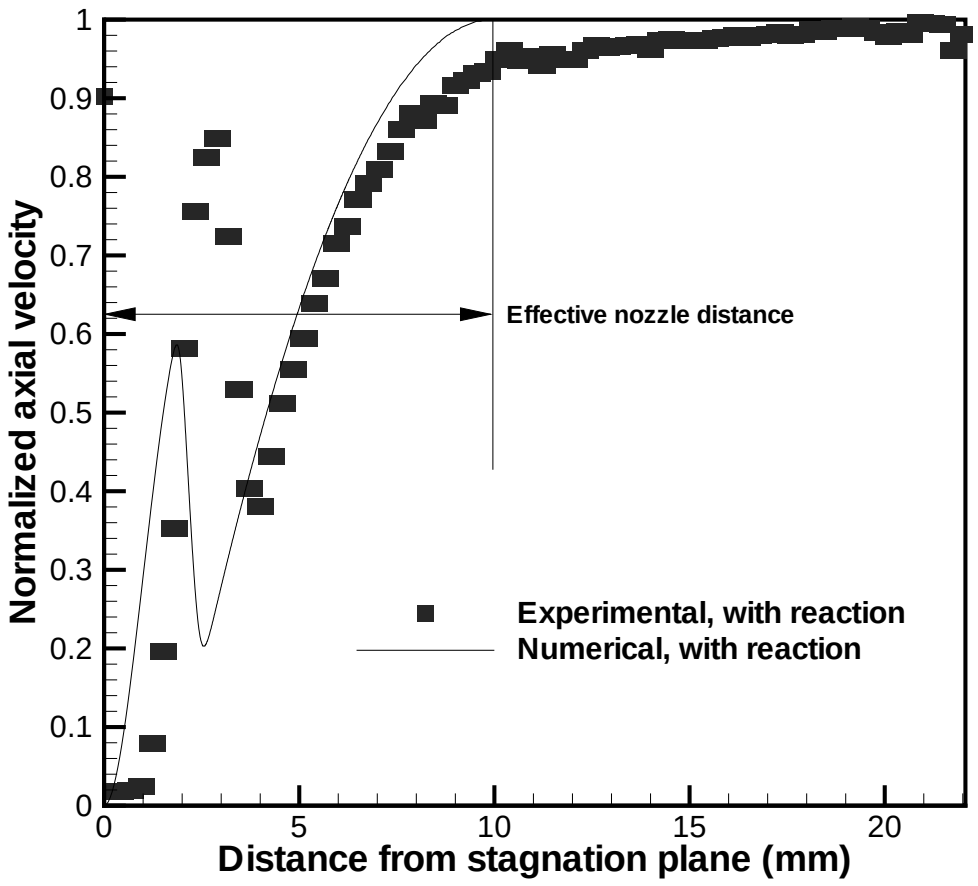


Figure 4.2: Numerical and experimental flow axial velocity profile along nozzle center line with chemical reaction.

*effective* nozzle distance is defined as the distance from the stagnation plane to the location where the velocity starts to drop monotonically up to $5\%$ of the peak value ($10$ mm from stagnation plane). The global strain rate for the experimental condition is determined based on the nozzle exit velocity and the effective nozzle distance.

Another major difficulty in cross-validation is to estimate the heat loss effect properly. Parameters such as substrate wall thickness (fixed as 1.27 cm), flow velocity and equivalence ratio can be easily measured and incorporated in the model. However, the heat conductivity ($k$) and radiation emissivity ($\epsilon$) of the material vary with temperature and it is

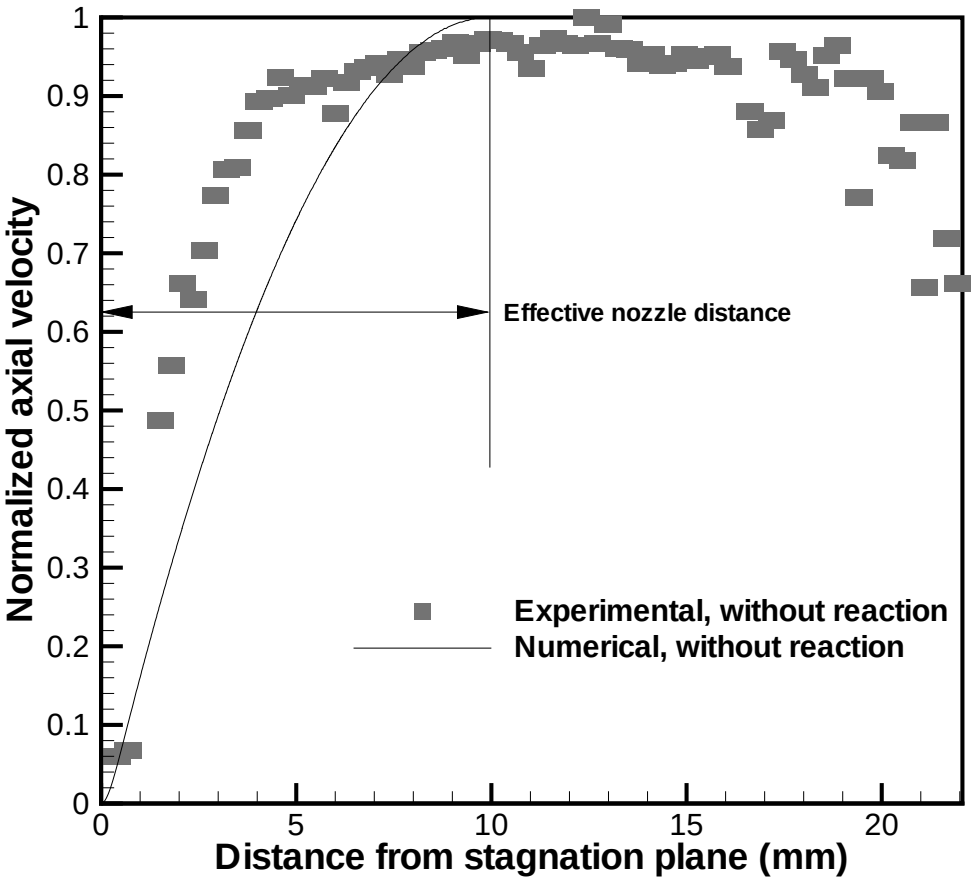


Figure 4.3: Numerical and experimental flow axial velocity profile along nozzle center line without chemical reaction.

difficult to estimate proper values for $k$ and $\epsilon$ separately. A trial-and-error approach was attempted by increasing the conductivity from zero until the modeled surface temperature reaches experimental condition. Unfortunately, the lowest simulated surface temperature at extinction was found to be always several hundred degrees (K) higher than the experimental results.

To reconcile this problem, the actual experimental measurements over a wide range of conditions were compiled and curve-fitted to extract the realistic heat transfer parameters. For each experiment case, temperature was measured at the stagnation plane and at the substrate backside. The calculation was then performed at the matched nozzle strain rate and equivalence ratio. By trial and error, the computation was then conducted with a guessed value of the heat transfer parameter until the computed stagnation plane temperature matches with the measured value. To minimize the number of free parameters, the radiative heat transfer effect was lumped into the *effective* conductivity $k_{eff}$, while allowing that $k_{eff}$ depends on temperature as well as the strain rate. For simplicity, the backside temperature in calculation was set to 300K in determining $k_{eff}$. In other words, $k_{eff}$ does not represent conductivity of any realistic solid material, but it rather emulates the net amount of heat loss.

Figures 4.4 and 4.5 show the measured temperature values and the resulting $k_{eff}$ over a wide range of conditions with non-catalytic and catalytic conditions, respectively. For a given strain rate condition, $k_{eff}$ tends to increase with the surface temperature, implying the increased radiative heat loss. Furthermore, $k_{eff}$ appears to decrease as the strain rate is increased. Based on these observations, within the narrow range of parameter conditions considered, a functional form for $k_{eff}$ is suggested in the following form:

$$k_{eff} = (a_1 U + b_1) T_{surf} + (a_2 U + b_2) \tag{4.1}$$

where the units for effective heat conductivity $k_{eff}$, average nozzle velocity $U$, and stagnation plane temperature $T_{surf}$ are W/m-K, m/s, and K, respectively. The resulting constants

are

$a_1 = -2.625$E-1, $b_1 = 2.038$E-1, $a_2 = 1.441$E+2, $b_2 = -1.084$E+2

for the noncatalytic surface and

$a_1 = -2.702$E-1, $b_1 = 2.176$E-1, $a_2 = 1.474$E+2, $b_2 = -1.169$E+2

for the catalytic surface. As will be discussed later, it was necessary to derive a distinct curve fit for noncatalytic and catalytic surfaces in order to reproduce the experimental results. This is attributed to the fact that the surface radiative properties differ significantly between the noncatalytic (bare silicon) and the catalytic (platinum) surface. A family of fitted lines following equation 4.1 are shown in Figures 4.4 and 4.5. Equation 4.1 was adopted for subsequent simulations discussed in the next section.

## 4.3 Results and Discussion

### 4.3.1 Comparison with Experiment

Using equation 4.1 in the simulation, calculations were performed for various strain rate conditions. For a given strain rate, the extinction equivalence ratio limit was identified by gradually decreasing the equivalence ratio until the flame extinction was observed. The computational results are then compared against experiment in terms of the stagnation plane temperature and the extinction equivalence ratio for different nozzle velocities.

Figure 4.6 shows both predicted and measured stagnation plane temperature. The level of agreement is good, with the relative errors within 10%. This is expected from the use of $k_{eff}$ fitted from the experimental data set. Furthermore, the two different sets of constants used for the noncatalytic and catalytic conditions yielded different surface temperature at the same strain rate conditions. While the surface temperature prediction appears reasonable, however, the comparison of predicted and measured extinction equivalence ratio shown in Fig. 4.7 does not yield the same level of agreement. Although the experiment tends to indicate that the extinction equivalence ratio becomes lower for the catalytic sur-

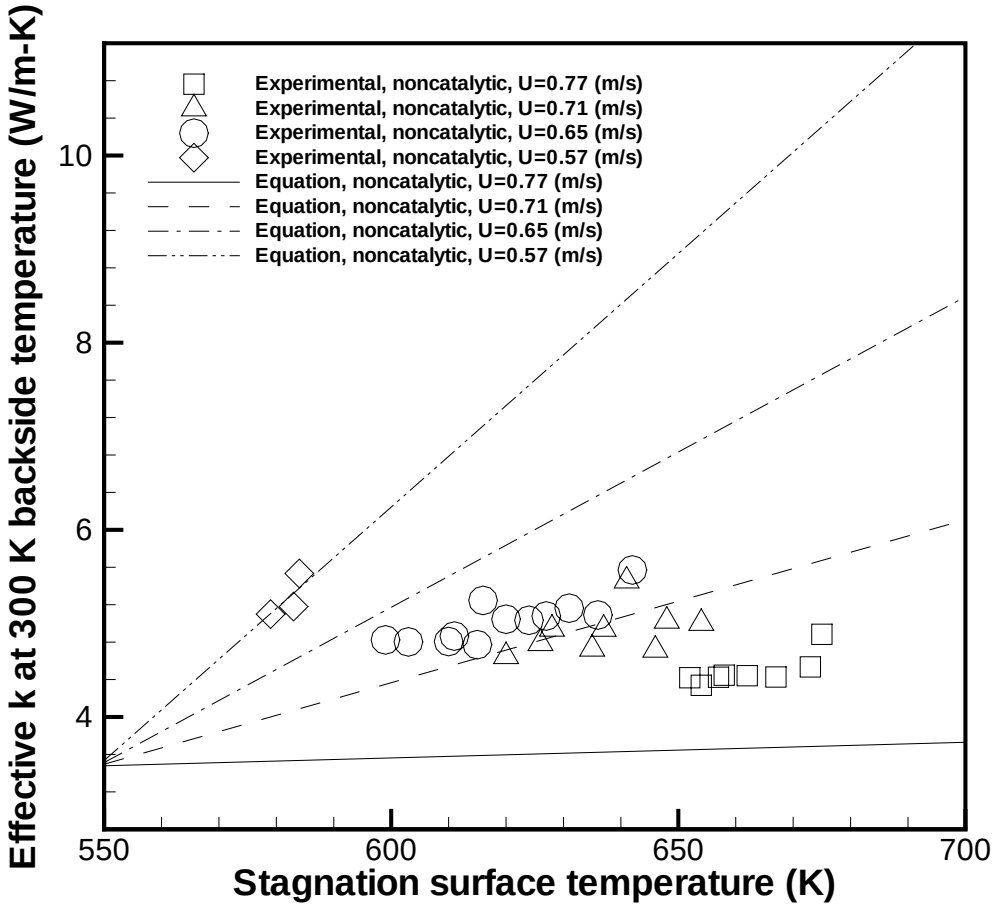


Figure 4.4: $k_{eff}$ versus the stagnation plane temperature for various strain rate and equivalence ratio conditions, with a noncatalytic surface.

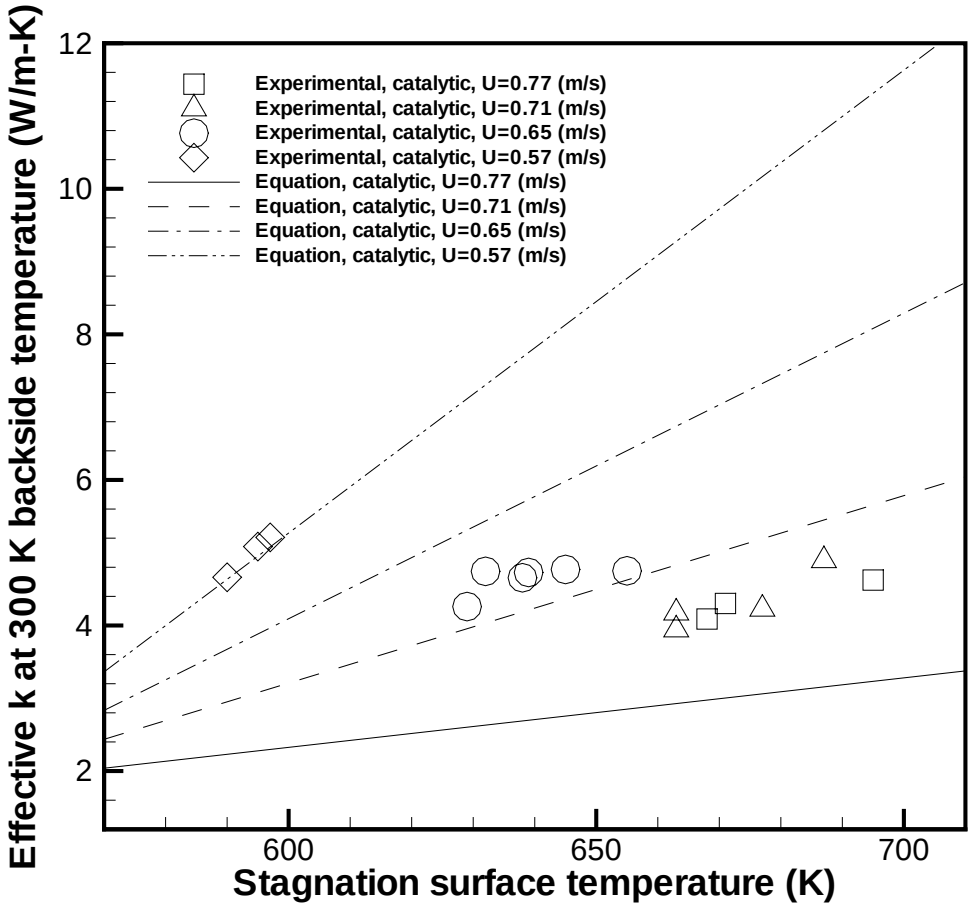


Figure 4.5: $k_{eff}$ versus the stagnation plane temperature for various strain rate and equivalence ratio conditions, with a catalytic surface.

face cases, hence suggesting that there exists a slight benefit in flammability extension by the use of catalytic surface, computational results revealed no discernable differences, despite the differences in the surface temperature between the two cases. These results imply that the differences in the surface temperature observed in the experiment was primarily due to the differences in the surface heat loss property, most likely the radiative property resulting from the two distinct surface materials. To demonstrate this further, equation 4.1 with averaged constants is adopoted to calculate heat loss for both catalytic and noncatalytic cases. Effect of distinct surface materials is eliminated numerically by doing this. Figure 4.8 shows extinction temperatures are same for catalytic and noncatalytic cases if their heat loss equation are same. Figure 4.7 suggests that no significant catalytic reaction existed under the conditions considered in the experiment. This is primarily due to the fact that the surface temperature was too low due to the large amount of heat loss, such that all the conditions were not ripe to activate catalytic reaction.

To explore the high surface temperature conditions in which the catalytic reactions are active, the experimental set-up is currently being modified and additional measurements are being taken by the experimental group. In the following, the potential benefit of flammability extension by catalytic reaction is explored by computational studies only.

### 4.3.2 Assessment of Flammability Extension

The comparison shown in the previous section provided explanation for the discrepancies in our earlier studies; while the flammability extension by catalytic reaction was demonstrated by computational modeling in Chapters 2 and 3, such results were never observed experimentally. By previous effort in this chapter in estimating real experimental parameters such as nozzle distance and heat loss condition, we are able to simulate experimental environments with numerical model. Both numerical and experimental results show no benefits of catalytic reaction. Since the numerical process is exactly the same as in chapters 2 and 3 except changed strain rate and heat loss condition, it is safe to conclude the

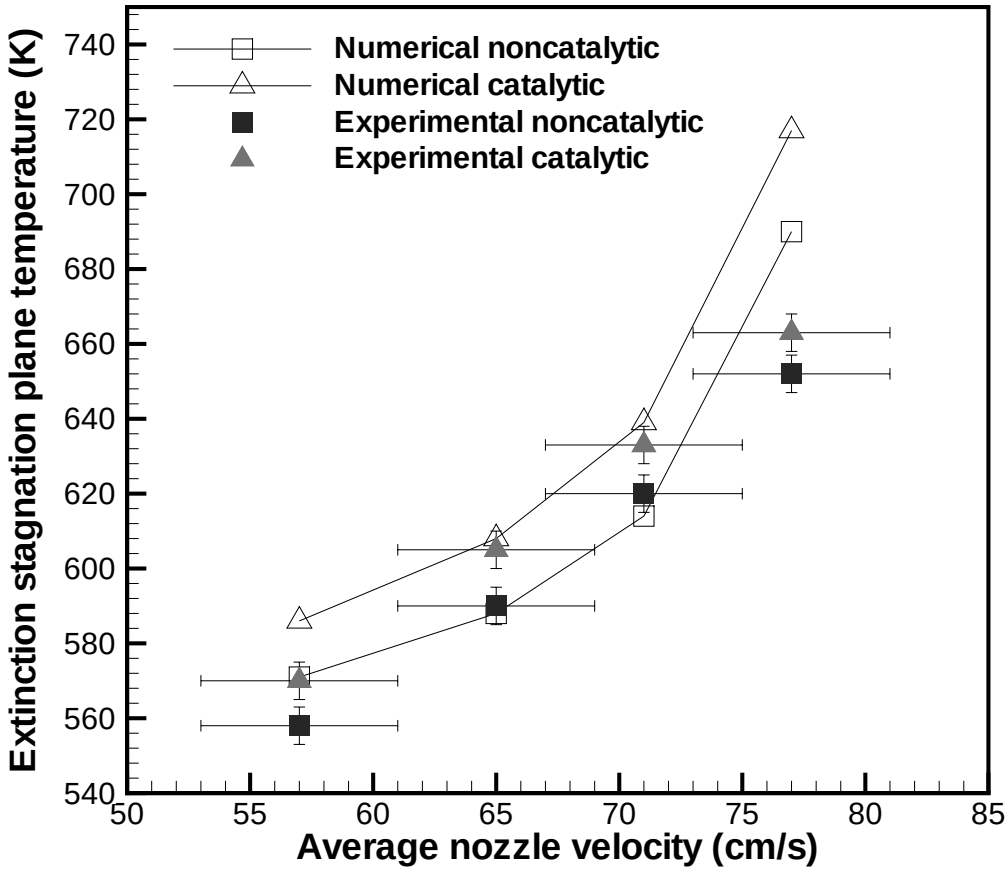


Figure 4.6: Extinction stagnation surface temperature from numerical and experimental results for catalytic/noncatalytic surface condition. Two equations for $k_{cata}/k_{noncata}$ is applied in calculation.

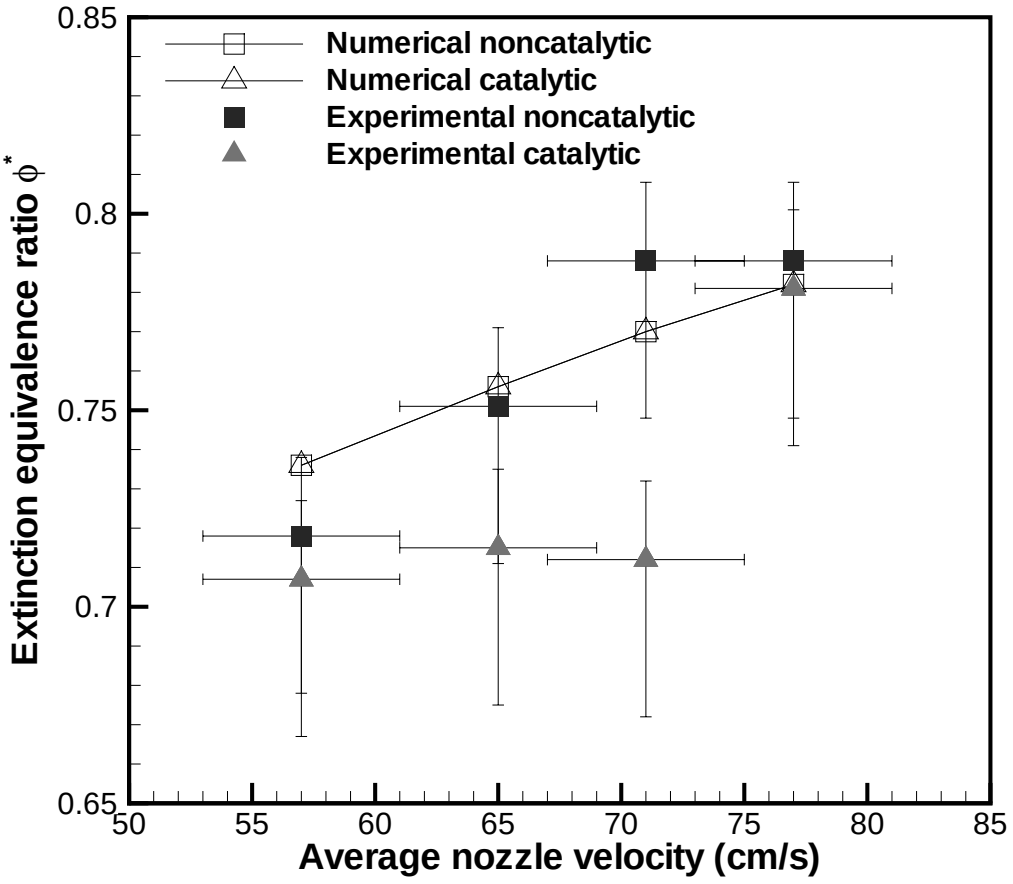


Figure 4.7: Extinction equivalence ratio from numerical and experimental results for catalytic/noncatalytic surface condition. Two equations for $k_{cata}/k_{noncata}$ is applied in calculation.

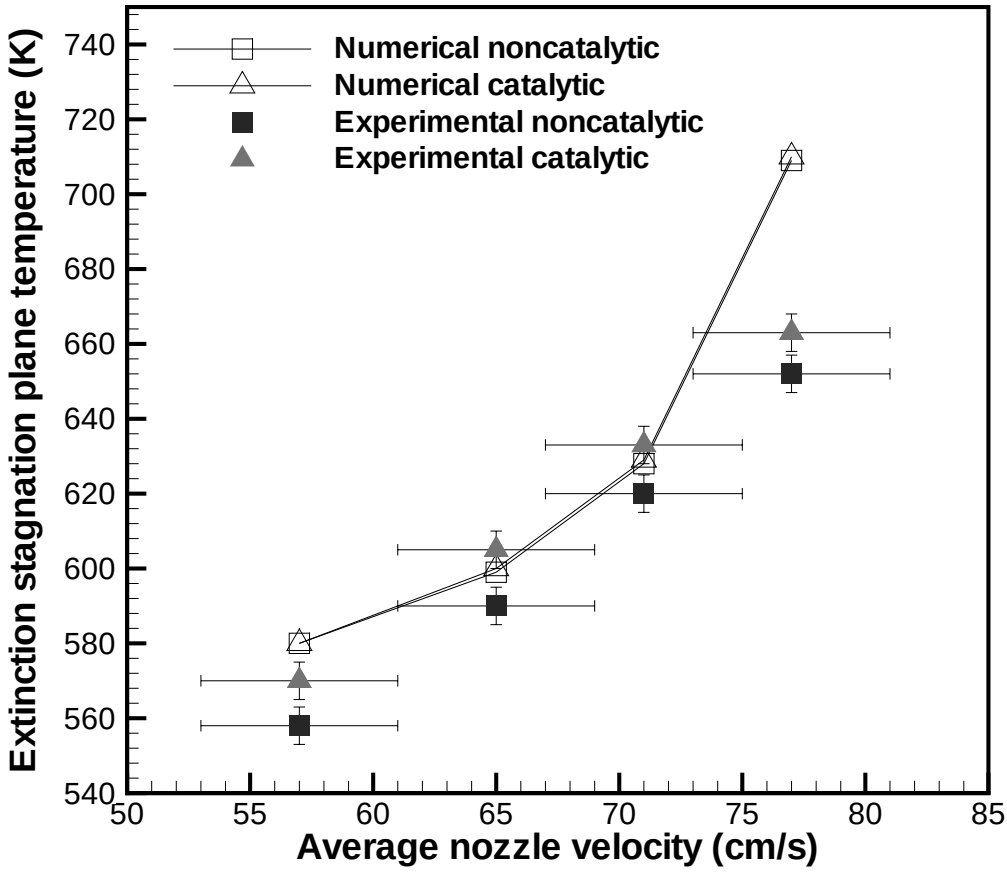


Figure 4.8: Extinction stagnation surface temperature from numerical and experimental results for catalytic/noncatalytic surface condition. Same equation for $k_{cata}/k_{noncata}$ is applied in calculation.

absence of catalytic effects as due to improper value of strain rate and heat loss condition. Rest part of of this chapter is trying to find a direction that can guide experiment validation to observe catalytic effects. It is found that catalytic reaction favors larger strain rate and lower heat loss. When heat loss hits some critical values (this value changes with strain rate), catalytic reaction will be triggered. As strain rate increasing and heat loss decreasing, benefits of catalytic reaction will be more and more obvious. Tremendous computational trial and error is required to find that critical heat loss value since it changes with strain rate. Here only two strain rates and two heat loss conditions are tried to demonstrate the conclusion that if we want to see catalytic effects in the experiments, we should increase strain rate or lower heat loss. Finding the critical trigging parameters could remain as future work.

Figures 4.9, 4.10, 4.11, 4.12, show extinction equivalence ratio and stagnation plane temperature for various surface reaction condition, nitrogen dilution, global strain rate and heat loss amount. Substrate backside temperature is fixed at 565 K which is at the same order as measured in experiments for these plots. By doing this, the fixed heat loss condition for Fig. 4.10, 4.12, is $7.874 W/m^2 - K$ which is a reasonable value for natural convection. On the contrary, if 300 K backside temperature is used as in previous part, a much lower $h$ has to be applied to produce the same heat loss amount which makes the heat loss parameter value abnormal.

In all these plots, catalytic and noncatalytic cases show obvious differences in both temperature and equivalence ratio. This means catalytic surface reaction is effective in the applied thermal boundary condition. Comparing adiabatic wall with heat loss wall for lower strain rate, extinction equivalence ratio of heat loss wall is obviously higher than that of adiabatic wall (Fig. 4.9, 4.10). Dilution makes both catalytic and noncatalytic extinction equivalence ratio higher but catalytic reaction starts to show benefits (cross over point of catalytic and noncatalytic lines in Fig. 4.9, 4.10) at a lower nitrogen dilution percentage for heat loss wall. These observations are also true for plots of higher strain rate. It has been

approved nitrogen dilution lowers both surface and gas phase reaction speed but affects the speed of gas phase reaction more [59]. However from current observations, that effect is more obvious for heat loss wall than for adiabatic wall. Comparing corresponding plots for lower and higher strain rate, extinction equivalence ratio of lower strain rate is lower than that of higher strain rate (Fig. 4.9, 4.11 and Fig. 4.10, 4.12). This is not surprising since lower strain rate is assumed to resist extinction better. Catalytic reaction starts to show benefits at a lower dilution percentage for higher strain rate. The conclusion is it is easier to see catalytic reaction's advantage over noncatalytic reaction with heat loss wall and larger strain rate.

## 4.4 Conclusions

In this chapter, numerical model was refined with adjustment in various physical parameters in order to reproduce experimental measurement data. The experimental results had shown that no discernable benefit of flammability extension was observed by the addition of catalytic surface. The numerical results confirmed that this is due to large wall heat loss which suppressed surface reaction. The level of differences in the surface temperature at extinction between the catalytic and noncatalytic cases is attributed to the different heat transfer properties on the bare silicon and platinum surfaces. Based on this observation, additional computational experiments were conducted to identify proper parametric range in which a clear catalytic flammability extension can be observed. In principle, this can be achieved at lower surface temperature and higher strain rate, both of which are expected to increase the disparity between the surface and gas-phase reaction time scales.

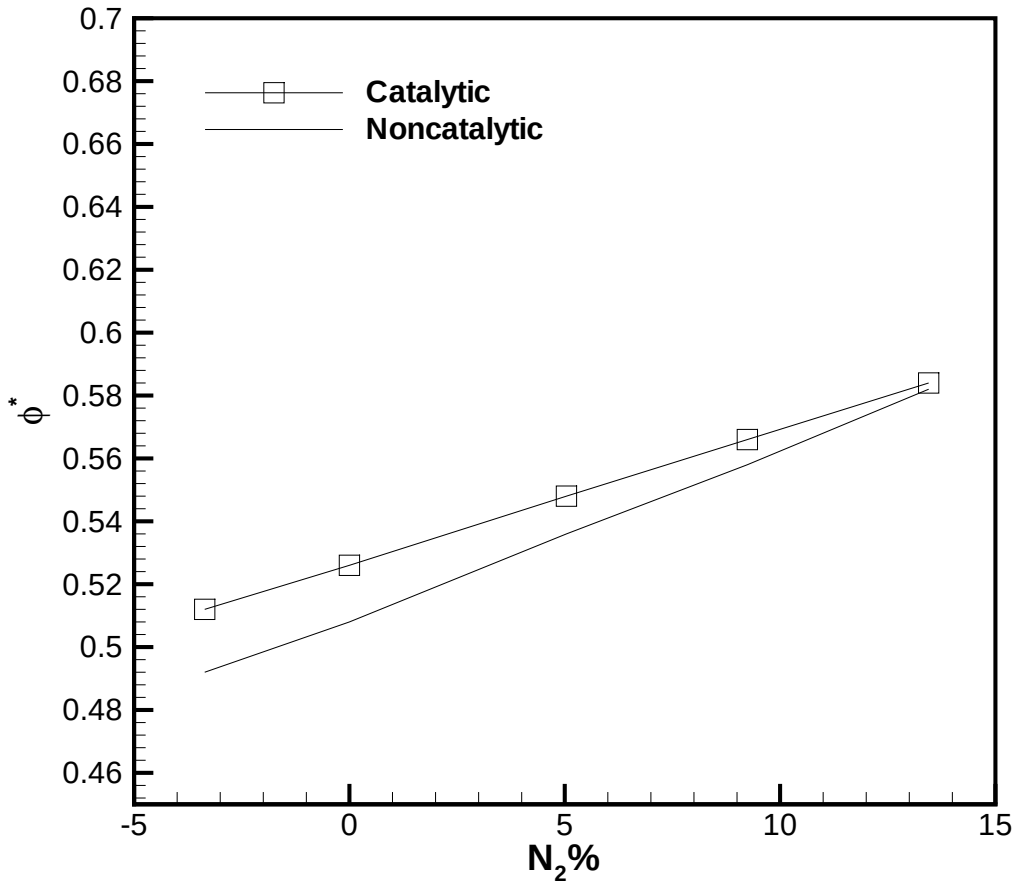


Figure 4.9: Extinction equivalence ratio from numerical results for catalytic/noncatalytic surface condition. Average nozzle velocity 74.4 cm/s, adiabatic wall.

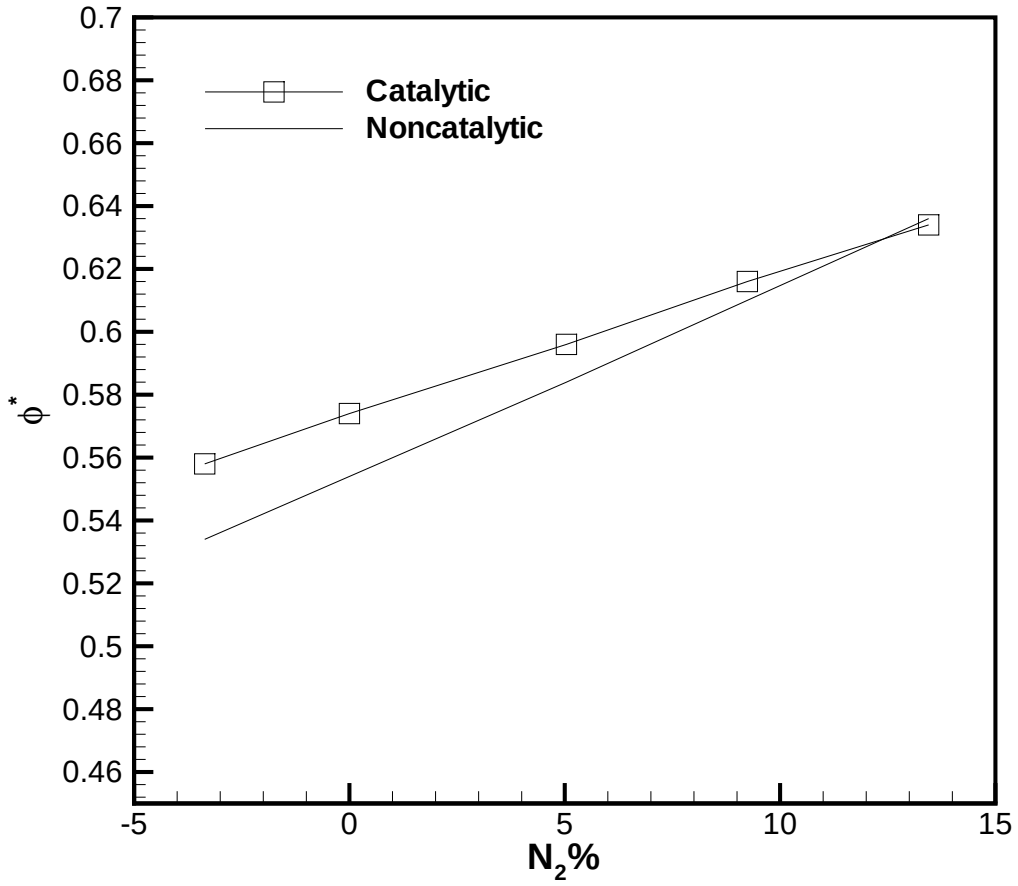


Figure 4.10: Extinction equivalence ratio from numerical results for catalytic/noncatalytic surface condition. Average nozzle velocity 74.4 cm/s, heat loss condition $h = k/\delta = 7.874 W/m^2 - K$.

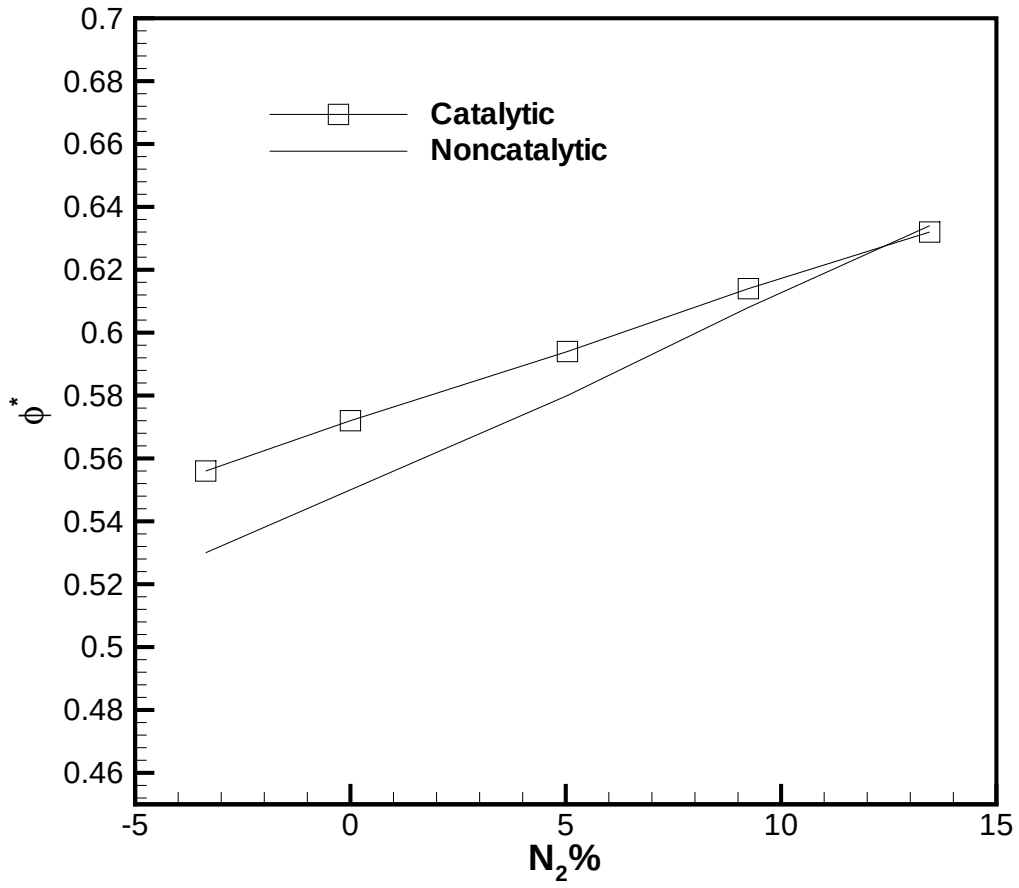


Figure 4.11: Extinction equivalence ratio from numerical results for catalytic/noncatalytic surface condition. Average nozzle velocity 138.6 cm/s, adiabatic wall.

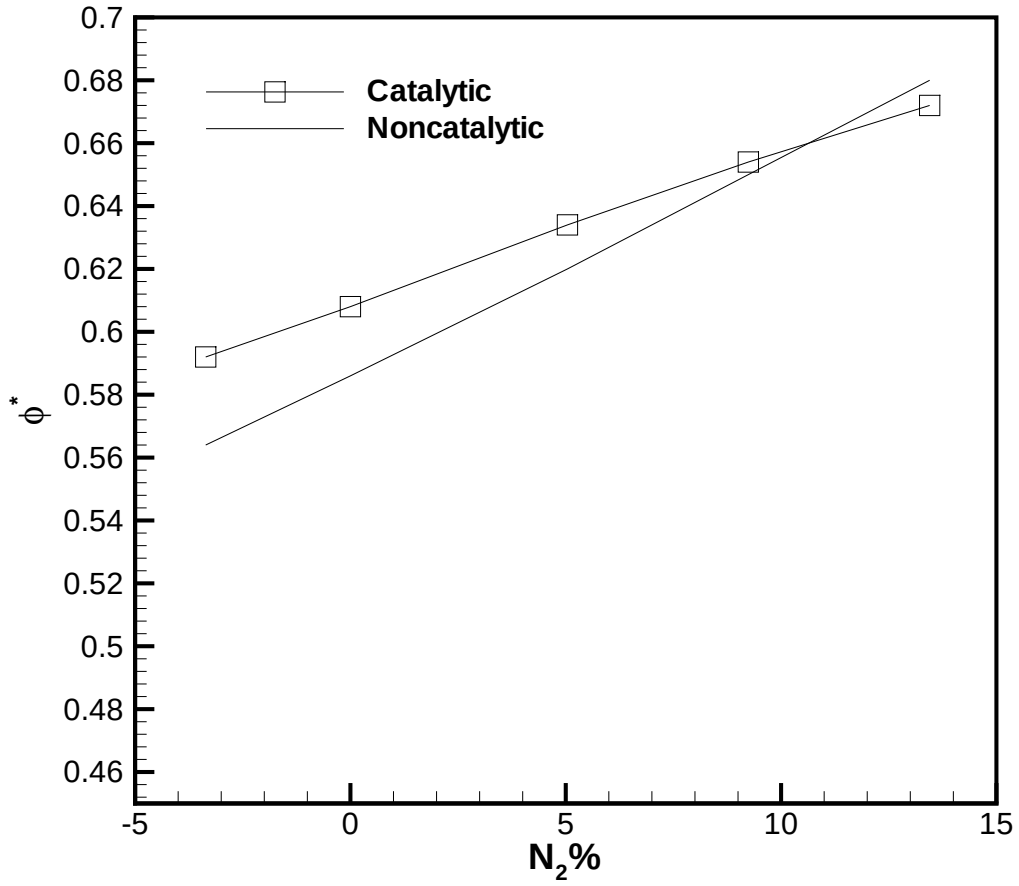


Figure 4.12: Extinction equivalence ratio from numerical results for catalytic/noncatalytic surface condition. Average nozzle velocity 138.6 cm/s, heat loss condition $h = k/\delta = 7.874 W/m^2 - K$.

# Chapter 5

# Flame Propagation and Extinction in a Narrow Channel

In this chapter, additional aspects relevant in development of micro-combustor are addressed, namely the gas-phase combustion characteristics within a narrow channel subjected to a large amount of heat loss. Adopting a canonical two-dimensional channel with conductive wall heat losses, the main objective of this study is to investigate the effects of wall heat loss on the shape of the premixed flame and the subsequent overall flame propagation speed. Flame Extinction condition is also investigated. All numerical results in this chapter are pure gas phase without introduction of surface catalytic reaction. Consideration of reactive channel walls is left for future work.

## 5.1 Numerical Model and Computational Condition

In this chapter, flame propagation and extinction behavior in different sized micro-scale plane channels are simulated by the high-fidelity reacting flow code employed in the study by Yoo and Im [60]. The code is a fully compressible Navier-Stokes solver coupled with an integrator for detailed chemistry, and is based on high-order finite differencing [61], high-order explicit Runge-Kutta time integration [62, 63], and a CHEMKIN-compatible description of gas-phase chemical kinetics [64].

A freely-propagating premixed flame within a narrow channel was considered. A two-dimensional rectangular domain with a channel length of 5 to 10 mm was used depending on the conditions, in order to ensure that the flame behavior is unaffected by the inflow and outflow boundaries. The width of channel was set at 2 mm and 0.7 mm which is approximately the quenching distance for hydrogen flames. The grid size was approximately 16 microns with further refinement in the transverse direction as needed to ensure sufficient grid resolution. A detailed reaction mechanism for hydrogen-air flames [65] was used in the simulation. For the initial condition, a one-dimensional premixed flame solution, generated from the Premix code [66], was uniformly mapped onto the two-dimensional domain as the initial condition. Note that, even for a flame that is propagating freely into a quiescent upstream, heat release generates a flow field behind the flame which must also satisfy the no-slip condition at the wall. Consequently, the downstream velocity distribution was modified into the parabolic profile in the transverse direction. Furthermore, to retain the flame within the computational domain during the calculation, a Galilean transformation was applied such that a uniform inflow velocity is imposed at the inlet boundary. Figure 5.1 shows the schematic of the transformation as well as the initial post-flame velocity profile. Since the flame speed is not known prior to the simulation, an iterative process was used to update the inflow velocity at each time step to the instantaneous bulk flame speed. A steady state solution is obtained through the process, which is then used for further analysis.

The composition is fixed at the inflow boundary and the improved Navier-Stokes characteristic boundary conditions developed by Yoo *et al.* [60, 67] were employed for the outflow and solid wall boundaries. As for the thermal boundary conditions, the heat loss through the wall was modeled by computing the heat flux as

$$q = h(T_{in} - T_{out}) \tag{5.1}$$

where $T_{out}$ was set at 300 K and the effective heat transfer coefficient $h$ was prescribed.

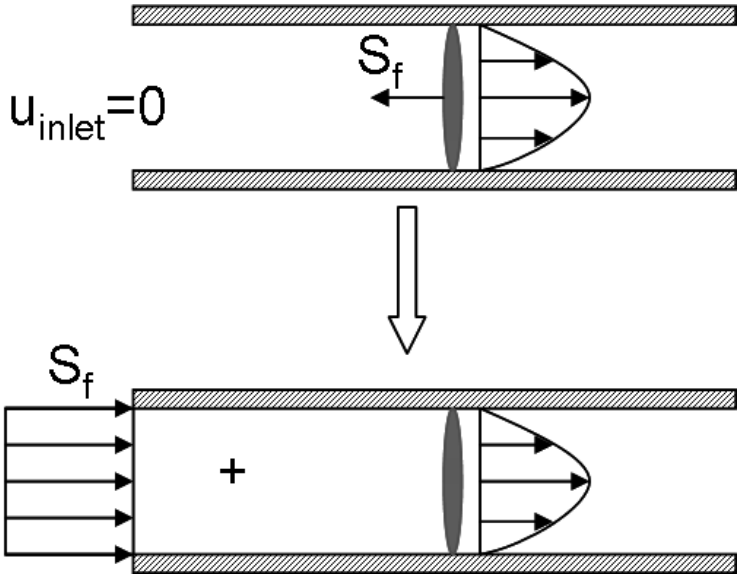


Figure 5.1: Schematic diagram of how Galilean transformation for velocity works.

The inner wall temperature $T_{in}$ was determined as part of the solution.

The main objectives of this study are to examine the effects of different level of wall heat loss conditions on the flame shape and the resulting bulk flame speed.

## 5.2 Results and Discussion

### 5.2.1 Effects of heat loss and mixture composition on the flame shape

Figure 5.2 shows the steady state solution for the heat release iso-contours for flames with various heat loss conditions. For the adiabatic wall condition, the flame curvature is determined by the pressure difference induced by the flame-generated vorticity along with the parabolic velocity profile due to the solid wall. A tulip flame shape is obtained only in the adiabatic wall condition. In the presence of wall heat loss; however, the flame speed near the wall is reduced due to heat loss, such that the flame curvature changes to a convex center to the upstream. As the level of heat loss is increased, local quenching of the flame near the wall is observed (Fig. 5.2(d)).

To investigate the effect of mixture composition, Fig. 5.3 shows the flame shape change

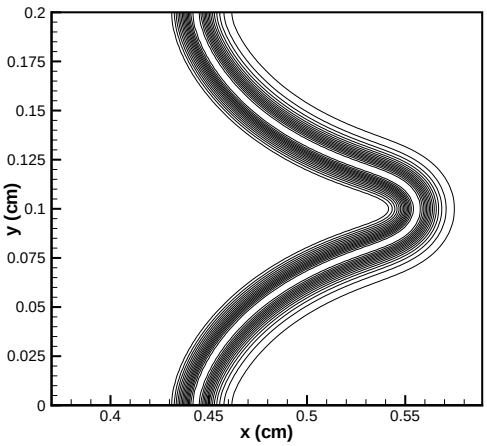


(a) $h = 0$

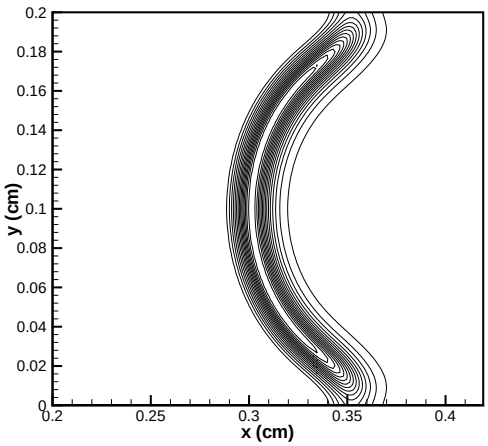


(b) $h = 5e - 9W/m^2 - K$

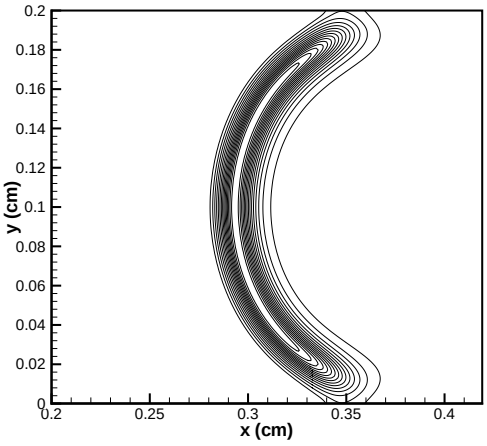


(c) $h = 10e - 9W/m^2 - K$

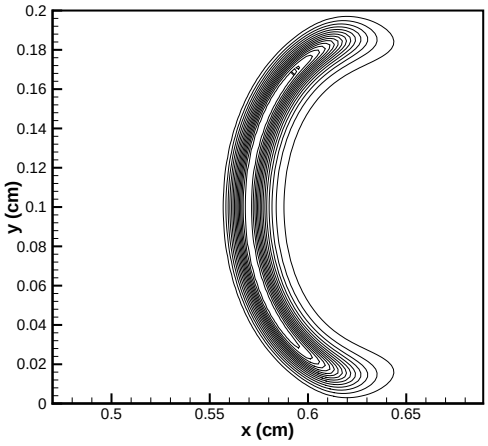


(d) $h = 32e - 9W/m^2 - K$

Figure 5.2: Flame shape change with heat loss in 2 mm channel, H2/air at $\phi = 0.5$.

with equivalence ratio in 2 mm channel for a fixed heat loss coefficient. It is obvious that the negative curvature (tulip flame) in the flame center reemerges as the equivalence ratio is increased, due to the enhanced flame-generated vortices. Therefore, there appear to be two competing effects to modify the flame shape in the narrow channel: the viscous friction on the wall coupled with flame-generated vortices versus the flame weakening near the wall due to heat loss.

Fig. 5.4 is a counterpart of Fig. 5.3 for 0.7 mm channel. Similar flame curvature in flame center is not observed in same parameter range. This is because heat loss in narrower channel is more important than in wider channel that equivalence ratio effect is not large enough to balance the heat loss effect.

### 5.2.2 Flame propagation speed change

Fig. 5.5 shows flame propagation speed as a function of equivalence ratio (Fig. 5.5 (a) or heat loss amount Fig. 5.5 (b)) in 2 mm channel. Flame speed increases unsurprisingly with increasing $\phi$ while increases slightly with increasing heat loss coefficient abnormally.

Fig. 5.6 is similar to Fig. 5.5 except it is for a 0.7 mm channel. From Fig. 5.6 (a), the flame speed for the two $h$ values does not change a lot. Though the flame speed with $h = 32e - 9W/m^2 - K$ as in Fig. 5.5 is not presented, it is expected that flame speed for $h = 32e - 9W/m^2 - K$ will be similar to $h = 40e - 9W/m^2 - K$ and $h = 50e - 9W/m^2 - K$. Comparing Fig. 5.5 (a) with Fig. 5.6 (a), it is observed that flame speed in narrower channel is lower than that in wider channel at same $\phi$ and $h$. This observation enforced the conclusion that the heat loss in a narrower channel is more important than in a wider channel. Fig. 5.6 (b) shows the flame speed increases slightly with heat loss for two higher equivalence ($\phi$=0.57 and 0.60) ratios but decreases slightly for the lower equivalence ratio ($\phi$=0.54) in 0.7 mm channel. Combine this observation with Fig. 5.5 (b). Since it has been concluded that the higher equivalence ratio and wider channel help the system to resist extinction due to heat loss, another conclusion can be made that the flame speed of

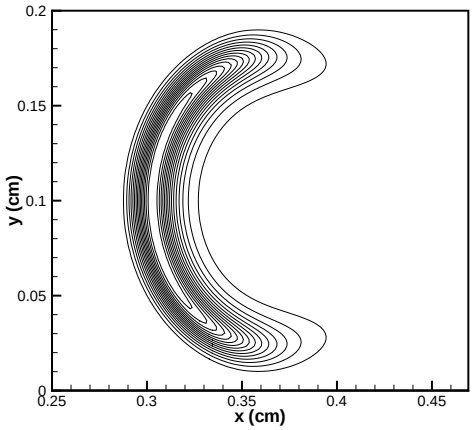


(a) $\phi = 0.4$

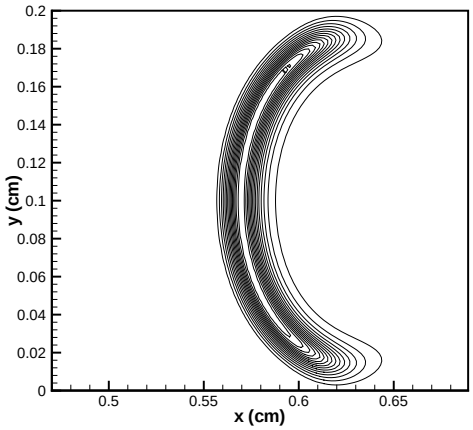


(b) $\phi = 0.5$

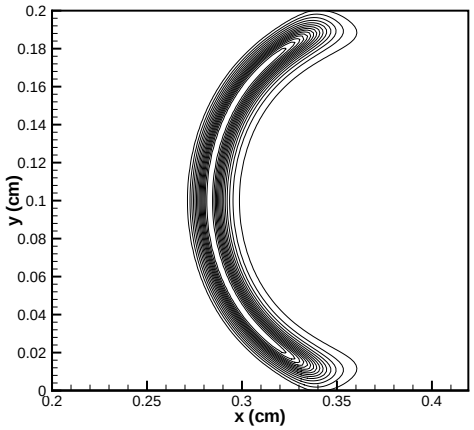


(c) $\phi = 0.6$

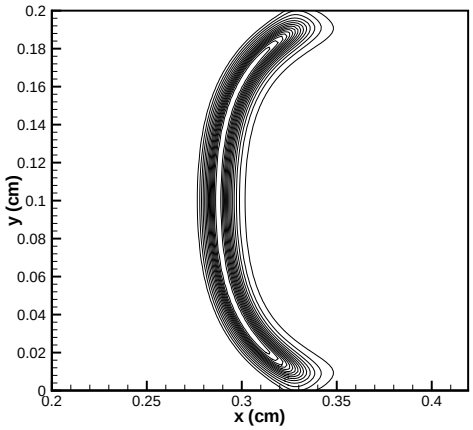


(d) $\phi = 0.7$

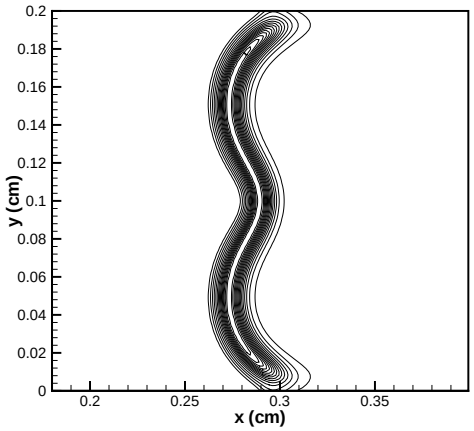


(e) $\phi = 0.8$

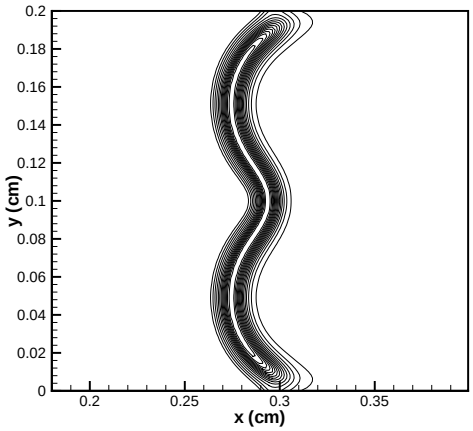


(f) $\phi = 0.9$

Figure 5.3: Flame shape change with equivalence ratio in 2 mm channel, $h = 32e - 9W/m^2 - K$.

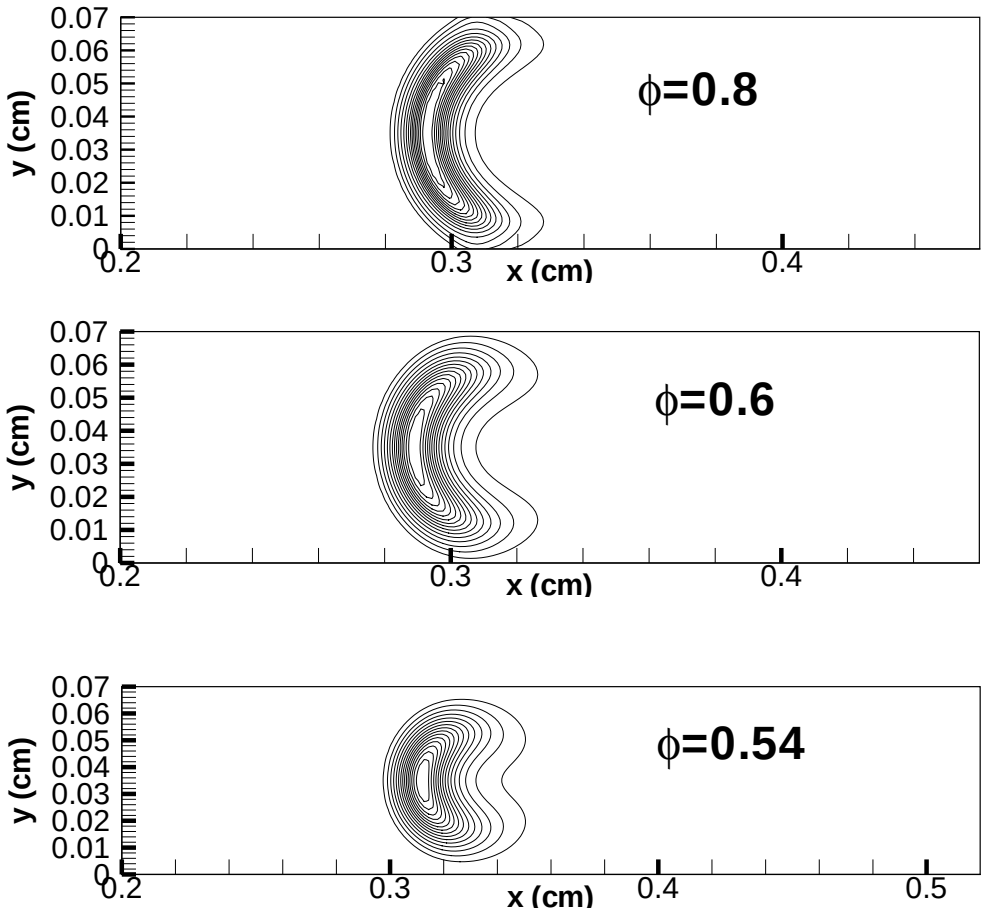


Figure 5.4: Flame shape with equivalence ratio in 0.7 mm channel, $h = 40e-9W/m^2-K$.

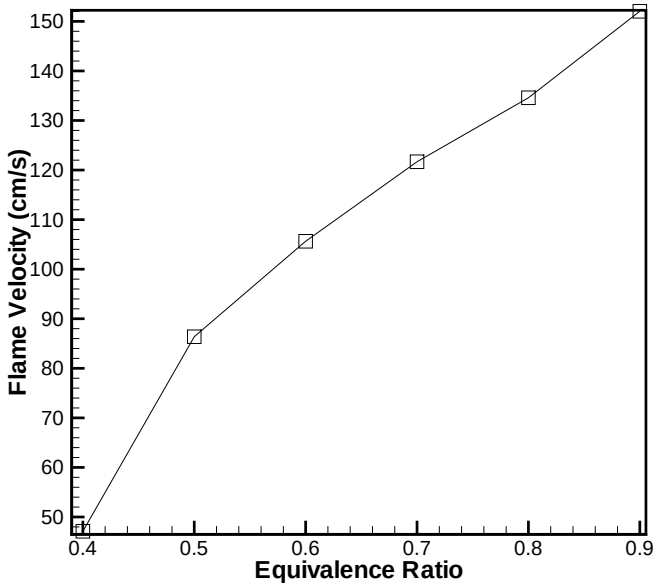


(a) Flame speed change with $\phi$, $h = 32e - 9W/m^2 - K$

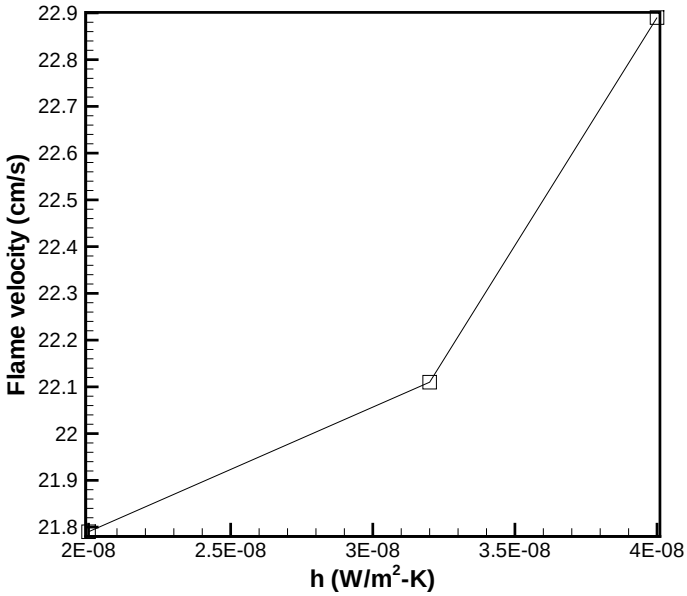


(b) Flame speed change with heat loss $h$, $\phi$=0.35

Figure 5.5: 2 mm channel.

systems with higher ability to resist extinction could increase with heat loss abnormally. Or it can be stated that the heat loss coefficient $h$ must be large enough to balance the effect of equivalence ratio and channel width to see the speed reduction due to heat loss.

Fig. 5.7 shows the flame extinction equivalence ratio with different heat loss in a 2mm and 0.7mm channel. The flame extinction equivalence ratio is not sensitive to this heat loss range but is sensitive to channel width. This conclusion might be different if the heat loss amount is increased largely. However, the code cannot capture the severe flow field change due to heat loss at the initial stage if $h$ is larger than $50e-9W/m^2-K$ with the current grid resolution. Larger resolution is not tractable for the current computer resources.

## 5.3 Conclusions

The velocity gradient induced pressure and heat loss through the channel wall are two competitive factors that determine flame shape. The first factor is strengthened by a larger equivalence ratio and the second factor is strengthened by a larger heat loss. However this observation is not obvious in the 0.7mm channel because the heat loss is more important in a narrower channel and the effect of equivalence ratio has been suppressed in that heat loss range. The flame is attached to the wall and heat release contour lines are vertical to the surface for the adiabatic wall. On the contrary, the flame is detached and contour lines could be parallel near to surface if the wall heat loss is large enough.

The flame speed increases with equivalence ratio and could increase or decrease with heat loss depending on the system's ability to resist extinction. Flame speed in a narrow channel is lower than in a wider channel for same $\phi$ and $h$ which is normal since heat loss effect is more important for narrower channel.

The extinction equivalence ratio is not sensitive to the heat loss coefficient $h$ in our parameter range but changes obviously with channel width. The first observation could be because the $h$ value is not large enough. For the 2 mm channel, the extinction $\phi$ is 0.34. For the 0.7 mm channel, the extinction $\phi$ is 0.53.

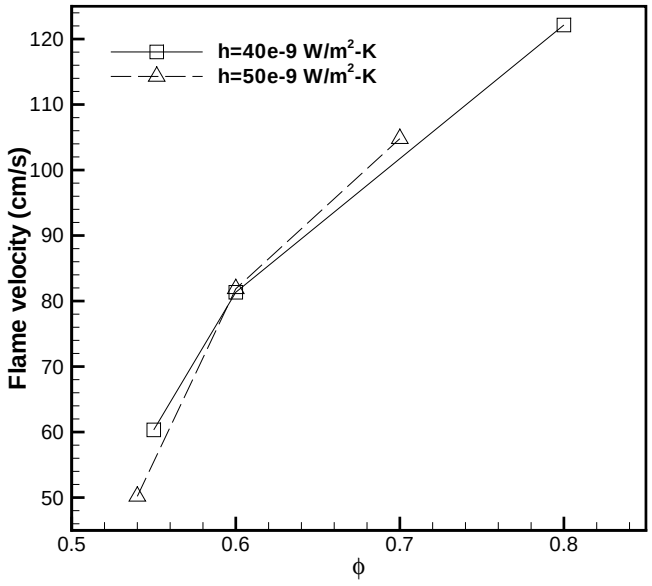


(a) Flame speed change with $\phi$.

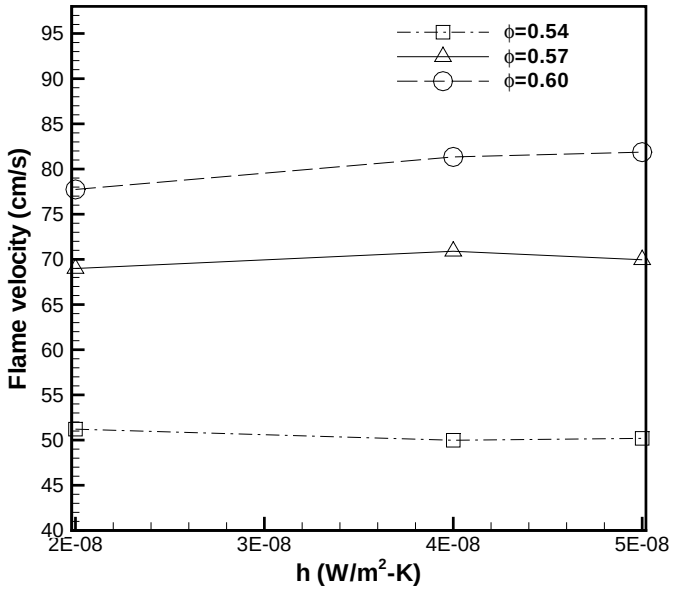


(b) Flame speed change with heat loss $h$.

Figure 5.6: 0.7 mm channel.

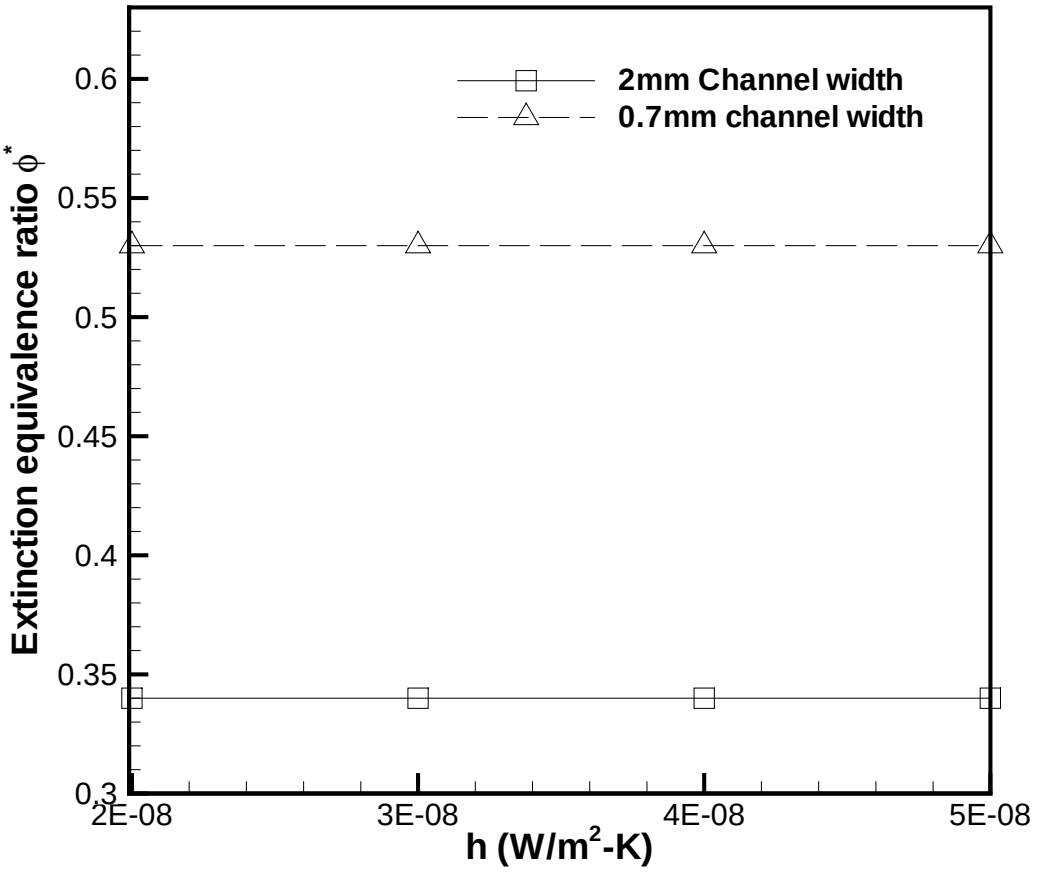


Figure 5.7: Extinction equivalence ratio with different wall heat loss and channel width.

# Chapter 6

# Conclusions

The Combustion process and extinction limit related with micro-combustor are studied in this dissertation. Stagnation-point flow and channel flow models are applied as numerical models. Experimental analysis was performed on the stagnation-point flow model. Due to the large surface to volume ratio of micro-sized combustors, heat loss through a combustor wall is the key factor that was paid attention to. Other parametric inputs include strain rate, equivalence ratio and nitrogen dilution. The whole study provides insights into performance optimization and combustion stability of micro-combustors. The following summarize the conclusions of this study.

**The strain rate extinction limit is extended by involving catalytic reaction** Strain-induced extinction limits over a range of physical parameters are analyzed using a stagnation-point flow model. An estimate of the characteristic chemical times based on the methane consumption rate confirms that the surface reaction has significantly shorter characteristic time scales, thereby sustaining reaction at lower flow residence times. The steady results showed that catalytic reaction can largely extend the extinction limit, while suppressing the gas phase reaction at lower strain rates. It was also found that the extension of the catalytic reaction quenching limit is highly sensitive to the mixture composition, suggesting the dominance of chemical aspects in catalytic combustion.

**Multiple physical solutions caused by catalytic surface reactions** In the steady state results of the stagnation-point flow model, the temperature versus strain rate response curves exhibit multiple branches of stable solutions, implying a possibility of hysteresis behavior in a coupled homogeneous-heterogeneous reactor. The branch with the higher temperature is dominated by gas phase reactions, partly with a detached flame and partly with an attached flame. The branch with the lower temperature is dominated by catalytic surface reactions without a visible flame. Characteristics of combustion behavior in each branch have been examined by the reaction zone structures. Different combination of equivalence ratio and heat loss could result in different branch shapes: a surface-dominant monotonic response, continuous two-branch response, and separated response showing an isolated surface-reaction island. Parametric mapping shows distinct regimes in terms of the mixture equivalence ratio and heat loss.

**Lean flammability extension due to catalytic reactions in diluted system** Despite a large strain rate, extinction due to low equivalence ratio is also studied. For the stagnation-point flow system, it was found that surface reactions actually attenuate the range of lean flammability limit due to their effect of radical scavenging. If the reactant is diluted with nitrogen properly; however, the catalytic reactions can indeed make extinction equivalence ratios lower than that of pure gas phase reactions and this effect is more obvious with additional dilution in the gas mixture. While the surface heat loss expectedly lowers the overall flammability of the system, it was found that the level of flammability extension by surface reactions is rather insensitive to the surface thermal conditions.

**Dynamic lean flammability extension** The stagnation-point flow system response to anoscillatory strain rate and equivalence ratio fluctuations showed overall consistent trends expected from the steady results. The overall flame response becomes attenuated as

the frequency of strain rate oscillation increases. It was also found that the benefit of flammability extension by catalytic reactions can be greater as the level of unsteadiness increases when the system is diluted enough.

**The experimental heat loss condition is too large to activate catalytic reaction** Experimental analysis was conducted for the stagnation-point flow model by another group while no similar catalytic effects were found as in numerical data. A meticulous numerical method is adopted to simulate real heat loss condition in experiments. It is found that the reason for no discrepancy was observed experimentally for catalytic and noncatalytic reaction is due to large wall heat loss which suppressed surface reaction. The minor extinction temperature discrepancy between catalytic and noncatalytic cases observed in experiments is mostly due to surface coating of catalytic material that changes surface emissivity other than the surface reaction effect. By further numerical study, it is believed that lower heat loss or larger strain rate should make it possible to observe catalytic effects in experiments. The triggering heat loss condition is expected to change with strain rate though parametric study is needed to demonstrate that. When the catalytic reaction is activated, its benefit over gas phase reaction is more obvious at larger strain rates and larger heat losses since catalytic reactions are less sensitive to those conditions.

**The flame shape in a channel is affected by heat loss and equivalence ratio** In a micro-channel combustor, the velocity gradient induced pressure and heat loss through the channel wall are two competitive factors that determine the flame curvature direction. The first factor is strengthened by larger equivalence ratios and the second factor is strengthened by larger heat losses. When they are comparable, the flame curvature could show a different direction at the center and edge.

**Lean extinction limit of micro-channel** Extinction equivalence ratio is not sensitive to the heat loss coefficient $h$ in our parameter range, but obviously depends on channel

width. For a 2 mm channel, the extinction $\phi$ is 0.34. For a 0.7 mm channel, the extinction $\phi$ is 0.53.

## 6.1 Directions for Future Work

Numerical analysis has been done with two types of micro-combustors to provide directions into improving combustor performance, optimize combustor design and show guidance for experimental analysis. Important observations have been researched carefully and theoretical explanations have been conducted. More analysis could be performed in the future to make this study more integrated.

It has been found that catalytic reaction needs a triggering heat loss condition in chapter 4. It is expected that this heat loss condition is a function of strain rate if keeping other parameters untouched. Parametric studies can be made in the future to find what theheat loss condition is. Is it a critical surface temperature or a critical heat loss amount or a nondimensional number which combines several parameters? Its relationship with strain rate needs to be solved by a large amount of numerical trial and error. Observations in chapter 3 imply that while dilution attenuate both gas phase and surface reactions, surface reactions are less sensitive to dilution. That causes the benefits of catalytic reactions to be more obvious with higher nitrogen dilution levels. In chapter 4, similar observation is found. While heat loss makes the whole system fragile, catalytic reactions are less affected by it thus the benefits of catalytic reactions over gas phase reactions are more obvious with larger heat loss. Further numerical sensitivity analysis should be done in the future to quantitatively demonstrate those conclusions.

Since the study of the micro-channel is in its initial stages and the observations and conclusions are preliminary, a lot of work can be done in the future on this model. It has been found that the flame speed increases with increasing equivalence ratio and increases with increasing heat loss. Those observations should be supplemented by applying multiple equivalence ratio values in heat loss versus flame speed plots and by applying multiple heat

loss values in equivalence ratio versus flame speed plots. Besides, flame strengthening by increasing equivalence ratio is expected, but flame speed increasing with larger heat loss is abnormal. More simulation should be conducted in the future to explain the heat loss effect on flame speed. Flame shape could also have effect on flame speed, and this could be analyzed by taking one-dimensional premixed flame speed comparison. The heat loss range is not wide enough in chapter 5 thus the heat loss effect is not obvious in extinction equivalence ratio which only changes with channel width. Numerical difficulties are encountered while heat loss amounts exceed current range due to a severe flow field change in the transitional stage from the initial field to the field that accommodates the heat loss. To solve this problem, a better initial field should be achieved in the future. Otherwise, grid numbers have to be increased in the boundary to capture the severe changes, and this will cause a huge consumption in computational resources and time. To take advantage of channel flow, fuel and oxidizer can be introduced to the channel separately to investigate effect of diffusion which cannot be conducted with the stagnation-point flow model. Another research direction that can be added to the micro-channel flow is to adopt catalytic reaction on channel wall. Coding issues on coupling gas phase and surface reactions, reaction characteristic time scale differences between gas phase and surface reactions could be a potential difficulty in achieving a converged solution. If those numerical problems could be solved in the future, this study will be useful in directing micro-combustor design that involves channel flow.

# Bibliography


[1] Spadaccini, C. M., Mehra, A., Lee, J., Zhang, X., Lukachko, S. and Waitz, I. A. (2003). High Power Density Silicon Combustion System for Micro Gas Turbine Engines. *Journal of Engineering for Gas Turbines and Power*, 125, pp. 709–719. v, 1, 2

[2] Peirs, J., Reynaerts, D. and Verplaetsen, F. (2004). A Microturbine for Electric Power Generation. *Sensors and Actuators, A: Physical*, 113, pp. 86–93. v, 2

[3] Zhang, C., Najafi, K., Bernal, L. P. and D., W. P. (2003). Micro Combustion-Thermionic Power Generation: Feasibility, Design and Initla Results. *The 12th International Conference on Solid State Sensors, Actuators and Microsystems*, Boston, USA. v, 2, 3

[4] Yang, W. M., Chou, S. K., Shu, C. and Li, Z. W. (2004). A Prototype Microthermophotovoltaic Power Generator. *Applied Physics Letters*, 84, pp. 3864–3866. v, 2, 3

[5] Wiswall, J. (2007). *Catalytic Effects on Methane and Propane Combustion on Platinum*. Master's thesis, University of Michigan, Ann Arbor. vi, 7, 51, 52, 53

[6] (2000). DARPA MEMS Project Summaries. Tech. rep., Defense Advanced Research Projects Agency, Department of Defense, http://www.arpa.mil/mto/mems/summaries/Projects. 1

[7] Fernandez-Pello, A. C. (2002). Micro-Power Generation Using Combustion: Issues and Approaches. *29th International Symposium on Combustion*, Sapporo, Japan. 1

[8] Epstein, A. H., Senturia, S. D., Anathasuresh, G., Ayon, A., Breuer, K., Chen, K.-S., Ehrich, F. E., Gauba, G., Ghodssi, R., Groshenry, C., Jacobson, S., Lang, J. H., Lin, C.-C., Mehra, A., Miranda, J. M., Nagle, S., Orr, D. J., Piekos, E., Schmidt, M. A., Shirley, G., Spearing, M. S., Tan, C. S., Tzeng, Y.-S. and Waitz, I. A. (1997). Power MEMS and Microengines. *1997 International Conference on Solid-State Sensors and Actuators*, Chicago, USA. 1

[9] Lee, D. H., Park, D. E., Yoon, E. and Kwon, S. (2003). A MEMS Piston-Cylinder Device Actuated by Combustion. *Journal of Heat Transfer*, 125, pp. 487–493. 1

[10] Green, D. V., Miller, C. G., Santavicca, D. A. and V., S. K. (2004). Pulsed Micro Catalytic Combustor for Use in A Solid Piston Microengine. *2004 ASME International Mechanical Engineering Congress and Exposition*, Anaheim, USA. 1

[11] Liedtke, O. and Schulz, A. (2003). Development of A New Lean Burning Combustor with Fuel Film Evaporation for A Micro Gas Turbine. *Experimental Thermal and Fluid Science*, 27, pp. 363–369. 1

[12] Mehra, A., Ayon, A. A., Waitz, I. A. and Schmidt, M. A. (1999). Microfabrication of High-Temperature Silicon Devices Using Wafer Bonding and Deep Reactive Ion Etching. *IEEE Journal of Microelectromechanical Systems*, 8, pp. 152–160. 1

[13] Spadaccini, C. M., Zhang, X., Cadou, C. P., Miki, N. and Waitz, I. A. (1999). Microfabrication of High-Temperature Silicon Devices Using Wafer Bonding and Deep Reactive Ion Etching. *IEEE Journal of Microelectromechanical Systems*, 8, pp. 152–160. 1, 3

[14] Fu, K., Knobloch, A., Martinez, F., Walther, D., Fernandez-Pello, A. C., Pisano, A., Liepmann, D., Miyaska, K. and Maruta, K. (2001). Design and Experimental Results of Small-Scale Rotary Engines. *Proceedings of the 2001 International Mechanical Engineering Congress and Exposition(IMECE)*, New York, USA. 1

[15] Arana, L. R., Schaevitz, S. B., Franz, A. J., Jenson, K. F. and Schmidt, M. A. (2002). A Microfabricated Suspended-Tube Chemical Reactor for Fuel Processing. *Proceedings of the IEEE Micro Electro Mechanical Systems (MEMS)*, pp. 232–235. 2

[16] Suzuki, Y., Horii, Y., Kasagi, N. and Matsuda, S. (2004). Micro Catalytic Combustor with Tailored Porous Alumina. *17th IEEE International Conference on Micro Electro Mechanical Systems (MEMS): Maastricht MEMS 2004 Technical Digest*, pp. 312–315. 2, 3

[17] Holladay, J. D., Jones, E. O., Dagle, R. A., Xia, G. G., Cao, C. and Wang, Y. (2004). High Efficiency and Low Carbon Monoxide Micro-Scale Methanol Processors. *Journal of Power Sources*, 131, pp. 69–72. 2

[18] Dalla Betta, R. A. (1997). Catalytic combustion gas turbine systems: The preferred technology for low emissions electric power production and co-generation. *Catalysis Today*, 35, pp. 129–135. 3

[19] Raja, L. L., Kee, R. J., Deutschmann, O., Warnatz, J. and Schmidt, L. D. (2000). Critical evaluation of Navier-Stokes, boundary-layer, and plug-flow models of the flow and chemistry in a catalytic-combustion monolith. *Catalysis Today*, 59, pp. 47–60. 3

[20] Kang, S. H., Im, H. G. and Baek, S. W. (2003). A computational study of Saffman-Taylor instability in premixed flames. *Combustion, Theory and Modelling*, 7, pp. 343–63. 4

[21] Mowery, D. L., Gardner, T. J., Frye-Mason, G. C., Kottenstette, R., Manginell, R. P. and Margolis, S. B. (2001). Development of a Novel On-Chip Catalytic Microcombustor Device. *17th North American Catalysis Society Meeting*, Toronto, Canada. 4

[22] Deutschmann, O., Schmidt, R., Behrendt, F. and Warnatz, J. (1996). Numerical Modeling of Catalytic Ignition. *Proc. Combust. Inst.*, 26, pp. 1747–1754. 4, 16, 38

[23] Law, C. K. and Sivashinsky, G. I. (1982). Catalytic Extension of Extinction Limits of Stretched Premixed Flames. *Combustion Science and Technology*, 29, pp. 277–286. 4

[24] Margolis, S. B. and Gardner, T. J. (2003). An Asymptotic Model of Nonadiabatic Catalytic Flames in Stagnation-Point Flow. *Siam J. Appl. Math.*, 63, pp. 1083–1103. 4, 27

[25] Fernandes, N. E., Park, Y. K. and Vlachos, D. G. (1999). The Autothermal Behavior of Platinum Catalyzed Hydrogen Oxidatin: Experiments and Modeling. *Combustion and Flame*, 118, pp. 164–178. 5

[26] Dupont, V., Zhang, S., Bentley, R. and Williams, A. (2002). Experimental and Modelling Studies of the Catalytic Combustion of Methane. *Fuel*, 81, pp. 799–810. 5

[27] Veser, G. and Schmidt, D. (1996). Ignition and Extinction in the Catalytic Oxidation of Hydrocarbons over Platinum. *AIChe Journal*, 42, pp. 1077–1087. 5

[28] Park, Y. K., Bui, P.-A. and Vlachos, D. G. (1998). Operation regimes in catalytic combustion: H2/air mixtures near Pt. *AIChE J.*, 44, pp. 2035–2043. 5

[29] Seo, Y. S., Kang, S. K. and Shin, H. D. (1999). Catalytic combustion of lean premixed mixture in catalytically stabilized thermal combustor. *Combustion Science and Technology*, 145, pp. 17–35. 5

[30] Im, H. G., Law, C. K., Kim, J. S. and Williams, F. A. (1995). Response of counterflow diffusion flames to oscillating strain rates. *Combust. Flame*, 100, pp. 21–30. 6, 45

[31] Im, H. G., Bechtold, J. K. and Law, C. K. (1995). Counterflow Diffusion Flames with Unsteady Strain Rates. *Combustion Science and Technology*, 106, pp. 345–361. 6

[32] Im, H. G., Bechtold, J. K. and Law, C. K. (1996). Response of counterflow premixed flames to oscillating strain rates. *Combustion and Flame*, 105, pp. 358–372. 6

[33] Egolfopoulos, F. N. and Campbell, C. S. (1996). Unsteady counterflowing strained diffusion flames: Diffusion-limited frequency response. *J. Fluid Mech.*, 318, pp. 1–29. 6, 45

[34] Ghoniem, A. F., Soteriou, M. C. and Knio, O. J. (1992). Effect of steady and periodic strain on unsteady flamelet combustion. *Proc. Combust. Inst.*, 25, pp. 223–230. 6

[35] Sung, C. J. and Law, C. K. (2000). Structural sensitivity, response, and extinction of diffusion and premixed flames in oscillating counterflow. *Combustion and Flame*, 123, pp. 375–388. 6

[36] Lauvergne, R. and Egolfopoulos, F. N. (2000). Unsteady response of C3H8/air laminar premixed flames submitted to mixture composition oscillations. *Proc. Combust. Inst.*, 28, pp. 1841–1849. 6

[37] Sankaran, R. and Im, H. G. (2002). Dynamic flammability limits of methane/air premixed flames with mixture composition fluctuations. *Proc. Combust. Inst.*, 29, pp. 77–84. 6, 46

[38] Maruta, K., Takeda, K., Sitzki, L., Borer, K., Ronney, P. D., Wussow, S. and Deutschmann, O. (2001). Catalytic Combustion in Microchannel for MEMS Power Generation. *3rd Asia-Pacific Conference on Combustion*, Seoul, Korea. 8

[39] Michaelis, B. and Rogg, B. (2004). FEM-simulation of laminar flame propagation. I: Two-dimensional flames. *Journal of Computational Physics*, 196, pp. 417–447. 8

[40] Kurdyumov, V., Fernandez-Tarrazo, E., Truffaut, J. M., Quinard, J., Wangher, A. and Searby, G. (2007). Experimental and numerical study of premixed flame flashback. *Proceedings of the Combustion Institute*, 31, pp. 1275–1282. 8

[41] Pizza, G., Frouzakis, C. E., Mantzaras, J., Tomboulides, A. G. and Boulouchos, K. (2008). Dynamics of premixed hydrogen/air flames in microchannels. *Combustion and Flame*, 152, pp. 433–450. 9

[42] Kee, R. J., Rupley, F. M. and Meeks, E. (1996). Chemkin-III: A Fortran Chemical Kinetics Package for the Analysis of Gas-Phase Chemical and Plasma Kinetics. Tech. Rep. SAND96-8216, Sandia National Lab. 12, 13, 16

[43] Raja, L. L., J., K. R. and Petzold, L. R. (1998). Simulation of the transient, compressible, gas-dynamic behavior of catalytic-combustion ignition in stagnation flow. *27th Symposium(intl.) on combustion*, pp. 2249–2257. 13

[44] Sankaran, R. (2004). *A Computational Study of Auto-Ignition and Flame Propagation in Stratified Mixtures Relevant to Modern Engines*. Ph.D. thesis, University of Michigan, Ann Arbor. 13

[45] Im, H. G., Raja, L. L., Kee, R. J., Lutz, A. E. and Petzold, L. R. (2000). Opus: A Fortran Program for Unsteady Opposed-Flow Flames. Tech. Rep. SAND2000-8211, Sandia National Lab. 13, 38

[46] Coltrin, M. E., Kee, R. J. and Rupley, F. M. (1990). SURFACE CHEMKIN: A Fortran Package for Analyzing Heterogeneous Chemical Kinetic at a Solid-Surface-Gas-Phase Interface. Tech. Rep. SAND90-8003B, Sandia National Lab. 13, 26

[47] Grcar, J. F. (1993). The Twopnt Program for Boundary Value Problems. Tech. Rep. SAND91-8230, Sandia National Lab. 13, 14

[48] Li, S. and Petzold, L. R. (1999). Design of New DASPK for Sensitivity Analysis. Tech. Rep. TRCS99-23, Computer Science Department, University of California, Santa Barbara. 13

[49] Kee, R. J., Dixon-Lewis, G., Warnatz, J., Coltrin, M. E. and Miller, J. A. (1986). A Fortran Computer Code Package for the Evaluation of Gas-Phase Multicomponent Transport Properties. Tech. Rep. SAND86-8246, Sandia National Lab. 13

[50] Keller, H. B. (1987). Lectures on Numerical Methods in Bifurcation Problems. Springer, New York. 14, 16

[51] Im, H. G. and Chen, J. H. (2000). Effects of flow transients on the burning velocity of laminar hydrogen/air premixed flames. *Proc. Combust. Inst.*, 28, pp. 1833–1840. 16, 45

[52] Law, C. K. (1988). Dynamics of Stretched Flames. *Proc. Combust. Inst.*, 22, pp. 1381–1402. 17

[53] Linan, A. and Williams, F. A. (1981). Note on Ignition by a Hot Catalytic Surface. *SIAM Journal on Applied Mathematics*, 40, p. 261. 19

[54] Bui, P. A., Vlachos, D. G. and Westmoreland, P. R. (1996). Homogeneous ignition of hydrogen-air mixtures over platinum. *Proc. Combust. Inst.*, 26, pp. 1763–1770. 19

[55] Ju, Y., Law, C. K., Maruta, K. and Niioka, T. (2000). Radiation-induced Instability of Stretched Premixed Flames. *Proceedings of Combustion Institute*, 28, pp. 1891–1900. 32

[56] Smith, G. P., Golden, D. M., Frenklach, M., Moriarty, N. W., Eiteneer, B., Goldenberg, M., Bowman, C. T., Hanson, R. K., Song, S., Gardiner, W. C., Lissianski, V. V. and Qin, Z. http://www.me.berkeley.edu/gri_mech. 38

[57] Deutschmann, O., Behrendt, F. and Warnatz, J. (1994). Modelling and simulation of heterogeneous oxidation of methane on a platinum foil. *Catalysis Today*, 21, pp. 461–470. 38

[58] Li, J. and Im, H. G. (2006). Extinction characteristics of catalyst-assisted combustion in a stagnation-point flow reactor. *Combust. Flame*, 145, pp. 390–400. 38, 39, 43

[59] Li, J. and Im, H. G. (2007). Effects of Dilution on the Extinction Characteristics of Strained Lean Premixed Flames Assisted by Catalytic Reaction. *Proceedings of the Combustion Institute*, 31, pp. 1189–1195. 65

[60] Yoo, C. S. and Im, H. G. (2007). Characteristic boundary conditions for simulations of compressible reacting flows with multi-dimensional, viscous and reaction effects. *Combustion Theory and Modelling*, 11, pp. 259–286. 70, 71

[61] Kennedy, C. A. and Carpenter, M. H. (1994). Several new numerical methods for compressible shear-layer simulations. *Appl. Num. Math*, 14, pp. 397–433. 70

[62] Kennedy, C. A., Carpenter, M. H. and Lewis, R. M. (2000). Low-storage, explicit Runge-Kutta scheme for the compressible Navier-Stokes equations. *Appl. Num. Math*, 35, pp. 177–219. 70

[63] Kennedy, C. A. and Carpenter, M. H. (2003). Additive Runge-Kutta schemes for convection-diffusion-reaction equations. *Appl. Num. Math*, 44, pp. 139–181. 70

[64] Kee, R. J., Rupley, F. M., Meeks, E. and Miller, J. A. (1996). Chemkin III: a fortran chemical kinetics package for the analysis of gas-phase chemical and plasma kinetics. Tech. Rep. SAN96-8216, Sandia National Lab. 70

[65] Mueller, M. A., Yetter, R. A. and Dryer, F. L. (1998). Measurement of the rate constant for $H+O_2+MHO_2+M$ ($M=N_2$, Ar) using kinetic modeling of the high-pressure$H_2/O_2$/NOx reaction. *Proceedings of the Combustion Institute*, 27, pp. 177–184. 71

[66] Kee, R. J., Grcar, J. F., Smooke, M. D. and Miller, J. A. (1985). A Fortran Program for Modeling Steady Laminar One-Dimensional Premixed Flames. Tech. Rep. SAND85-8240, Sandia National Lab. 71

[67] Yoo, C. S., Wang, Y., Trouve, A. and Im, H. G. (2005). Characteristic boundary conditions for direct simulations of turbulent counterflow flames. *Combustion Theory and Modelling*, 9, pp. 617–646. 71